

# Signatures of archaic adaptive introgression in present-day human populations

Fernando Racimo<sup>a</sup>, Davide Marnetto<sup>b</sup>, Emilia Huerta-Sánchez<sup>c</sup>

<sup>a</sup>Department of Integrative Biology, University of California Berkeley, CA, USA

<sup>b</sup>Department of Molecular Biotechnology and Health Sciences, University of Torino, Turin, Italy

<sup>c</sup>School of Natural Sciences, University of California Merced, CA, USA

---

## Abstract

Comparisons of DNA from archaic and modern humans show that these groups interbred, and in some cases received an evolutionary advantage from doing so. This process - adaptive introgression - may lead to a faster rate of adaptation than is predicted from models with mutation and selection alone. Within the last couple of years, a series of studies have identified regions of the genome that are likely examples of adaptive introgression. In many cases, once a region was ascertained as being introgressed, commonly used statistics based on both haplotype as well as allele frequency information were employed to test for positive selection. Introgression by itself, however, changes both the haplotype structure and the distribution of allele frequencies, thus confounding traditional tests for detecting positive selection. Therefore, patterns generated by introgression alone may lead to false inferences of positive selection. Here we explore models involving both introgression and positive selection to investigate the behavior of various statistics under adaptive introgression. In particular, we find that the number and allelic frequencies of sites that are uniquely shared between archaic humans and specific present-day populations are particularly useful for detecting adaptive introgression. We then examine the 1000 Genomes dataset to characterize the landscape of uniquely shared archaic alleles in human populations. Finally, we identify regions that were likely subject to adaptive introgression and discuss some of the most promising candidate genes located in these regions.

**Keywords:** Neanderthal, Denisova, Adaptive Introgression, Ancient DNA

---

## 1. Introduction

There is now a large body of evidence supporting the idea that certain modern human populations admixed with archaic groups of humans after expanding out of Africa. In particular, non-African populations have 1 – 2% Neanderthal ancestry [1, 2], while Melanesians and East Asians have 3% and 0.2% ancestry, respectively, from Denisovans [3, 4, 2].

Recently, it has become possible to identify the fragments of the human genome that were introgressed and survive in present-day individuals [5, 6, 2, 7, 8, 7]. Researchers have also detected which of these introgressed regions are present at high frequencies in certain present-day non-African populations. Some of these regions are likely to have undergone positive selection in those populations after they were introgressed, a phenomenon known as adaptive introgression (AI). One particularly striking example of AI is the gene *EPAS1* [9] which confers a selective advantage in Tibetans by making them less prone to hypoxia at high altitudes [10, 11, 12, 13, 14, 15, 16, 17]. The selected Tibetan haplotype is likely to have been introduced in the human gene pool by Denisovans or a population closely related to them [18, 19].

In this study, we first use simulations to assess the power to detect AI using different exploratory summary statistics that do not require the introgressed fragments to be identified *a priori*. Some of these are inspired by the signatures observed in *EPAS1*, which contains an elevated number of sites with alleles uniquely shared between the Denisovan genome and Tibetans. We then apply these statistics to real human genomic data from phase 3 of the 1000 Genomes Project [20], to detect AI in human populations, and find candidate genes. While these statistics are sensitive to adaptive introgression, they may also be sensitive to other phenomena that generate genomic patterns similar to those generated by AI, like ancestral population structure and incomplete lineage sorting. These processes, however, should not generate long regions of the genome where haplotypes from the source and the recipient population

19 are highly similar. As additional confirmation that the candidates we found with our statistics are generated by AI, we explored the  
20 haplotype structure of some of the most promising candidates, and used a probabilistic method [21] that infers introgressed segments  
21 along the genome by looking at the spatial arrangement of SNPs that are consistent with introgression. This allows us to verify that  
22 the candidate regions contain introgressed haplotypes at high frequencies: a hallmark of AI.

## 23 **2. Results**

### 24 *2.1. Statistics for detecting AI*

25 We began by evaluating the performance of various statistics at detecting AI. In addition to testing statistics that have already  
26 been previously defined in the literature ( $D$ ,  $f_D$ ,  $D'$ ,  $r^2$ ,  $\pi$ ), we define three new types of statistics that we find are particularly  
27 powerful at detecting AI (Table 1). We briefly describe the new statistics here, but more extensive descriptions of all tested statistics  
28 can be found in the Methods section below.

29 First, in a region under AI, one would expect the sequence divergence between an individual from the source population and an  
30 admixed individual to be smaller than the sequence divergence between an individual from the source population and a non-admixed  
31 individual. Thus, we define  $R_D$  as the average ratio of the sequence divergence between a panel from the source population and a  
32 panel from the admixed population, over the sequence divergence between the source panel and a non-admixed panel, computed  
33 in a genomic window of the genome.

34 Second, under AI we would expect a large number of sites containing archaic alleles at high frequency in the admixed population,  
35 but absent or at low frequency in a non-admixed population. Therefore, we define the statistic  $U_{A,B,C}(w, x, y)$  to be equal to the  
36 number of sites within a genomic window where a sample C from an archaic source population has a particular allele at frequency  $y$ ,  
37 and that allele is at a frequency smaller than  $w$  in a panel A of a non-admixed population but larger than  $x$  in a panel B of an admixed  
38 population (Figure 1). Throughout the text, we denote panels A, B and C as the “outgroup”, “target” and “bait” panels, respectively.  
39 If we have samples from two different archaic populations (for example, a Neanderthal genome and a Denisova genome), we can  
40 define  $U_{A,B,C,D}(w, x, y, z)$  as the number of sites where the archaic sample C has a particular allele at frequency  $y$  and the archaic  
41 sample D has that allele at frequency  $z$ , while the same allele is at a frequency smaller than  $w$  in an outgroup panel A and larger than  
42  $x$  in a target panel B (Figure S1).

43 Finally, if we do not want to set a hard cutoff for what we consider “high-frequency” archaic alleles, we can just take a summary  
44 statistic of the site-frequency spectrum in the target panel, conditional on the archaic allele being at low frequency in the outgroup.  
45 This statistic should be high when a region contains many alleles at especially high frequencies in the target. We therefore define  
46  $Q95_{A,B,C}(w, y)$  to be equal to the 95<sup>th</sup> percentile of derived frequencies in a target panel B of all SNPs that have a derived allele  
47 frequency  $y$  in the bait (archaic) panel C, but where the derived allele is at a frequency smaller than  $w$  in an outgroup panel A from a  
48 non-admixed population (Figure 1).

### 49 *2.2. Simulations under AI*

50 We use simulations to assess the performance of the statistics mentioned above at detecting AI. Figures S3, S4 and S5 show  
51 the distribution of statistics that rely on patterns of shared allele configurations between source and introgressed populations ( $\pi$ ,  $D$ ,  
52  $f_D$ ,  $U_{A,B,C}$ ,  $Q95_{A,B,C}$  and  $R_D$ ), for different choices of the selection coefficient  $s$ , and under 2%, 10% and 25% admixture rates,  
53 respectively. For  $Q95_{A,B,C}(w, 100\%)$  and  $U_{A,B,C}(w, x, 100\%)$ , we tested different choices of the outgroup cutoff  $w$  (1%, 10%)  
54 and the target cutoff  $x$  (0%, 20%, 50% and 80%).

55 Some statistics, like  $Q95_{A,B,C}(1\%, 100\%)$  and  $f_D$  show strong separation between the selection regimes. For example, with  
56 an admixture rate of 2%,  $Q95_{A,B,C}(1\%, 100\%)$  has 100% sensitivity at a specificity of 99%, for both  $s=0.1$  and  $s=0.01$ . Some  
57 parameterizations of the U statistic are not as effective, however. For example,  $U_{A,B,C}(1\%, 0\%, 100\%)$  shows some power when  
58 the admixture rate is low (2%), but almost no power when the admixture rate is high (25%). This is because setting the minimum

59 frequency of the archaic allele in the test population at  $x = 0\%$  means that any site with some archaic allele in the test panel will be  
60 counted, regardless of the allele frequency, so long as the archaic allele is at low frequency in the outgroup panel. At high admixture  
61 rates, low- and medium-frequency archaic alleles would naturally occur under neutrality, so they would not be informative about AI.

62 We also evaluated the effectiveness of LD-based statistics at detecting AI (Figure S6). We tested the performance of  $D'$  and  
63  $r^2$  by either computing each of these in the admixed panel only ( $D'[\text{intro}]$ ,  $r^2[\text{intro}]$ ) or in the combination of the admixed and  
64 non-admixed panels ( $D'[\text{comb}]$ ,  $r^2[\text{comb}]$ ). While  $D'[\text{intro}]$ ,  $D'[\text{comb}]$  and  $r^2[\text{comb}]$  are modestly increased by AI, this is not  
65 the case with  $r^2[\text{intro}]$  under strong selection and admixture regimes. This is because  $r^2$  will tend to decrease if the minor allele  
66 frequency is very small, which will occur if this frequency is only measured in the population undergoing AI. In general, these statistics  
67 are not as powerful for detecting AI as allele configuration statistics like  $U$  or  $Q95$ .

68 To jointly explore the power and specificity of all these statistics, we generated receiving operating characteristic (ROC) curves  
69 under various selection and admixture regimes (Figures 3 and S7). In general,  $Q95_{A,B,C}(1\%, 100\%)$ ,  $Q95_{A,B,C}(10\%, 100\%)$   
70 and  $f_D$  are very powerful statistics for detecting AI under strong ( $s=0.1$ ) and intermediate ( $s=0.01$ ) selection pressures. The number  
71 of uniquely shared sites  $U_{A,B,C}(w, x, y)$  is also powerful, so long as the population in the target panel ( $B$ ) is large. Additionally,  
72 for different choices of  $x$ , using  $w = 1\%$  yields a more powerful statistic than using  $w = 10\%$ . We also tested AI scenarios with  
73 weak selection ( $s=0.001$ ), in which all statistics performed rather poorly, with  $Q95$  and  $f_D$  performing comparably better than the rest  
74 (Figure S8). However, under these conditions, it is very unlikely that the selected allele will reach appreciable frequencies (Figure  
75 S2), so the lack of sensitivity of all statistics here is largely a reflection of the fact that in most simulations the selected allele is  
76 not successful, especially when the probability of admixture is low. Conditioning on survival of the allele should therefore increase  
77 sensitivity.

78 We were also interested in the joint distribution of pairs of these statistics. Figure S9 shows the joint distribution of  $Q95_{A,B,C}(1\%, 100\%)$   
79 in the y-axis and four other statistics ( $R_D$ ,  $\pi$ ,  $D$  and  $f_D$ ) in the x-axis, under different admixture and selection regimes. One can ob-  
80 serve, for example, that while  $Q95_{A,B,C}(1\%, 100\%)$  increases with increasing selection intensity and admixture rates,  $\pi$  increases  
81 with increasing admixture rates, but decreases with increasing selection intensity. Thus, under AI the two forces cancel each other  
82 out, and we obtain a similar value of  $\pi$  as under neutrality. Furthermore, the joint distributions of  $Q95_{A,B,C}(1\%, 100\%)$  and  $f_D$  or  
83  $R_D$  show particularly good separation among the different AI scenarios.

84 Another joint distribution that is especially good at separating different AI regimes is the combination of  $Q95_{A,B,C}(w, 100\%)$   
85 and  $U_{A,B,C}(w, x, 100\%)$ . In Figure 4, we show this joint distribution, for different choices of  $w$  (1%, 10%) and  $x$  (20%, 50%). Here,  
86 with increasing intensity of selection and admixture, the number of uniquely shared sites and the quantile statistic increase, but the  
87 quantile statistic tends to only reach high values when selection is strong, even if admixture rates are low.

### 88 2.3. Alternative demographic scenarios

89 We evaluated the performance of our statistics under various alternative demographic scenarios. First, we simulated a 5X  
90 bottleneck occurring in population B 1,600 generations before the admixture event, and lasting 200 generations, to observe its  
91 effects on the power of the statistics for detecting AI (Figure 2.B). Though we observe a reduction in power - most evident in the  
92 heterozygosity statistics - none of the statistics are very strongly affected by this event (Figure S10). We also simulated a bottleneck  
93 of equal size but occurring after the admixture event - starting 1,400 generations ago, and lasting 200 generations (Figure 2.C). In this  
94 case, the sensitivity of all the statistics is strongly reduced when the admixture rate is low (Figure S11). For example, when looking  
95 at the raw values of the  $U_{A,B,C}$  and  $Q95_{A,B,C}$  statistics, we observe that for low admixture rates the distribution under selection  
96 has a larger overlap with the distribution under neutrality, which explains the low power (Figures S12, S13). Additionally,  $U_{A,B,C}$   
97 (but not  $Q95$ ) seems to display more elevated values under neutrality in the bottleneck model than in the constant population size  
98 model. However, the relative performance of each statistic with respect to all the others does not appear to change substantially  
99 (Figure S11).

100 We next explored a model where the introgressed haplotype was not immediately adaptive in the Eurasian population, but instead

101 underwent an intermediate period of neutral drift, before it becomes advantageous (Figure 2.D). In such a situation, our power to  
102 detect AI is reduced, for all statistics (Figure S14). This is particularly an issue when the admixture rate is low, as in those cases the  
103 starting frequency of the selected allele in the Eurasian population is low, so it is more likely to drift to extinction during the neutral  
104 period, before it can become advantageous.

105 We also evaluated the performance of our statistics under selective scenarios that did not involve adaptive introgression, to check  
106 which of them were sensitive to these models and which were not. Under a model of selection from de novo mutation (SDN, Figure  
107 2.E) - in which a single mutation appears in the receiving population after the split time between it and the non-admixed population -  
108 the heterozygosity ( $\pi$ ) and linkage disequilibrium statistics ( $r^2[intra]$  and  $D'[intro]$ ) are the most sensitive ones (Figure S15). This  
109 is expected, given that classical selective sweeps are known to strongly affect patterns of heterozygosity and linkage disequilibrium  
110 in the neighborhood of the selected site [22, 23, 24]. Since all other statistics have very poor sensitivity to detect SDN, we expect to  
111 be able to distinguish signatures generated from SDN and AI. One caveat to this is the scenario in which a *de novo* selected mutation  
112 occurs on an introgressed haplotype immediately after an introgression event - before the haplotype has a chance to expand and  
113 recombine in the population - in which case our statistics will not be able to distinguish SDN from AI.

114 We also simulated a model of selection from standing variation (Figure 2.F), by randomly selecting 20% of haplotypes within the  
115 introgressed population to be advantageous, after the split time between it and the non-introgressed population. In this case, all statis-  
116 tics perform poorly, especially when admixture is low. Interestingly, when admixture is high (Figure S16),  $Q95_{A,B,C}(1\%, 100\%)$   
117 and  $U_{A,B,C}(1\%, 0\%, 100\%)$  are the best performing statistics. This is likely because some of the haplotypes that are randomly  
118 chosen to be selected also happen to be ancestrally polymorphic and present in the archaic humans.

119 When we set ancestral structure to be our null model, we observe different behaviors depending on the strength of the migration  
120 rates. When the migration rates are strong (Figure S17), we have excellent power to detect AI with several statistics, including  
121  $Q95_{A,B,C}(1\%, 100\%)$ ,  $D$ ,  $f_D$ ,  $R_D$  and  $U_{A,B,C}(1\%, 50\%, 100\%)$ . When the rates are of medium strength (Figure S18), the  
122 power is slightly reduced, but the same statistics are the ones that perform best. When the migration rates are weak - meaning  
123 ancestral structure is very strong -  $Q95_{A,B,C}(1\%, 100\%)$  loses power, and the best-performing statistics are  $R_D$ ,  $D$  and  $f_D$   
124 (Figure S19). We note, though, that the genome-wide  $D$  observed under this last ancestral structure model ( $D = 0.24$ ) is much  
125 more extreme than the genome-wide  $D$  observed empirically between any Eurasian population and Neanderthals or Denisovans,  
126 suggesting that if there was ancestral structure between archaic and modern humans, it was likely not of this magnitude.

#### 127 2.4. Global features of uniquely shared archaic alleles

128 Before identifying candidate genes for adaptive introgression, we investigated the frequency and number of uniquely shared  
129 sites at the genome-wide level. Specifically, we wanted to know whether human populations varied in the number of sites with  
130 uniquely shared archaic alleles, and whether they also varied in the frequency distribution of these alleles. Therefore, we computed  
131  $U_{A,B,Nea,Den}(1\%,x,y,z)$  and  $Q95_{A,B,Nea,Den}(1\%,y,z)$  for different choices of  $x$ ,  $y$  and  $z$ . We used different cutoffs for the frequency  
132 of the archaic allele ( $x$ ) in the target population B: 0%, 20% and 50%. To look for alleles uniquely shared with the Altai Neanderthal  
133 genome only, we set  $y = 100\%$  and  $z = 0\%$ . To look for alleles uniquely shared with the Denisovan genome only, we set  $y = 0\%$   
134 and  $z = 100\%$ . Finally, to look for uniquely shared alleles matching both of the archaic genomes, we set  $y = 100\%$  and  $z = 100\%$ .

135 We used each of the non-African panels in the 1000 Genomes Project phase 3 data [20] as the “target” panel (B), and chose  
136 the outgroup panel (A) to be the combination of all African populations (YRI, LWK, GWD, MSL, ESN), excluding admixed African-  
137 Americans. We note that this is a conservative reference panel, as some of the African panels - like LWK - are from populations with  
138 a substantial amount of Eurasian ancestry [20], likely preventing the detection of introgressed segments at some loci.

139 When setting  $x = 0\%$  (i.e. not imposing a frequency cutoff in the target panel B), South Asians as a target population show  
140 the largest number of archaic alleles (Figure 5.A). However, East Asians have a larger number of high-frequency uniquely shared  
141 archaic alleles than Europeans and South Asians, for both  $x = 20\%$  and  $x = 50\%$  (Figure 5.B-C). Population-specific D-statistics  
142 (using YRI as the non-admixed population) also follow this trend (Figure S20) and we observe this pattern when looking only at the X

143 chromosome as well (Figure S21). These results hold in comparisons with both archaic human genomes, but we observe a stronger  
144 signal when looking at Neanderthal-specific shared alleles. To correct for the fact that some panels have more segregating sites  
145 than others (and may therefore have more archaic-like segregating sites), we also scaled the number of uniquely shared sites by the  
146 total number of segregating sites per population panel (Figure 5.D-F), and we see in general the same patterns, with the exception of  
147 a Peruvian panel, which we discuss further below. We also observe similar patterns when calculating  $Q95_{A,B,Nea,Den}(1\%, y, z)$   
148 genome-wide (Figure S22). The elevation in  $U_{A,B,Nea,Den}$  and  $Q95_{A,B,Nea,Den}$  in East Asians may possibly result from higher  
149 levels of archaic ancestry in East Asians than in Europeans [25], which some studies argue could be due to additional admixture  
150 events occurring in East Asians [26, 27].

151 Surprisingly, the Peruvians (PEL) harbor the largest amount of high frequency mutations of archaic origin than any other single  
152 population, especially when using Neanderthals as bait (Figures 5.B-C,S21). It is unclear whether this signal is due to increased  
153 drift or selection in this population. Skoglund et al. [28] argue via simulations that if one analyzes a population with high amounts of  
154 recent genetic drift and excludes SNPs where the minor allele is at low frequency, some statistics that are meant to detect archaic  
155 ancestry - like D - may be artificially inflated. Our filtering procedure to select uniquely shared archaic alleles necessarily excludes  
156 sites where the archaic allele is at low frequency in the target panel, and the PEL panel comes from a population with a history of  
157 low effective population sizes (high drift) relative to other Non-Africans [20], which could explain this pattern. This could also explain  
158 why the effect is not seen when  $x = 0\%$  (Figure 5.A), or when computing D-statistics (Figure S20), both of which include sites with  
159 low-frequency alleles in their computation. Additionally, scaling the uniquely shared sites by the total number of segregating sites  
160 per population panel mitigates (but does not completely erase) this pattern. After scaling, PEL shows levels of archaic allele sharing  
161 within the range of the East Asian populations at  $x = 20\%$  (Figure 5.E), but is still the panel with the largest number of archaic sites  
162 at  $x = 50\%$  (Figure 5.F).

163 Furthermore, we plotted the values of  $U_{AFR,X,Nea,Den}(1\%, x, y, z)$  and  $Q95_{AFR,X,Nea,Den}(1\%, y, z)$  jointly for each pop-  
164 ulation X, under different frequency cutoffs  $x$ . When  $x = 0\%$ , there is a generally inversely proportional relationship between the  
165 two scores (Figure S23), but this becomes a directly proportional relationship when  $x = 20\%$  (Figure 6) or  $x = 50\%$  (Figure S27).  
166 Here, we also clearly observe that PEL is an extreme panel with respect to both the number and frequency of archaic shared derived  
167 alleles, and that East Asian and American populations have more high-frequency archaic shared alleles than Europeans.

168 We checked via simulations if the observed excess of high frequency archaic derived mutations in Americans and especially  
169 Peruvians could be caused by genetic drift, as a consequence of the bottleneck that occurred in the ancestors of Native Americans  
170 as they crossed Beringia. We observe that if the introgressed population B undergoes a bottleneck, this can lead to a larger number  
171 of  $U_{A,B,C}(w, x, y, z)$  for large values of  $x$  (Figures S12,S13,S24). Indeed, population structure analyses of the 1000 Genomes  
172 samples suggest that Peruvians have the largest amount of Native American ancestry [20] and show a bottleneck with a lack of  
173 recent population growth, which could explain this pattern. We also observe an increase in the variance of the distribution of  $U$  and  
174  $Q95$  in the presence of a bottleneck, especially when long and severe (Figures S25, S26).

## 175 2.5. Candidate regions for adaptive introgression

176 To identify adaptively introgressed regions of the genome, we computed  $U_{A,B,C,D}(w, x, y, z)$  and  $Q95_{A,B,C,D}(w, y, z)$  in  
177 40 kb non-overlapping windows along the genome, using the low-coverage sequencing data from phase 3 of the 1000 Genomes  
178 Project [20]. We used this window size because the mean length of introgressed haplotypes in ref. [2] was 44,078 bp (Supplementary  
179 Information 13). Our motivation was to find regions under AI in a particular panel B, using panel A as a non-introgressed outgroup  
180 (generally Africans, unless otherwise stated). We used the high-coverage Altai Neanderthal genome [2] as bait panel C and the  
181 high-coverage Denisova genome [4] as bait panel D. We deployed these statistics in three ways: a) to look for Neanderthal-specific  
182 AI, we set  $y = 100\%$  and  $z = 0\%$ ; b) to look for Denisova-specific AI, we set  $y = 0\%$  and  $z = 100\%$ ; c) to look for AI matching  
183 both of the archaic genomes, we set  $y = 100\%$  and  $z = 100\%$  (Figure S1, Table S3). To try to determine the adaptive pressure  
184 behind the putative AI event, we obtained all the CCDS-verified genes located inside each window [29].

185 For guidance as to how high a value of  $U$  and  $Q_{95}$  we would expect under neutrality, we used the simulations from Figure  
186 2 to obtain 95% empirical quantiles of the distribution of these scores under neutrality. Tables S1 and S2 show the 95% quan-  
187 tiles for these two statistics under various models of adaptive introgression and ancestral structure, for different choices of pa-  
188 rameter values (see Methods Section). When examining our candidates for AI below, we focused on windows whose values for  
189  $U_{A,B,Nea,Den}(w, x, y, z)$  and  $Q_{95_{A,B,Nea,Den}}(w, y, z)$  were both in the 99.9% quantile of their respective genome-wide distri-  
190 butions. We verified via simulations that, under a simple model of neutral admixture at a genome-wide rate of 2%, the estimated  
191 probability of obtaining values as high as these (or the false positive rate, FPR) was between 10.6% and 0%, depending on the  
192 target population chosen. The highest rates correspond to the African-American (ASW) admixed panel, as this panel contains high  
193 proportions of ancestry from the outgroup panel (unadmixed Africans) and are therefore not well-suited for our statistics. Excluding  
194 ASW, the highest estimated FPR was 5.5%.

195 We also calculated  $D$  and  $f_D$  along the same windows (using Africans as the non-admixed population), and saw good agreement  
196 with the new statistics presented here (Table S3). Finally, we further validated the regions most likely to have been adaptively  
197 introgressed by searching for archaic tracts of introgression within them that were at high frequency, using a Hidden Markov Model  
198 (see below).

### 199 2.5.1. Continental populations

200 When focusing on adaptive introgression in continental populations, we first looked for uniquely shared archaic alleles specific to  
201 Europeans that were absent or almost absent ( $< 1\%$  frequency) in Africans and East Asians. Conversely, we also looked for uniquely  
202 shared archaic alleles in East Asians, which were absent or almost absent in Africans and Europeans. In this continental survey, we  
203 ignored Latin American populations as they have high amounts of European and African ancestry, which could confound our analyses.  
204 Figure 7 shows the number of sites with uniquely shared alleles for increasing frequency cutoffs in the introgressed population, and  
205 for different types of archaic alleles (Neanderthal-specific, Denisova-specific or common to both archaic humans). In other words, we  
206 calculated  $U_{AFR, EUR, Nea, Den}(1\%, x, y, z)$  and  $U_{AFR, EAS, Nea, Den}(1\%, x, y, z)$  for different values of  $x$  (0%, 20%, 50% and  
207 80%) and different choices of  $y$  and  $z$ , depending on which type of archaic alleles we were looking for. We observe that the regions  
208 in the extreme of the distributions for  $x = 50\%$  corresponded very well to genes that had been previously found to be candidates for  
209 adaptive introgression from archaic humans in these populations, using more complex probabilistic methods [6, 5] or gene-centric  
210 approaches [30]. These include *BNC2* (involved in skin pigmentation [31, 32]), *POU2F3* (involved in skin keratinocyte differentiation  
211 [33, 34]), *HYAL2* (involved in the response to UV radiation on human keratinocytes [35]), *SIPA1L2* (involved in neuronal signaling  
212 [36]) and *CHMP1A* (a regulator of cerebellar development [37]). To be more rigorous in our search for adaptive introgression, we  
213 looked at the joint distribution of the  $U$  statistic and the  $Q_{95}$  statistic for the same choices of  $w$ ,  $y$  and  $z$ , and then selected the regions  
214 that were in the 99.9% quantiles of the distributions of both statistics (Figures 8, S28, S29). We find that the strongest candidates  
215 here are *BNC2*, *POU2F3*, *SIPA1L2* and the *HYAL2* region.

216 We also scanned for regions of the genome where South Asians (SAS) had uniquely shared archaic alleles at high frequency,  
217 which were absent or almost absent in Europeans, East Asians and Africans. In this case, we focused on  $x = 20\%$  because we  
218 found that  $x = 50\%$  left us with no candidate regions. Among the candidate regions sharing a large number of high-frequency  
219 Neanderthal alleles in South Asians, we find genes *ASTN2*, *SFMBT1*, *MUSTN1* and *MAML2* (Figure S30). *ASTN2* is involved in  
220 neuronal migration [38] and is associated with schizophrenia [39, 40]. *SFMBT1* is involved in myogenesis [41] and is associated  
221 with hydrocephalus [42]. *MUSTN1* plays a role in the regeneration of the musculoskeletal system [43]. Finally, *MAML2* codes for a  
222 signaling protein [44, 45], and is associated with cutaneous carcinoma [46] and lacrimal gland cancer [47].

### 223 2.5.2. Eurasia

224 We then looked for AI in all Eurasians (EUA=EUR+SAS+EAS, ignoring American populations) using Africans as the non-admixed  
225 population (AFR, ignoring admixed African-Americans). Figure 8 shows the extreme outlier regions that are in the 99.9% quantiles for

226 both  $U_{EUA,AFR,Nea,Den}(1\%, 20\%, y, z)$  and  $Q95_{EUA,AFR,Nea,Den}(1\%, y, z)$ , while Figure S31 shows the entire distribution.  
227 We focused on  $x = 20\%$  because we found that  $x = 50\%$  left us with almost no candidate regions. In this case, the region with by  
228 far the largest number of uniquely shared archaic alleles is the one containing genes *OAS1* and *OAS3*, involved in innate immunity  
229 [48, 49, 50, 51]. This region was previously identified as a candidate for AI from Neanderthals in non-Africans [52]. Another region  
230 that we recover and was previously identified as a candidate for AI is the one containing genes *TLR1* and *TLR6* [53, 54]. These  
231 genes are also involved in innate immunity and have been shown to be under positive selection in some non-African populations  
232 [55, 56].

233 Interestingly, we find that a very strong candidate region in Eurasia contains genes *TBX15* and *WARS2*. This region has been  
234 associated with a variety of traits, including adipose tissue differentiation [57], body fat distribution [58, 59, 60, 61], hair pigmentation  
235 [62], facial morphology [63, 64], ear morphology [65], stature [64] and skeletal development [66, 64]. It was previously identified  
236 as being under positive selection in Greenlanders [67], and it shows particularly striking signatures of adaptive introgression, so we  
237 devote a separate study to its analysis [68].

### 238 2.5.3. Population-specific signals of adaptive introgression

239 To identify population-specific signals of AI, we looked for archaic alleles at high frequency in a particular non-African panel X,  
240 which were also at less than 1% frequency in all other non-African and African panels, excluding X (Table S3). This is a very restrictive  
241 requirement, and indeed, we only find a few windows in a single panel (PEL) with archaic alleles at more than 20% frequency. One  
242 of the regions with the largest number of uniquely shared Neanderthal sites in PEL contains gene *CHD2*, which codes for a DNA  
243 helicase [69] involved in myogenesis (UniProtKB by similarity), and that is associated with epilepsy [70, 71]. We note, however,  
244 that the presence of these extreme regions could be due to the global elevation in the U statistic caused by higher levels of drift in  
245 Peruvians, as explained above.

### 246 2.5.4. Shared signals among populations

247 In the previous section, we focused on regions where archaic alleles were uniquely at high frequencies in particular populations,  
248 but at low frequencies in all other populations. This precludes us from detecting AI regions that are shared across more than one  
249 non-African population. To address this, we conditioned on observing the archaic allele at less than 1% frequency in a non-admixed  
250 outgroup panel composed of all the African panels (YRI, LWK, GWD, MSL, ESN), excluding African-Americans, and then looked  
251 for archaic alleles at high frequency in particular non-African populations. Unlike the previous section, we did not condition on the  
252 archaic allele being at low frequency in other non-African populations as well. The whole joint distributions of  $U$  and  $Q95$  for this  
253 choice of parameters for each non-African panel are shown in figs. S32 to S50, while regions in the 99.9% quantile for both statistics  
254 are shown in Figure 8.

255 Here, we recapitulate many of the findings from our Eurasian and continental-specific analyses above, like *TLR1/TLR6*, *BNC2*,  
256 *OAS1/OAS3*, *POU2F3*, *LIPA* and *TBX15/WARS2* (Figure 8). For example, just as we found that *POU2F3* was an extreme region  
257 in the East Asian (EAS) continental panel, we separately find that almost all populations composing that panel (CHB, KHV, CHS,  
258 CDX, JPT) have archaic alleles in that region at disproportionately high frequency, relative to their frequency in Africans. Additionally  
259 though, we can learn things we would not have detected at the continental level. For example, the Bengali from Bangladesh (BEB)  
260 - a South Asian population - also have archaic alleles at very high frequencies in this region.

261 We detected several genes that appear to show signatures of AI across various populations (Figure 8). One of the most extreme  
262 examples is a 120 kb region containing the *LARS* gene, with 76 uniquely shared Neanderthal alleles at  $< 1\%$  frequency in Africans  
263 and  $> 50\%$  frequency in Peruvians, which are also at  $> 20\%$  frequency in Mexicans. *LARS* codes for a leucine-tRNA synthetase  
264 [72], and is associated with liver failure syndrome [73]. Additionally, a region containing gene *ZFH3* displays an elevated number  
265 of uniquely shared Neanderthal sites in PEL, and we also observe this when looking more broadly at East Asians (EAS) and - based  
266 on the patterns of inferred introgressed tracts (see below) - in various American (AMR) populations as well. *ZFH3* is involved in the  
267 inhibition of estrogen receptor-mediated transcription [74] and has been associated with prostate cancer [75].

268 We also find several Neanderthal-specific uniquely shared sites in American panels (PEL, CLM, MXL) in a region previously  
269 identified as harboring a risk haplotype for type 2 diabetes (chr17:6880001-6960000) [76]. This is consistent with previous findings  
270 suggesting the risk haplotype was introgressed from Neanderthals and is specifically present at high frequencies in Latin Americans  
271 [76]. The region contains gene *SLC16A11*, whose expression is known to alter lipid metabolism [76]. We also find that the genes  
272 *FAP/IFIH1* have signals consistent with AI, particularly in PEL. This region has been previously associated with type 1 diabetes  
273 [77, 78]. A previous analysis of this region has suggested that the divergent haplotypes in it resulted from ancestral structure or  
274 balancing selection in Africa, followed by local episodes of positive selection in Europe, Asia and the Americas [79]. A more recent  
275 analysis has found this as a region of archaic AI in Melanesians as well [7].

276 Another interesting candidate region contains two genes involved in lipid metabolism: *LIPA* and *CH25H*. We find a 40 kb region  
277 with 11 uniquely shared Denisovan alleles that are at low ( $< 1\%$ ) frequency in Africans and at very high ( $> 50\%$ ) frequency in  
278 various South and East Asian populations (JPT, KHV, CHB, CHS, CDX and BEB). The Q95 and D statistics in this region are also  
279 high across all of these populations, and we also find this region to have extreme values of these statistics in our broader Eurasian  
280 scan. The *LIPA* gene codes for a lipase [80] and is associated with cholesterol ester storage disease [81] and Wolman disease  
281 [82]. In turn, the *CH25H* gene codes for a membrane hydroxylase involved in the metabolism of cholesterol [83] and associated with  
282 Alzheimer's disease [84] and antiviral activity [85].

283 Finally, we find a region harboring between 3 and 10 uniquely shared Neanderthal alleles (depending on the panel used) in  
284 various non-African populations. This region was identified earlier by ref. [5] and contains genes *PPDPF*, *PTK6* and *HELZ2*. *PPDPF*  
285 codes for a probable regulator of pancreas development (UniProtKB by similarity). *PTK6* codes for an epithelial signal transducer  
286 [86] and *HELZ2* codes for a helicase that works as a transcriptional coactivator for nuclear receptors [87, 88].

## 287 2.6. The X chromosome

288 Previous studies have observed lower levels of archaic introgression in the X chromosome relative to the autosomes [5, 6]. Here,  
289 we observe a similar trend: compared to the autosomes, the X chromosome contains a smaller number of windows with sites that  
290 are uniquely shared with archaic humans (Figure 7). For example, for  $w = 1\%$  and  $x = 20\%$ , we observe that, in Europeans, 0.4%  
291 of all windows in the autosomes have at least one uniquely shared site with Neanderthals or Denisovans, while only 0.05% of all  
292 windows in the X chromosome have at least one uniquely shared site ( $P = 4.985 \times 10^{-4}$ , chi-squared test assuming independence  
293 between windows). The same pattern is observed in East Asians ( $P = 1.852 \times 10^{-8}$ ).

294 Nevertheless, we do identify some regions in the X chromosome exhibiting high values for both  $U_{A,B,C,D}(w, x, y, z)$  and  
295  $Q_{95A,B,C,D}(w, y, z)$ . For example, a region containing gene *DHRX* contains a uniquely shared site where a Neanderthal allele  
296 is at  $< 1\%$  frequency in Africans, but at  $> 50\%$  frequency in a British panel (GBR). The site is also at high frequency (29% – 47%) in  
297 the other European panels, but never as high as in GBR (55%). It is also surrounded by 5 neighboring SNPs that have intermediate  
298 Neanderthal allele frequencies (24% – 41%) in GBR. Another region contains gene *DMD* and harbors two uniquely shared sites where  
299 two archaic (Denisovan/Neanderthal) alleles are also at low ( $< 1\%$ ) frequency in Africans but at  $> 50\%$  frequency in Peruvians.  
300 *DHRX* codes for an oxidoreductase enzyme [89], while *DMD* is a well-known gene because mutations in it cause muscular dystrophy  
301 [90], and was also previously identified as having signatures of archaic introgression in non-Africans [91]. We note, however, that  
302 our simulations do not account for the particular inheritance and recombination patterns of the X chromosome, so caution should be  
303 taken when calling these regions as under AI.

## 304 2.7. Introgressed haplotypes in candidate loci

305 We inspected the haplotype patterns of candidate loci with support in favor of AI. We displayed the haplotypes for selected  
306 populations at seven regions: *POU2F3* (Figure 9.A), *BNC2* (Figure 9.B), *LARS* (Figure 9.C), *FAP/IFIH1* (Figure 9.D), *OAS1* (Figure  
307 9.E), *LIPA* (Figure 9.F) and *SLC16A11* (Figure S51.C). We included continental populations that show a large number of uniquely  
308 shared archaic alleles, and included YRI as a representative African population. We then clustered and ordered the haplotypes by



309 similarity to the closest archaic genome (Altai Neanderthal or Denisova) (Figure 9). As can be observed, all these regions tend to  
310 show sharp distinctions between the putatively introgressed haplotypes and the non-introgressed ones. This is also evident when  
311 looking at the cumulative number of differences of each haplotype to the closest archaic haplotype, where we see a sharp rise in the  
312 number of differences, indicating strong differentiation between the two sets of haplotypes. Additionally, the YRI haplotypes tend to  
313 predominantly belong to the non-introgressed group, as expected.

### 314 2.7.1. Consequences of relaxing the outgroup frequency cutoff

315 When using a more lenient cutoff for the outgroup panel (10% maximum frequency, rather than 1%), we find a few genes that  
316 display values of the  $U$  statistic that are suggestive of AI, and that have been previously found to be under strong positive selection  
317 in particular human populations [92, 93]. The most striking examples are *TYRP1* in EUR (using EAS+AFR as outgroup) and *OCA2*  
318 in EAS (using EUR+AFR as outgroup)(Table S3). Both of these genes are involved in pigmentation. We caution, however, that the  
319 reason why they carry archaic alleles at high frequency may simply be because their respective selective sweeps pushed an allele  
320 that was segregating in both archaic and modern humans to high frequency in modern humans, but not necessarily via introgression.

321 In fact, *TYRP1* only stands out as an extreme region for the number of archaic shared alleles in EUR when using the lenient 10%  
322 cutoff, but not when using the more stringent 1% cutoff. When looking at these SNPs in more detail, we find that their allele frequency  
323 in Africans ( $\sim 20\%$ ) is even higher than in East Asians ( $\sim 1\%$ ), largely reflecting population differentiation across Eurasia due to  
324 positive selection [93], rather than adaptive introgression. When exploring the haplotype structure of this gene (Figure S51.B), we  
325 find one haplotype that shows similarities to archaic humans but is at low frequency. In the combined YRI+EUR panel, just 6.37% of  
326 all haplotypes have 36 or less differences to the Neanderthal genome, and this number is roughly the point of transition between the  
327 archaic-like and the non-archaic-like haplotypes (Figures S51.B). There is a second - more frequent - haplotype that is more distinct  
328 from archaic humans but present at high frequency in Europeans. The uniquely shared sites obtained using the lenient ( $< 10\%$ )  
329 allele frequency outgroup cutoff are tagging both haplotypes together, rather than just the highly differentiated archaic-like haplotype.

330 *OCA2* has several sites with uniquely shared alleles in EAS (AFR+EUR as outgroup) when using the lenient 10% cutoff, but  
331 only a few (2) shared archaic sites when using the  $< 1\%$  outgroup frequency cutoff. When exploring the haplotype structure of this  
332 gene, we fail to find a clear-cut differentiation between putatively introgressed and non-introgressed haplotypes, so the evidence for  
333 adaptive introgression in this region is also weak. A close inspection of its haplotype structure shows that *OCA2* does not show a  
334 large number of differences between the haplotype classes that are closer and those that are distant from the archaic humans (Figure  
335 S51.A).

336 Finally, using the lenient outgroup cutoff of  $< 10\%$  and a target cutoff of  $> 20\%$ , we find the gene with the highest number  
337 of uniquely shared sites among all the populations and cutoffs we tested: *MUC19*. This region is rather impressive in containing  
338 115 sites where the archaic alleles are shared between the Mexican panel (MXL) and the Denisovan genome at more than 20%  
339 frequency, when using all populations that are not MXL as the outgroup. However, the actual proportion of individuals that contain  
340 a Denisova-like haplotype (though highly differentiated from the rest of present-day human haplotypes) is very small. Only 11.86%  
341 of haplotypes in the combined YRI+AMR panel show 69 differences or less to the closest archaic genome (Denisova), and the next  
342 closest haplotype has 134 differences (Figure S51.D).

343 Overall, a finer investigation of these three cases suggests that using a lenient outgroup frequency cutoff may lead to misleading  
344 inferences. Nevertheless, the haplotype structure of these genes and their relationship to their archaic human counterparts are quite  
345 unusual. It remains to be determined whether these patterns could be caused by either positive selection or introgression alone, or  
346 whether a combination of these or other demographic forces is required to explain them.

### 347 2.8. Inferred introgressed tracts

348 We used an HMM [21] to verify that the strongest candidate regions effectively contained archaic segments of a length that would  
349 be consistent with introgression after the population divergence between archaic and modern humans. For each region, we used

350 the closest archaic genome (Altai Neanderthal or Denisova) as the putative source of introgression. We then plotted the inferred  
351 segments in non-African continental populations for genes with strong evidence for AI. Among these, genes with Neanderthal as the  
352 closest source (figs. S52 to S59) include: *POU2F3* (EAS,SAS), *BNC2* (EUR), *OAS1* (Eurasians), *LARS* (AMR), *FAP/IFIH1* (PEL),  
353 *CHD2* (PEL), *TLR1-6* (EAS) and *ZFX3* (PEL). Genes with Denisova as the closest source (figs. S60 and S61) include: *LIPA* (EAS,  
354 SAS, AMR) and *MUSTN1* (SAS).

### 355 2.9. Testing for enrichment in genic regions

356 We aimed to test whether uniquely shared archaic alleles at high frequencies were enriched in genic regions of the genome. We  
357 looked at archaic alleles at high frequency in any of the Non-African panels that were also at low frequency ( $< 1\%$ ) in Africans. As  
358 background, we used all archaic alleles that were at any frequency larger than 0 in the same Non-African populations, and that were  
359 also at low frequency in Africans. We then tested whether the high-frequency archaic alleles tended to occur in genic regions more  
360 often than expected.

361 SNPs in introgressed blocks will tend to cluster together and have similar allele frequencies, which could cause a spurious en-  
362 richment signal. To correct for the fact that SNPs at similar allele frequencies will cluster together (as they will tend to co-occur in the  
363 same haplotypes), we performed linkage disequilibrium (LD) pruning using two methods. In one (called “LD-1”), we downloaded the  
364 approximately independent European LD blocks published in ref. [94]. For each set of high frequency derived sites, we randomly  
365 sampled one SNP from each block. In a different approach (called “LD-2”), for each set of high frequency derived sites, we sub-  
366 sampled SNPs such that each SNP was at least 200 kb apart from each other. We then tested these two types of LD-pruned SNP  
367 sets against 1000 SNP sets of equal length that were also LD-pruned and that were obtained randomizing frequencies and collecting  
368 SNPs in the same ways as described above.

369 Regardless of which LD method we used, we find no significant enrichment in genic regions for high-frequency ( $> 50\%$ ) Nean-  
370 derthal alleles (LD-1  $P=352$ , LD-2  $P=0.161$ ) or Denisovan alleles (LD-1  $P=0.348$ , LD-2  $P=0.192$ ). Similarly, we find no enrichment for  
371 medium-to-high-frequency ( $> 20\%$ ) Neanderthal alleles (LD-1  $P=0.553$ , LD-2  $P=0.874$ ) or Denisovan alleles (LD-1  $P=0.838$ , LD-2  
372  $P=0.44$ ).

## 373 3. Discussion

374 Here, we carried out one of the first investigations into the joint dynamics of archaic introgression and positive selection, to  
375 develop statistics that are informative of AI. We find that one of the most powerful ways to detect AI is to look at both the number and  
376 allele frequency of mutations that are uniquely shared between the introgressed and the archaic populations. Such mutations should  
377 be abundant and at high-frequencies in the introgressed population if AI occurred. In particular, we identified two novel summaries  
378 of the data that capture this pattern quite well: the statistics  $Q_{95}$  and  $U$ . These statistics can recover loci under AI and are easy to  
379 compute from genomic data, as they do not require phasing.

380 We have also studied the general landscape of archaic alleles and their frequencies in present-day human populations. While  
381 scanning the present-day human genomes from phase 3 of the 1000 Genomes Project [20] using these and other summary statistics,  
382 we were able to recapitulate previous AI findings (like the *TLR* [53, 54] and *OAS* regions [52]) as well as identify new candidate regions  
383 for AI in Eurasia (like the *LIPA* gene and the *FAP/IFIH1* region). These mostly include genes involved in lipid metabolism, pigmentation  
384 and innate immunity, as observed in previous studies [5, 6, 95]. Phenotypic changes in these systems may have allowed archaic  
385 humans to survive in Eurasia during the Pleistocene, and may have been passed on to present-day human populations during their  
386 expansion out of Africa.

387 When using more lenient definitions of what we consider to be “uniquely shared archaic alleles” we find sites containing these  
388 alleles in genes that have been previously found to be under positive selection (like *OCA2* and *TYRP1*) but not necessarily under  
389 adaptive introgression. While these do not show as strong signatures of adaptive introgression as genes like *BNC2* and *POU2F3*,  
390 their curious haplotype patterns and their relationship to archaic genomes warrants further exploration.

391 We tested whether uniquely shared archaic alleles at high frequencies in non-Africans were significantly more likely to be found in  
392 genic regions, relative to all shared archaic alleles, but did not find a significant enrichment. Though this suggests archaic haplotypes  
393 subject to AI may not be preferentially found near or inside genes, it may also be a product of a lack of power, or of the fact that  
394 not all uniquely shared archaic alleles may be truly introgressed. As mentioned before, some of these alleles may be present due  
395 to incomplete lineage sorting, which could add noise to the test signal. A more rigorous - and possibly more powerful - test could  
396 involve testing whether HMM-inferred introgressed archaic segments at high frequency tend to be found in genic regions, relative to  
397 all inferred introgressed archaic segments, while controlling for features like the length of introgressed segments and the sensitivity  
398 of the HMM to different regions of the genome. However, in this study, we did not pursue this line of research further.

399 In this study, we have mostly focused on positive selection for archaic alleles. One should remember, though, that a larger  
400 proportion of introgressed genetic material was likely maladaptive to modern humans, and therefore selected against. Indeed, two  
401 recent studies have shown that negative selection on archaic haplotypes may have reduced the initial proportion of archaic material  
402 present in modern humans immediately after the hybridization event(s) [96, 97].

403 Another caveat is that some regions of the genome display patterns that could be consistent with multiple introgression events,  
404 followed by positive selection on one or more distinct archaic haplotypes [53]. In this study, we have simply focused on models  
405 with a single pulse of admixture - followed immediately by selection or with an intermediate neutrality period in the introgressed  
406 population. We have not considered complex scenarios with multiple sources of introgression. Additionally, the currently limited  
407 availability of high-coverage archaic human genomes may prevent us from detecting AI events for which the source may not have  
408 been closely related to the sequenced Denisovan or Altai Neanderthal genomes. This may include other Neanderthal or Denisovan  
409 subpopulations, or other (as yet unsampled) archaic groups that may have lived in Africa and Eurasia.

410 It is also worth noting that positive selection for archaic haplotypes may be due to heterosis, rather than adaptation to particu-  
411 lar environments [96]. That is, archaic alleles may not have been intrinsically beneficial, but simply protective against deleterious  
412 recessive modern human alleles, and therefore selected after their introduction into the modern human gene pool. The degree of  
413 dominance of deleterious alleles in humans remains elusive, so it is unclear how applicable this model would be to archaic admixture  
414 in humans.

415 Many of the statistics we introduced in this study have their drawbacks: notably, they depend on simulations to assess significance  
416 and some - like U - may be sensitive to local variation in mutation rates across the genome. Nevertheless they serve as useful  
417 exploratory tools, as they highlight a characteristic signature left by AI in present-day human genomes. Future avenues of research  
418 could involve developing ways to incorporate uniquely shared sites into a robust test of selection that specifically targets regions  
419 under AI. For example, one could think about modifying statistics based on local between-population population differentiation, like  
420 PBS [10], so that they are only sensitive to allele frequency differences at sites that show signatures of archaic introgression.

421 Finally, while this study has largely focused on human AI, several other species also show suggestive signatures of AI [98].  
422 Assessing the extent and prevalence of AI and uniquely shared sites in other biological systems could provide new insights into their  
423 biology and evolutionary history. This may also serve to better understand how populations of organisms respond to introgression  
424 events, and to derive general principles about the interplay between admixture and natural selection.

## 425 **4. Methods**

### 426 *4.1. Summary statistics sensitive to adaptive introgression*

427 Several statistics have been previously deployed to detect AI events (reviewed in Racimo et al. [99]). We briefly describe these  
428 below, as well as three new statistics tailored specifically to find this signal (Table 1). One of the simplest approaches consists of  
429 applying the  $D$  statistic [1, 100] locally over windows of the genome. The  $D$  statistic was originally applied to compare a single human  
430 genome against another human genome, so as to detect excess shared ancestry between one of the genomes and a genome from  
431 an outgroup population. Application of this statistic comparing non-Africans and Africans served as one of the pieces of evidence

432 in support of Neanderthal admixture into non-Africans. However, it can also be computed from large panels of multiple individuals  
433 instead of single genomes. This form of the  $D$  statistic has been applied locally over windows of the genome to detect regions of  
434 excess shared ancestry between an admixed population and a source population [101, 102].

435 The  $D$  statistic, however, can be confounded by local patterns of diversity, as regions of low diversity may artificially inflate the  
436 statistic even when a region was not adaptively introgressed. To correct for this, Martin et al. [103] developed a similar statistic  
437 called  $f_D$  which is less sensitive to differences in diversity along the genome. Both of these patterns exploit the excess relatedness  
438 between the admixed and the source population.

439 AI is also expected to increase linkage disequilibrium (LD), as an introgressed fragment that rises in frequency in the population  
440 will have several closely linked loci that together will be segregating at different frequencies than they were in the recipient population  
441 before admixture. Thus, two well-known statistics that are informative about the amount of LD in a region -  $D'$  and  $r^2$  - could also  
442 be informative about adaptive introgression. To apply them over regions of the genome, we can take the average of each of the two  
443 statistics over all SNP pairs in a window. In the section below, we calculate these statistics in two ways: a) using the introgressed  
444 panel only ( $D'$ [*intro*] and  $r^2$ [*intro*]), and b) using the combination of the introgressed and the non-introgressed panels ( $D'$ [*comb*]  
445 and  $r^2$ [*comb*]). The first way (*intro*) should capture patterns of within-population LD in the introgressed population under AI, while  
446 the second way (*comb*) should capture patterns of global LD across both populations. If the introgressed population has a particular  
447 set of archaic haplotypes at high frequency that are highly differentiated from the non-archaic haplotypes in the non-introgressed  
448 panel, we expect the second way to be more powerful at distinguishing AI from neutrality.

449 We also introduce three new statistics that one would expect, *a priori*, to be particularly effective at identifying windows of the  
450 genome that are likely to have undergone adaptive introgression:  $R_D$ ,  $U$  and  $Q_{95}$ .  $R_D$  is computed by calculating - in a window of  
451 the genome - the ratio of the sequence divergence between an individual from the source population and an admixed individual, and  
452 the sequence divergence between an individual from the source population and a non-admixed individual. One can then take the  
453 average of this ratio over all individuals in the admixed and non-admixed panels. This average should be larger if the introgressed  
454 haplotype is present in a large number of individuals of the admixed population. We call this statistic  $R_D$ .

455 Second, for a window of arbitrary size, let  $U_{A,B,C}(w, x, y)$  be defined as the number of sites where a sample C (the “bait”) from  
456 an archaic source population (which could be as small as a single diploid individual) has a particular allele at frequency  $y$ , and that allele  
457 is at a frequency smaller than  $w$  in a sample A (the “outgroup”) of a population but larger than  $x$  in a sample B (the “target”) of another  
458 population (Figure 1). In other words, we are looking for sites that contain alleles shared between an archaic human genome and a  
459 test population, but absent or at very low frequencies in an outgroup (usually non-admixed) population. For example, suppose we  
460 are looking for Neanderthal adaptive introgression in the Han Chinese (CHB). In that case, we can consider CHB as our target panel,  
461 and use Africans as the outgroup panel and a single Neanderthal genome as the bait. If  $U_{AFR,CHB,Nea}(1\%, 20\%, 100\%) = 4$  in  
462 a window of the genome, that means there are 4 sites in that window where the Neanderthal genome is homozygous for a particular  
463 allele and that allele is present at a frequency smaller than 1% in Africans but larger than 20% in Han Chinese. In other words, there  
464 are 4 sites that are uniquely shared at more than 20% frequency between Han Chinese and Neanderthal, but not with Africans.

465 This statistic can be further parametrized if we have samples from two different archaic populations (for example, a Neanderthal  
466 genome and a Denisova genome). In that case, we can define  $U_{A,B,C,D}(w, x, y, z)$  as the number of sites where the archaic  
467 sample C has a particular allele at frequency  $y$  and the archaic sample D has that allele at frequency  $z$ , while the same allele is at a  
468 frequency smaller than  $w$  in an outgroup panel A and larger than  $x$  in a target panel B (Figure S1). For example, if we were interested  
469 in looking for Neanderthal-specific AI, we could set  $y = 100\%$  and  $z = 0\%$ , to find alleles uniquely shared with Neanderthal, but  
470 not Denisova. If we were interested in archaic alleles shared with both Neanderthal and Denisova, we could set  $y = 100\%$  and  
471  $z = 100\%$ .

472 Another statistic that we found to be useful for finding AI events is  $Q_{95_{A,B,C}}(w, y)$ , and is here defined as the 95<sup>th</sup> per-  
473 centile of derived frequencies in an admixed sample B of all SNPs that have a derived allele frequency  $y$  in the archaic sample C,  
474 but where the derived allele is at a frequency smaller than  $w$  in a sample A of a non-admixed population (Figure 1). For example,

475  $Q95_{AFR,CHB,Nea}(1\%, 100\%) = 0.65$  means that if one computes the 95% quantile of all the Han Chinese derived allele fre-  
476 quencies of SNPs where the Neanderthal genome is homozygous derived and the derived allele has frequency smaller than 1% in  
477 Africans, that quantile will be equal to 0.65. The motivation for this statistic is that AI will produce archaic SNPs at high frequen-  
478 cies in the introgressed population. The 95<sup>th</sup> percentile should be an effective way of summarizing the frequencies of these SNPs  
479 while downweighting other SNPs that may also share the same allelic state as the archaic genomes, but that are segregating at low  
480 frequencies in the target panel and are therefore not informative about AI. In other words, it is a summary of the allele frequency  
481 spectrum in the introgressed population, conditional on only looking at alleles uniquely shared with the source population and at low  
482 frequency in the non-admixed population. As before, we can generalize this statistic if we have a sample D from a second archaic  
483 population. Then,  $Q95_{A,B,C,D}(w, y, z)$  is the 95<sup>th</sup> percentile of derived frequencies in the sample B of all SNPs that have a derived  
484 allele frequency  $y$  in the archaic sample C and derived allele frequency  $z$  in the archaic sample D, but where the derived allele is at  
485 a frequency smaller than  $w$  in the sample A (Figure S1).

486 A common statistic that is indicative of population variation - expected heterozygosity ( $\pi$ ) was previously found to be affected by  
487 archaic introgression in a serial founder model of human history [104]. We measured  $\pi$  as the average of  $2p*(1-p)$  over all sites in  
488 a window, where  $p$  is the sample derived allele frequency in the introgressed population.

#### 489 4.2. Simulations

490 None of these statistics have been explicitly vetted under scenarios of AI so far, though the performance of  $D$  and  $f_D$  has  
491 been previously evaluated for detecting local introgression [103]. Therefore, we aimed to test how each of the statistics described  
492 above performed in detecting AI in a 40 kb window. We chose this window size because the mean length of introgressed haplotypes  
493 in ref. [2] was 44,078 bp (Supplementary Information 13) and because 40kb is well above the length needed to reject incomplete  
494 lineage sorting for regions with moderate recombination rates [18]. We began by simulating a three population tree in Slim [105]  
495 with constant  $N_e = 10,000$ , mutation rate equal to  $1.5 * 10^{-8}$  per bp per generation, recombination rate equal to  $10^{-8}$  per  
496 bp per generation, and split times emulating the African-Eurasian and Neanderthal-modern human split times (4,000 and 16,000  
497 generations ago, respectively). We allowed for admixture between the most distantly diverged population and one of the closely  
498 related sister populations, at different rates: 2%, 10% and 25% (Figure 2.A). We use the lower (2%) rate to represent the Neanderthal  
499 genome-wide admixture into Eurasians, with Africans as the non-admixed population. The higher (10% and 25%) rates are meant to  
500 represent cases when a researcher is focusing on a particular region of the genome that has some *a priori* evidence for having been  
501 introgressed, thus pushing the local probability of introgression to high values, even though the genome-wide rate may be lower.  
502 Under each of the three admixture rate scenarios, we simulated regions that were evolving neutrally, regions where the central SNP  
503 was under weak positive additive selection ( $s = 0.01$ ) and regions with a central SNP under strong selection ( $s = 0.1$ ). We required  
504 the selected allele to be fixed in the archaic population prior to introgression, but allowed the allele to rise or decrease in frequency  
505 in the introgressed population, as determined by the strength of selection, its probability of entering the introgressed population and  
506 its starting frequency after introgression. Figure S2 shows the distributions of frequencies of the selected alleles in the introgressed  
507 population in the present.

508 We also tested how the statistics perform at detecting adaptive introgression when the alternative model is not a neutral intro-  
509 gression model, but a neutral model with ancestral structure (Figure 2.G). We followed a model described in Huerta-Sanchez et al  
510 (2014) and simulated a population in which an African population splits from archaic humans before Eurasians, but is allowed to  
511 exchange migrants with them. Afterwards, we split Eurasians and archaic humans. At that point, we stop the previous migration and  
512 only allow for migration between the Eurasian and African populations until the present, at double the previous rate. This is meant to  
513 generate loci where Eurasians and archaic humans share a more recent common ancestor with each other than with Africans, but  
514 because of ancient shared ancestry, not recent introgression. We simulated 3 scenarios, in which we set the per-generation ancient  
515 migration rate to be 0.01, 0.001 and 0.0001, respectively, and the recent migration rate to be 0.02, 0.002 and 0.0002, respectively.  
516 We call these the strong-, medium-, and weak-migration scenarios, respectively. The stronger the migration, the weaker the ancestral

517 structure, as archaic-shared segments in Eurasians will tend to be removed by migration with Africans.

#### 518 4.3. Plotting haplotype structure

519 The *Haplostrips* software (Marnetto et al. in prep.) was used to produce plots of haplotypes at candidate regions for AI. This  
520 software displays each SNP within a predefined region as a column, while each row represents a phased haplotype: the result is a  
521 heatmap. Each haplotype is labeled with a color that corresponds to the 1000 Genomes panel of its carrier individual. The haplotypes  
522 were first hierarchically clustered via the single agglomerative method based on Manhattan distances, using the *stats* library in R.  
523 The resulting dendrogram of haplotypes was then re-ordered by decreasing similarity to a reference sequence constructed so that it  
524 contains all the derived alleles found in the archaic genome (Altai Neanderthal or Denisova). The reordering is performed using the  
525 minimum distance method, so that haplotypes with more derived alleles shared with the archaic population are at the top of the plot.  
526 Derived alleles are represented as black spots and ancestral alleles are represented as white spots. Variant positions were filtered  
527 out when the site in the archaic genome had mapping quality less than 30 or genotype quality less than 40, or if the minor allele had  
528 a population frequency smaller than 5% in each of the present-day human populations included in the plot.

#### 529 4.4. Hidden Markov Model

530 As haplotypes could look archaic simply because of ancestral structure or incomplete lineage sorting, we used a Hidden Markov  
531 Model (HMM) described in ref. [21] (which assumes an exponential distribution of admixture tract lengths [106, 107]), in order to  
532 verify that our candidate regions truly had archaic introgressed segments. This procedure also allowed us to confirm which of the  
533 archaic genomes was closest to the original source of introgression, as using a distant archaic source as input (for example, the  
534 Denisova genome when the true source is closest to the Neanderthal genome) produced shorter or less frequent inferred segments  
535 in the HMM output than when using the closer source genome.

536 The HMM we used requires us to specify a prior for the admixture rate. We tried two priors: 2% and 50%. The first was chosen  
537 because it is consistent with the genome-wide admixture rate for Neanderthals into Eurasians. The second, larger, value was chosen  
538 because each candidate region should *a priori* have a larger probability of being admixed, as they were found using statistics that  
539 are indicative of admixture in the first place. We observe almost no differences in the number of haplotypes inferred using either  
540 value. For example, for BNC2 - a well known candidate for AI [5, 6] - the frequency of sequences in EUR with inferred introgressed  
541 haplotypes under the 2% prior is 92.5%, while it is 93.1% under the 50% prior. However, the larger prior leads to longer and less  
542 fragmented introgressed chunks, as the HMM is less likely to transition into a non-introgressed state between two introgressed states.  
543 Therefore, all figures we show below were obtained using a 50% admixture prior. The admixture time was set to 1,900 generations  
544 ago and the recombination rate parameter was set to the local recombination rate in each region, following the recombination rate  
545 map in ref. [108]. A tract was called as introgressed if the posterior probability for introgression was higher than 90%. Under these  
546 parameters, the HMM has a specificity of 99.56%, a sensitivity of 36.07% and a false discovery rate of 1.15%.

## 547 5. Acknowledgments

548 We are grateful to Montgomery Slatkin, Rasmus Nielsen, Fergal P. Casey, Kirk Lohmueller and Amy Ko for helpful advice and  
549 comments. E.H.S. is supported by UC Merced start-up funds and National Science Foundation grant NSF-DEB-1557151. D.M.  
550 is supported by a University of Torino PhD Scholarship. F.R. is supported by National Institutes of Health grant R01HG003229 to  
551 Rasmus Nielsen.

## 552 6. References

553 [1] R. E. Green, J. Krause, A. W. Briggs, T. Maricic, U. Stenzel, M. Kircher, N. Patterson, H. Li, W. Zhai, M. H.-Y. Fritz, et al., A  
554 draft sequence of the Neandertal genome, *science* 328 (2010) 710–722.

- 555 [2] K. Prüfer, F. Racimo, N. Patterson, F. Jay, S. Sankararaman, S. Sawyer, A. Heinze, G. Renaud, P. H. Sudmant, C. de Filippo,  
556 et al., The complete genome sequence of a Neanderthal from the Altai mountains, *Nature* 505 (2014) 43–49.
- 557 [3] D. Reich, R. E. Green, M. Kircher, J. Krause, N. Patterson, E. Y. Durand, B. Viola, A. W. Briggs, U. Stenzel, P. L. Johnson,  
558 et al., Genetic history of an archaic hominin group from Denisova cave in Siberia, *Nature* 468 (2010) 1053–1060.
- 559 [4] M. Meyer, M. Kircher, M.-T. Gansauge, H. Li, F. Racimo, S. Mallick, J. G. Schraiber, F. Jay, K. Prüfer, C. de Filippo, et al., A  
560 high-coverage genome sequence from an archaic Denisovan individual, *Science* 338 (2012) 222–226.
- 561 [5] S. Sankararaman, S. Mallick, M. Dannemann, K. Prüfer, J. Kelso, S. Pääbo, N. Patterson, D. Reich, The genomic landscape  
562 of Neanderthal ancestry in present-day humans, *Nature* 507 (2014) 354–357.
- 563 [6] B. Vernot, J. M. Akey, Resurrecting surviving Neandertal lineages from modern human genomes, *Science* 343 (2014) 1017–  
564 1021.
- 565 [7] B. Vernot, S. Tucci, J. Kelso, J. G. Schraiber, A. B. Wolf, R. M. Gitterman, M. Dannemann, S. Grote, R. C. McCoy, H. Norton,  
566 L. B. Scheinfeldt, D. A. Merriwether, G. Koki, J. S. Friedlaender, J. Wakefield, S. Pääbo, J. M. Akey, Excavating Neandertal  
567 and Denisovan DNA from the genomes of Melanesian individuals, *Science* (2016).
- 568 [8] S. Sankararaman, S. Mallick, N. Patterson, D. Reich, The combined landscape of Denisovan and Neanderthal ancestry in  
569 present-day humans, *Current Biology* (2016).
- 570 [9] C.-J. Hu, L.-Y. Wang, L. A. Chodosh, B. Keith, M. C. Simon, Differential roles of hypoxia-inducible factor 1 $\alpha$  (HIF-1 $\alpha$ ) and  
571 HIF-2 $\alpha$  in hypoxic gene regulation, *Molecular and cellular biology* 23 (2003) 9361–9374.
- 572 [10] X. Yi, Y. Liang, E. Huerta-Sanchez, X. Jin, Z. X. P. Cuo, J. E. Pool, X. Xu, H. Jiang, N. Vinckenbosch, T. S. Korneliussen,  
573 et al., Sequencing of 50 human exomes reveals adaptation to high altitude, *Science* 329 (2010) 75–78.
- 574 [11] A. Bigham, M. Bauchet, D. Pinto, X. Mao, J. M. Akey, R. Mei, S. W. Scherer, C. G. Julian, M. J. Wilson, D. L. Herráez, et al.,  
575 Identifying signatures of natural selection in Tibetan and Andean populations using dense genome scan data, *PLoS Genet* 6  
576 (2010) e1001116.
- 577 [12] C. M. Beall, G. L. Cavalleri, L. Deng, R. C. Elston, Y. Gao, J. Knight, C. Li, J. C. Li, Y. Liang, M. McCormack, et al., Natural  
578 selection on EPAS1 (hif2 $\alpha$ ) associated with low hemoglobin concentration in Tibetan highlanders, *Proceedings of the National  
579 Academy of Sciences* 107 (2010) 11459–11464.
- 580 [13] Y. Peng, Z. Yang, H. Zhang, C. Cui, X. Qi, X. Luo, X. Tao, T. Wu, H. Chen, H. Shi, et al., Genetic variations in Tibetan  
581 populations and high-altitude adaptation at the Himalayas, *Molecular biology and evolution* 28 (2011) 1075–1081.
- 582 [14] S. Xu, S. Li, Y. Yang, J. Tan, H. Lou, W. Jin, L. Yang, X. Pan, J. Wang, Y. Shen, et al., A genome-wide search for signals of  
583 high-altitude adaptation in Tibetans, *Molecular biology and evolution* 28 (2011) 1003–1011.
- 584 [15] B. Wang, Y.-B. Zhang, F. Zhang, H. Lin, X. Wang, N. Wan, Z. Ye, H. Weng, L. Zhang, X. Li, et al., On the origin of Tibetans  
585 and their genetic basis in adapting high-altitude environments, *PLoS One* 6 (2011) e17002.
- 586 [16] C. Jeong, G. Alkorta-Aranburu, B. Basnyat, M. Neupane, D. B. Witonsky, J. K. Pritchard, C. M. Beall, A. Di Rienzo, Admixture  
587 facilitates genetic adaptations to high altitude in Tibet, *Nature communications* 5 (2014).
- 588 [17] S. Hackinger, T. Kraaijenbrink, Y. Xue, M. Mezzavilla, G. van Driem, M. A. Jobling, P. de Knijff, C. Tyler-Smith, Q. Ayub, et al.,  
589 Wide distribution and altitude correlation of an archaic high-altitude-adaptive EPAS1 haplotype in the Himalayas, *Human  
590 genetics* (2016) 1–10.

- 591 [18] E. Huerta-Sánchez, X. Jin, Z. Bianba, B. M. Peter, N. Vinckenbosch, Y. Liang, X. Yi, M. He, M. Somel, P. Ni, et al., Altitude  
592 adaptation in Tibetans caused by introgression of Denisovan-like DNA, *Nature* 512 (2014) 194–197.
- 593 [19] E. Huerta-Sanchez, F. P. Casey, Archaic inheritance: supporting high altitude life in Tibet, *Journal of Applied Physiology* 119  
594 (2015) 1129–1134.
- 595 [20] A. Auton, et al., A global reference for human genetic variation, *Nature* 526 (2015) 68–74.
- 596 [21] A. Seguin-Orlando, T. S. Korneliussen, M. Sikora, A.-S. Malaspinas, A. Manica, I. Moltke, A. Albrechtsen, A. Ko, A. Margaryan,  
597 V. Moiseyev, et al., Genomic structure in Europeans dating back at least 36,200 years, *Science* 346 (2014) 1113–1118.
- 598 [22] N. H. Barton, The effect of hitch-hiking on neutral genealogies, *Genetical Research* 72 (1998) 123–133.
- 599 [23] Y. Kim, W. Stephan, Detecting a local signature of genetic hitchhiking along a recombining chromosome, *Genetics* 160 (2002)  
600 765–777.
- 601 [24] Y. Kim, R. Nielsen, Linkage disequilibrium as a signature of selective sweeps, *Genetics* 167 (2004) 1513–1524.
- 602 [25] J. D. Wall, M. A. Yang, F. Jay, S. K. Kim, E. Y. Durand, L. S. Stevison, C. Gignoux, A. Woerner, M. F. Hammer, M. Slatkin,  
603 Higher levels of Neanderthal ancestry in East Asians than in Europeans, *Genetics* 194 (2013) 199–209.
- 604 [26] B. Vernot, J. M. Akey, Complex history of admixture between modern humans and Neandertals, *The American Journal of*  
605 *Human Genetics* 96 (2015) 448–453.
- 606 [27] B. Y. Kim, K. E. Lohmueller, Selection and reduced population size cannot explain higher amounts of Neanderthal ancestry in  
607 East Asian than in European human populations, *The American Journal of Human Genetics* (2015).
- 608 [28] P. Skoglund, M. Jakobsson, Archaic human ancestry in East Asia, *Proceedings of the National Academy of Sciences* 108  
609 (2011) 18301–18306.
- 610 [29] K. D. Pruitt, J. Harrow, R. A. Harte, C. Wallin, M. Diekhans, D. R. Maglott, S. Searle, C. M. Farrell, J. E. Loveland, B. J. Ruff,  
611 et al., The consensus coding sequence (CCDS) project: identifying a common protein-coding gene set for the human and  
612 mouse genomes, *Genome research* 19 (2009) 1316–1323.
- 613 [30] Q. Ding, Y. Hu, S. Xu, J. Wang, L. Jin, Neanderthal introgression at chromosome 3p21. 31 was under positive natural selection  
614 in East Asians, *Molecular biology and evolution* (2013) mst260.
- 615 [31] A. Vanhoutteghem, P. Djian, Basonuclins 1 and 2, whose genes share a common origin, are proteins with widely different  
616 properties and functions, *Proceedings of the National Academy of Sciences* 103 (2006) 12423–12428.
- 617 [32] L. C. Jacobs, A. Wollstein, O. Lao, A. Hofman, C. C. Klaver, A. G. Uitterlinden, T. Nijsten, M. Kayser, F. Liu, Comprehensive  
618 candidate gene study highlights UGT1A and BNC2 as new genes determining continuous skin color variation in europeans,  
619 *Human genetics* 132 (2013) 147–158.
- 620 [33] A. Cabral, D. F. Fischer, W. P. Vermeij, C. Backendorf, Distinct functional interactions of human Skn-1 isoforms with Ese-1  
621 during keratinocyte terminal differentiation, *Journal of Biological Chemistry* 278 (2003) 17792–17799.
- 622 [34] H. Takemoto, K. Tamai, E. Akasaka, D. Rokunohe, N. Takiyoshi, N. Umegaki, K. Nakajima, T. Aizu, T. Kaneko, H. Nakano,  
623 et al., Relation between the expression levels of the POU transcription factors Skn-1a and Skn-1n and keratinocyte differenti-  
624 ation, *Journal of dermatological science* 60 (2010) 203–205.



- 625 [35] M. Hašová, T. Crhák, B. Šafránková, J. Dvořáková, T. Muthný, V. Velebný, L. Kubala, Hyaluronan minimizes effects of UV  
626 irradiation on human keratinocytes, *Archives of dermatological research* 303 (2011) 277–284.
- 627 [36] C. Spilker, M. R. Kreutz, Rapgaps in brain: multipurpose players in neuronal Rap signalling, *European Journal of Neuroscience*  
628 32 (2010) 1–9.
- 629 [37] G. H. Mochida, V. S. Ganesh, M. I. de Michelena, H. Dias, K. D. Atabay, K. L. Kathrein, H.-T. Huang, R. S. Hill, J. M. Felie,  
630 D. Rakiec, et al., CHMP1A encodes an essential regulator of BMI1-INK4A in cerebellar development, *Nature genetics* 44  
631 (2012) 1260–1264.
- 632 [38] P. M. Wilson, R. H. Fryer, Y. Fang, M. E. Hatten, Astn2, a novel member of the astrotactin gene family, regulates the trafficking  
633 of ASTN1 during glial-guided neuronal migration, *The Journal of Neuroscience* 30 (2010) 8529–8540.
- 634 [39] T. Vrijenhoek, J. E. Buizer-Voskamp, I. van der Stelt, E. Strengman, G. Risk, C. Sabatti, A. G. van Kessel, H. G. Brunner, R. A.  
635 Ophoff, J. A. Veltman, et al., Recurrent CNVs disrupt three candidate genes in schizophrenia patients, *The American Journal*  
636 *of Human Genetics* 83 (2008) 504–510.
- 637 [40] K.-S. Wang, X.-F. Liu, N. Aragam, A genome-wide meta-analysis identifies novel loci associated with schizophrenia and bipolar  
638 disorder, *Schizophrenia research* 124 (2010) 192–199.
- 639 [41] S. Lin, H. Shen, J.-L. Li, S. Tang, Y. Gu, Z. Chen, C. Hu, J. C. Rice, J. Lu, L. Wu, Proteomic and functional analyses reveal  
640 the role of chromatin reader SFMBT1 in regulating epigenetic silencing and the myogenic gene program, *Journal of Biological*  
641 *Chemistry* 288 (2013) 6238–6247.
- 642 [42] T. Kato, H. Sato, M. Emi, T. Seino, S. Arawaka, C. Iseki, Y. Takahashi, M. Wada, T. Kawanami, Segmental copy number loss  
643 of SFMBT1 gene in elderly individuals with ventriculomegaly: a community-based study, *Internal Medicine* 50 (2011) 297–303.
- 644 [43] M. Krause, J. Moradi, S. Coleman, D. D'Souza, C. Liu, M. Kronenberg, D. Rowe, T. Hawke, M. Hadjiargyrou, A novel GFP  
645 reporter mouse reveals *Mustn1* expression in adult regenerating skeletal muscle, activated satellite cells and differentiating  
646 myoblasts, *Acta Physiologica* 208 (2013) 180–190.
- 647 [44] L. Wu, J. Liu, P. Gao, M. Nakamura, Y. Cao, H. Shen, J. D. Griffin, Transforming activity of MECT1-MAML2 fusion oncoprotein  
648 is mediated by constitutive CREB activation, *The EMBO journal* 24 (2005) 2391–2402.
- 649 [45] S.-E. Lin, T. Oyama, T. Nagase, K. Harigaya, M. Kitagawa, Identification of new human mastermind proteins defines a family  
650 that consists of positive regulators for notch signaling, *Journal of Biological Chemistry* 277 (2002) 50612–50620.
- 651 [46] M. Winnes, L. Mölne, M. Suurküla, Y. Andrén, F. Persson, F. Enlund, G. Stenman, Frequent fusion of the *CRTC1* and *MAML2*  
652 genes in clear cell variants of cutaneous hidradenomas, *Genes, Chromosomes and Cancer* 46 (2007) 559–563.
- 653 [47] S. L. Von Holstein, A. Fehr, S. Heegaard, M. H. Therkildsen, G. Stenman, *CRTC1-MAML2* gene fusion in mucoepidermoid  
654 carcinoma of the lacrimal gland, *Oncology reports* 27 (2012) 1413–1416.
- 655 [48] E. Hamano, M. Hijikata, S. Itoyama, T. Quy, N. C. Phi, H. T. Long, V. Van Ban, I. Matsushita, H. Yanai, F. Kirikae, et al.,  
656 Polymorphisms of interferon-inducible genes *oas-1* and *MxA* associated with SARS in the vietnamese population, *Biochemical*  
657 *and biophysical research communications* 329 (2005) 1234–1239.
- 658 [49] J. K. Lim, A. Lisco, D. H. McDermott, L. Huynh, J. M. Ward, B. Johnson, H. Johnson, J. Pape, G. A. Foster, D. Krysztow, et al.,  
659 Genetic variation in *OAS1* is a risk factor for initial infection with West Nile virus in man (2009).

- 660 [50] S. Knapp, L. Yee, A. Frodsham, B. Hennig, S. Hellier, L. Zhang, M. Wright, M. Chiaramonte, M. Graves, H. Thomas, et al.,  
661 Polymorphisms in interferon-induced genes and the outcome of hepatitis C virus infection: roles of MxA, OAS-1 and PKR,  
662 *Genes and immunity* 4 (2003) 411–419.
- 663 [51] M. Fedetz, F. Matesanz, A. Caro-Maldonado, O. Fernandez, J. Tamayo, M. Guerrero, C. Delgado, J. López-Guerrero, A. Al-  
664 cina, OAS1 gene haplotype confers susceptibility to multiple sclerosis, *Tissue antigens* 68 (2006) 446–449.
- 665 [52] F. L. Mendez, J. C. Watkins, M. F. Hammer, Neandertal origin of genetic variation at the cluster of OAS immunity genes,  
666 *Molecular biology and evolution* 30 (2013) 798–801.
- 667 [53] M. Dannemann, A. M. Andrés, J. Kelso, Introgression of Neandertal-and Denisovan-like haplotypes contributes to adaptive  
668 variation in human toll-like receptors, *The American Journal of Human Genetics* 98 (2016) 22–33.
- 669 [54] M. Deschamps, G. Laval, M. Fagny, Y. Itan, L. Abel, J.-L. Casanova, E. Patin, L. Quintana-Murci, Genomic signatures of  
670 selective pressures and introgression from archaic hominins at human innate immunity genes, *The American Journal of*  
671 *Human Genetics* 98 (2016) 5–21.
- 672 [55] S. Akira, S. Uematsu, O. Takeuchi, Pathogen recognition and innate immunity, *Cell* 124 (2006) 783–801.
- 673 [56] L. B. Barreiro, M. Ben-Ali, H. Quach, G. Laval, E. Patin, J. K. Pickrell, C. Bouchier, M. Tichit, O. Neyrolles, B. Gicquel, et al.,  
674 Evolutionary dynamics of human Toll-like receptors and their different contributions to host defense, *PLoS Genet* 5 (2009)  
675 e1000562.
- 676 [57] V. Gburcik, W. P. Cawthorn, J. Nedergaard, J. A. Timmons, B. Cannon, An essential role for Tbx15 in the differentiation  
677 of brown and “brite” but not white adipocytes, *American Journal of Physiology-Endocrinology and Metabolism* 303 (2012)  
678 E1053–E1060.
- 679 [58] I. M. Heid, A. U. Jackson, J. C. Randall, T. W. Winkler, L. Qi, V. Steinthorsdottir, G. Thorleifsson, M. C. Zillikens, E. K. Speliotes,  
680 R. Mägi, et al., Meta-analysis identifies 13 new loci associated with waist-hip ratio and reveals sexual dimorphism in the genetic  
681 basis of fat distribution, *Nature genetics* 42 (2010) 949–960.
- 682 [59] C.-T. Liu, M. L. Buchkovich, T. W. Winkler, I. M. Heid, I. Borecki, C. S. Fox, K. L. Mohlke, K. E. North, L. A. Cupples, A. A.  
683 A. G. Consortium, et al., Multi-ethnic fine-mapping of 14 central adiposity loci, *Human molecular genetics* (2014) ddu183.
- 684 [60] C.-T. Liu, K. L. Monda, K. C. Taylor, L. Lange, E. W. Demerath, W. Palmas, M. K. Wojczynski, J. C. Ellis, M. Z. Vitolins, S. Liu,  
685 et al., Genome-wide association of body fat distribution in African ancestry populations suggests new loci, *PLoS Genet* 9  
686 (2013) e1003681.
- 687 [61] D. Shungin, T. W. Winkler, D. C. Croteau-Chonka, T. Ferreira, A. E. Locke, R. Mägi, R. J. Strawbridge, T. H. Pers, K. Fischer,  
688 A. E. Justice, et al., New genetic loci link adipose and insulin biology to body fat distribution, *Nature* 518 (2015) 187–196.
- 689 [62] S. Candille, C. D. Van Raamsdonk, C. Chen, S. Kuijper, Y. Chen-Tsai, A. Russ, F. Meijlink, G. S. Barsh, Dorsoventral patterning  
690 of the mouse coat by Tbx15, *PLoS biology* 2 (2004) E3–E3.
- 691 [63] L. F. Pallares, P. Carbonetto, S. Gopalakrishnan, C. C. Parker, C. L. Ackert-Bicknell, A. A. Palmer, D. Tautz, Mapping of  
692 craniofacial traits in outbred mice identifies major developmental genes involved in shape determination, *PLOS Genet* 11  
693 (2015) e1005607.

- 694 [64] E. Lausch, P. Hermanns, H. F. Farin, Y. Alanay, S. Unger, S. Nikkel, C. Steinwender, G. Scherer, J. Spranger, B. Zabel, et al.,  
695 TBX15 mutations cause craniofacial dysmorphism, hypoplasia of scapula and pelvis, and short stature in cousin syndrome,  
696 *The American Journal of Human Genetics* 83 (2008) 649–655.
- 697 [65] G. Curry, Genetical and developmental studies on droopy-eared mice, *Journal of embryology and experimental morphology*  
698 7 (1959) 39–65.
- 699 [66] M. K. Singh, M. Petry, B. Haenig, B. Lescher, M. Leitges, A. Kispert, The t-box transcription factor Tbx15 is required for skeletal  
700 development, *Mechanisms of development* 122 (2005) 131–144.
- 701 [67] M. Fumagalli, I. Moltke, N. Grarup, F. Racimo, P. Bjerregaard, M. E. Jørgensen, T. S. Korneliusson, P. Gerbault, L. Skotte,  
702 A. Linneberg, et al., Greenlandic Inuit show genetic signatures of diet and climate adaptation, *Science* 349 (2015) 1343–1347.
- 703 [68] F. Racimo, D. Gokhman, M. Fumagalli, T. Hansen, I. Moltke, A. Albrechtsen, L. Carmel, E. Huerta-Sanchez, R. Nielsen,  
704 Archaic adaptive introgression in TBX15/WARS2, *bioRxiv* (2015) 033928.
- 705 [69] T. Woodage, M. A. Basrai, A. D. Baxevanis, P. Hieter, F. S. Collins, Characterization of the CHD family of proteins, *Proceedings*  
706 *of The National Academy of Sciences* 94 (1997) 11472–11477.
- 707 [70] A. Rauch, D. Wieczorek, E. Graf, T. Wieland, S. Ende, T. Schwarzmayr, B. Albrecht, D. Bartholdi, J. Beygo, N. Di Donato,  
708 et al., Range of genetic mutations associated with severe non-syndromic sporadic intellectual disability: an exome sequencing  
709 study, *The Lancet* 380 (2012) 1674–1682.
- 710 [71] G. L. Carvill, S. B. Heavin, S. C. Yendle, J. M. McMahon, B. J. O’Roak, J. Cook, A. Khan, M. O. Dorschner, M. Weaver,  
711 S. Calvert, et al., Targeted resequencing in epileptic encephalopathies identifies de novo mutations in CHD2 and SYNGAP1,  
712 *Nature genetics* 45 (2013) 825–830.
- 713 [72] R. E. Giles, N. Shimizu, F. H. Ruddle, Assignment of a human genetic locus to chromosome 5 which corrects the heat sensitive  
714 lesion associated with reduced leucyl-tRNA synthetase activity in ts025Cl Chinese hamster cells, *Somatic cell genetics* 6 (1980)  
715 667–687.
- 716 [73] J. P. Casey, P. McGettigan, N. Lynam-Lennon, M. McDermott, R. Regan, J. Conroy, B. Bourke, J. O’Sullivan, E. Crushell,  
717 S. Lynch, et al., Identification of a mutation in LARS as a novel cause of infantile hepatopathy, *Molecular genetics and*  
718 *metabolism* 106 (2012) 351–358.
- 719 [74] X.-Y. Dong, X. Sun, P. Guo, Q. Li, M. Sasahara, Y. Ishii, J.-T. Dong, ATBF1 inhibits estrogen receptor (ER) function by  
720 selectively competing with AIB1 for binding to the ER in ER-positive breast cancer cells, *Journal of Biological Chemistry* 285  
721 (2010) 32801–32809.
- 722 [75] X. Sun, H. F. Frierson, C. Chen, C. Li, Q. Ran, K. B. Otto, B. M. Cantarel, R. L. Vessella, A. C. Gao, J. Petros, et al., Frequent  
723 somatic mutations of the transcription factor ATBF1 in human prostate cancer, *Nature genetics* 37 (2005) 407–412.
- 724 [76] S. T. . D. Consortium, et al., Sequence variants in SLC16A11 are a common risk factor for type 2 diabetes in Mexico, *Nature*  
725 506 (2014) 97–101.
- 726 [77] H.-Q. Qu, L. Marchand, R. Grabs, C. Polychronakos, The association between the IFIH1 locus and type 1 diabetes, *Diabetolo-*  
727 *gia* 51 (2008) 473–475.

- 728 [78] S. Liu, H. Wang, Y. Jin, R. Podolsky, M. P. L. Reddy, J. Pedersen, B. Bode, J. Reed, D. Steed, S. Anderson, et al., IFIH1  
729 polymorphisms are significantly associated with type 1 diabetes and IFIH1 gene expression in peripheral blood mononuclear  
730 cells, *Human molecular genetics* 18 (2009) 358–365.
- 731 [79] M. Fumagalli, R. Cagliani, S. Riva, U. Pozzoli, M. Biasin, L. Piacentini, G. P. Comi, N. Bresolin, M. Clerici, M. Sironi, Population  
732 genetics of IFIH1: ancient population structure, local selection, and implications for susceptibility to type 1 diabetes, *Molecular  
733 biology and evolution* 27 (2010) 2555–2566.
- 734 [80] T. G. Warner, L. M. Dambach, J. H. Shin, J. S. O'Brien, Separation and characterization of the acid lipase and neutral esterases  
735 from human liver., *American journal of human genetics* 32 (1980) 869.
- 736 [81] H. Klima, K. Ullrich, C. Aslanidis, P. Fehring, K. Lackner, G. Schmitz, A splice junction mutation causes deletion of a 72-  
737 base exon from the mRNA for lysosomal acid lipase in a patient with cholesteryl ester storage disease, *Journal of Clinical  
738 Investigation* 92 (1993) 2713.
- 739 [82] C. Aslanidis, S. Ries, P. Fehring, C. Büchler, H. Klima, G. Schmitz, Genetic and biochemical evidence that cesd and wolman  
740 disease are distinguished by residual lysosomal acid lipase activity, *Genomics* 33 (1996) 85–93.
- 741 [83] E. G. Lund, T. A. Kerr, J. Sakai, W.-P. Li, D. W. Russell, cDNA cloning of mouse and human cholesterol 25-hydroxylases,  
742 polytopic membrane proteins that synthesize a potent oxysterol regulator of lipid metabolism, *Journal of Biological Chemistry*  
743 273 (1998) 34316–34327.
- 744 [84] N. Shibata, T. Kawarai, J. H. Lee, H.-S. Lee, E. Shibata, C. Sato, Y. Liang, R. Duara, R. P. Mayeux, P. H. St George-Hyslop,  
745 et al., Association studies of cholesterol metabolism genes (CH25H, ABCA1 and CH24H) in Alzheimer's disease, *Neuroscience  
746 letters* 391 (2006) 142–146.
- 747 [85] S.-Y. Liu, R. Aliyari, K. Chikere, G. Li, M. D. Marsden, J. K. Smith, O. Pernet, H. Guo, R. Nusbaum, J. A. Zack, et al., Interferon-  
748 inducible cholesterol-25-hydroxylase broadly inhibits viral entry by production of 25-hydroxycholesterol, *Immunity* 38 (2013)  
749 92–105.
- 750 [86] T. Kamalati, H. E. Jolin, P. J. Mitchell, K. T. Barker, L. E. Jackson, C. J. Dean, M. J. Page, B. A. Gusterson, M. R. Crompton,  
751 Brk, a breast tumor-derived non-receptor protein-tyrosine kinase, sensitizes mammary epithelial cells to epidermal growth  
752 factor, *Journal of Biological Chemistry* 271 (1996) 30956–30963.
- 753 [87] S. Surapureddi, S. Yu, H. Bu, T. Hashimoto, A. V. Yeldandi, P. Kashireddy, M. Cherkaoui-Malki, C. Qi, Y.-J. Zhu, M. S.  
754 Rao, et al., Identification of a transcriptionally active peroxisome proliferator-activated receptor  $\alpha$ -interacting cofactor complex  
755 in rat liver and characterization of PRIC285 as a coactivator, *Proceedings of the National Academy of Sciences* 99 (2002)  
756 11836–11841.
- 757 [88] T. Tomaru, T. Satoh, S. Yoshino, T. Ishizuka, K. Hashimoto, T. Monden, M. Yamada, M. Mori, Isolation and characterization of  
758 a transcriptional cofactor and its novel isoform that bind the deoxyribonucleic acid-binding domain of peroxisome proliferator-  
759 activated receptor- $\gamma$ , *Endocrinology* 147 (2006) 377–388.
- 760 [89] B. Persson, Y. Kallberg, J. E. Bray, E. Bruford, S. L. Dellaporta, A. D. Favia, R. G. Duarte, H. Jörnvall, K. L. Kavanagh,  
761 N. Kedishvili, et al., The SDR (short-chain dehydrogenase/reductase and related enzymes) nomenclature initiative, *Chemico-  
762 biological interactions* 178 (2009) 94–98.
- 763 [90] D. S. Wood, M. Zeviani, A. Prella, E. Bonilla, G. Salviati, A. F. Miranda, S. DiMauro, L. P. Rowland, Is nebulin the defective  
764 gene product in Duchenne muscular dystrophy?, *N Engl J Med* 1987 (1987) 107–108.

- 765 [91] V. Yotova, J.-F. Lefebvre, C. Moreau, E. Gbeha, K. Hovhannesian, S. Bourgeois, S. Bédarida, L. Azevedo, A. Amorim,  
766 T. Sarkisian, et al., An X-linked haplotype of neandertal origin is present among all non-African populations, *Molecular Biology*  
767 *and Evolution* 28 (2011) 1957–1962.
- 768 [92] B. F. Voight, S. Kudaravalli, X. Wen, J. K. Pritchard, A map of recent positive selection in the human genome, *PLoS Biol* 4  
769 (2006) e72.
- 770 [93] J. K. Pickrell, G. Coop, J. Novembre, S. Kudaravalli, J. Z. Li, D. Absher, B. S. Srinivasan, G. S. Barsh, R. M. Myers, M. W.  
771 Feldman, et al., Signals of recent positive selection in a worldwide sample of human populations, *Genome research* 19 (2009)  
772 826–837.
- 773 [94] T. Berisa, J. K. Pickrell, Approximately independent linkage disequilibrium blocks in human populations, *Bioinformatics* 32  
774 (2016) 283–285.
- 775 [95] E. E. Khrameeva, K. Bozek, L. He, Z. Yan, X. Jiang, Y. Wei, K. Tang, M. S. Gelfand, K. Prufer, J. Kelso, et al., Neanderthal  
776 ancestry drives evolution of lipid catabolism in contemporary Europeans, *Nature communications* 5 (2014).
- 777 [96] K. Harris, R. Nielsen, The genetic cost of Neanderthal introgression, *bioRxiv* (2015) 030387.
- 778 [97] I. Juric, S. Aeschbacher, G. Coop, The strength of selection against Neanderthal introgression, *bioRxiv* (2015) 030148.
- 779 [98] P. W. Hedrick, Adaptive introgression in animals: examples and comparison to new mutation and standing variation as sources  
780 of adaptive variation, *Molecular ecology* 22 (2013) 4606–4618.
- 781 [99] F. Racimo, S. Sankararaman, R. Nielsen, E. Huerta-Sánchez, Evidence for archaic adaptive introgression in humans, *Nature*  
782 *Reviews Genetics* 16 (2015) 359–371.
- 783 [100] E. Y. Durand, N. Patterson, D. Reich, M. Slatkin, Testing for ancient admixture between closely related populations, *Molecular*  
784 *biology and evolution* 28 (2011) 2239–2252.
- 785 [101] M. R. Kronforst, M. E. Hansen, N. G. Crawford, J. R. Gallant, W. Zhang, R. J. Kulathinal, D. D. Kapan, S. P. Mullen, Hybridization  
786 reveals the evolving genomic architecture of speciation, *Cell reports* 5 (2013) 666–677.
- 787 [102] J. Smith, M. R. Kronforst, Do *Heliconius* butterfly species exchange mimicry alleles?, *Biology letters* 9 (2013) 20130503.
- 788 [103] S. H. Martin, J. W. Davey, C. D. Jiggins, Evaluating the use of ABBA–BABA statistics to locate introgressed loci, *Molecular*  
789 *biology and evolution* 32 (2015) 244–257.
- 790 [104] M. DeGiorgio, M. Jakobsson, N. A. Rosenberg, Explaining worldwide patterns of human genetic variation using a coalescent-  
791 based serial founder model of migration outward from Africa, *Proceedings of the National Academy of Sciences* 106 (2009)  
792 16057–16062.
- 793 [105] P. W. Messer, SLiM: simulating evolution with selection and linkage, *Genetics* 194 (2013) 1037–1039.
- 794 [106] J. E. Pool, R. Nielsen, Inference of historical changes in migration rate from the lengths of migrant tracts, *Genetics* 181 (2009)  
795 711–719.
- 796 [107] S. Gravel, Population genetics models of local ancestry, *Genetics* 191 (2012) 607–619.
- 797 [108] S. Myers, L. Bottolo, C. Freeman, G. McVean, P. Donnelly, A fine-scale map of recombination rates and hotspots across the  
798 human genome, *Science* 310 (2005) 321–324.

- 799 [109] J. F. Crow, M. Kimura, et al., An introduction to population genetics theory., An introduction to population genetics theory.  
800 (1970).
- 801 [110] R. Lewontin, The interaction of selection and linkage. i. general considerations; heterotic models, *Genetics* 49 (1964) 49.
- 802 [111] W. Hill, A. Robertson, Linkage disequilibrium in finite populations, *Theoretical and Applied Genetics* 38 (1968) 226–231.

803 7. Tables

Table 1: Summary statistics mentioned in the main text.

Statistic	Explanation	Reference
$D$	D-statistic: measures excess allele sharing between a test population and an outgroup using a sister population that is more closely related to the test than the outgroup	[1][100]
$f_D$	Similar to the D-statistic, but serves to better control for local variation in diversity patterns if one is interested in finding loci with excess ancestry from an admixing population.	[103]
$R_D$	Average ratio of the sequence divergence between an individual from the source population and an individual from the admixed population, and the sequence divergence between an individual from the source population and an individual from the non-admixed population. This is computed by taking the average over all pairs of admixed and non-admixed individuals.	This study
$U_{A,B,C}(w, x, y)$	Number of sites in which any allele is at a frequency lower than $w$ in panel $A$ , higher than $x$ in panel $B$ and equal to $y$ in panel $C$ .	This study
$U_{A,B,C,D}(w, x, y, z)$	Number of sites in which any allele is at a frequency lower than $w$ in panel $A$ , higher than $x$ in panel $B$ , equal to $y$ in panel $C$ and equal to $z$ in panel $D$ .	This study
$Q95_{A,B,C}(w, y)$	95% quantile of the distribution of derived allele frequencies in panel $B$ , for sites where the derived allele is at a frequency lower than $w$ in panel $A$ and equal to $y$ in panel $C$ .	This study
$Q95_{A,B,C,D}(w, y, z)$	95% quantile of the distribution of derived allele frequencies in panel $B$ , for sites where the derived allele is at a frequency lower than $w$ in panel $A$ , equal to $y$ in panel $C$ and equal to $z$ in panel $D$ .	This study
$\pi$	Expected heterozygosity, measured as the average of $2p(1-p)$ over all sites in a window, where $p$ is the frequency of an arbitrarily chosen allele.	[109]
$D' [intro]$	A measure of linkage disequilibrium. Computed as $D/D_{max}$ where $D = p_{XY} - p_X p_Y$ , $p_{XY}$ is the frequency of haplotype $XY$ , $p_X$ is the frequency of allele $X$ , $p_Y$ is the frequency of allele $Y$ , and $D_{max}$ is the maximum theoretical value that $D$ can take. $D' [intro]$ is computed only using frequencies from the introgressed panel. When we compute this in a window, the value is obtained by taking the average over all pairs of SNPs.	[110]
$D' [comb]$	$D'$ computed using haplotype and allele frequencies from the combination of the introgressed and non-introgressed panels.	[110]
$r^2 [intro]$	A measure of linkage disequilibrium. Computed as $D^2 / (p_X(1-p_X)p_Y(1-p_Y))$ . $r^2 [intro]$ is computed only using frequencies from the introgressed panel. When we compute this in a window, the value is obtained by taking the average over all pairs of SNPs.	[111]
$r^2 [comb]$	$r^2$ computed using haplotype and allele frequencies from the combination of the introgressed and non-introgressed panels.	[111]

804 **8. Figures**

Example Statistics

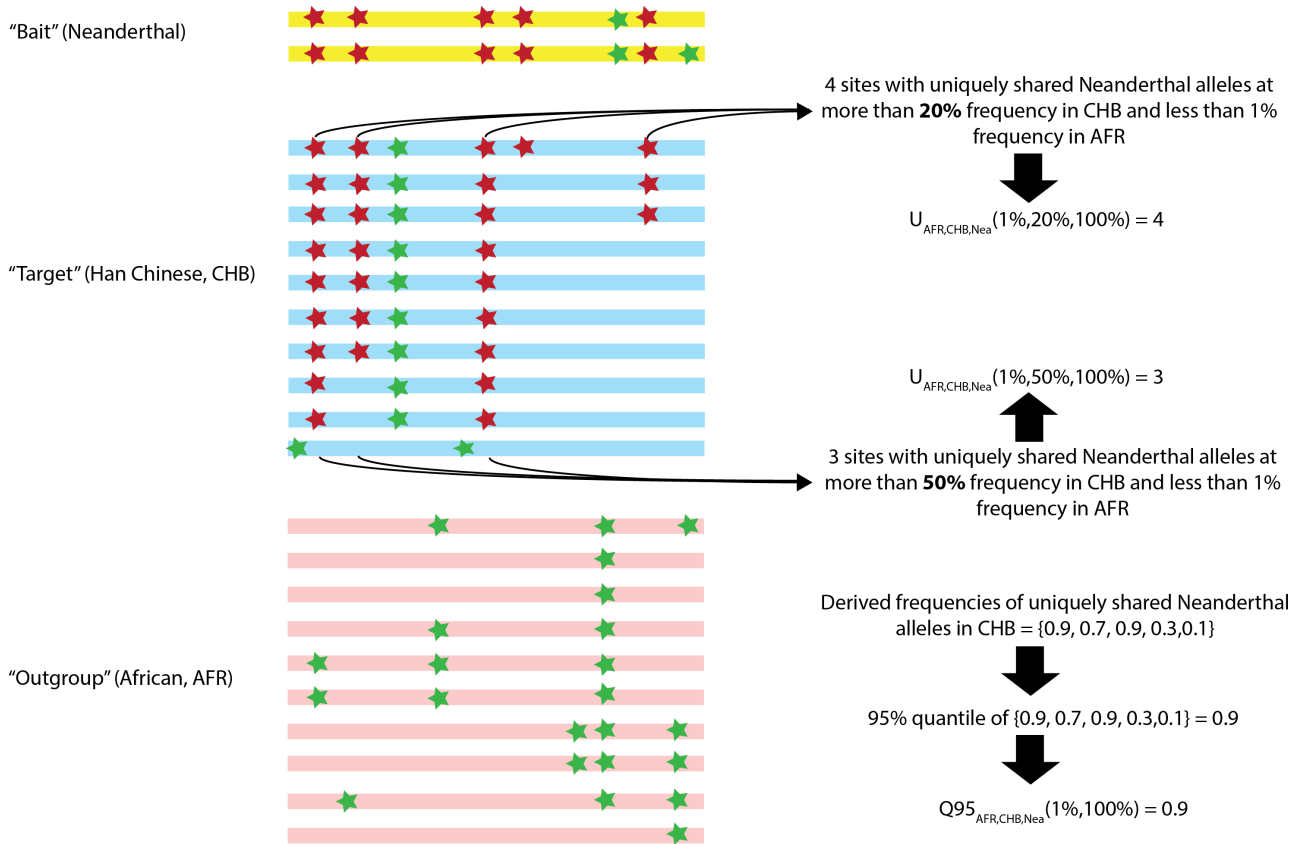


Figure 1: Schematic illustration of the way the  $U_{A,B,C}$  and  $Q95_{A,B,C}$  statistics are calculated.



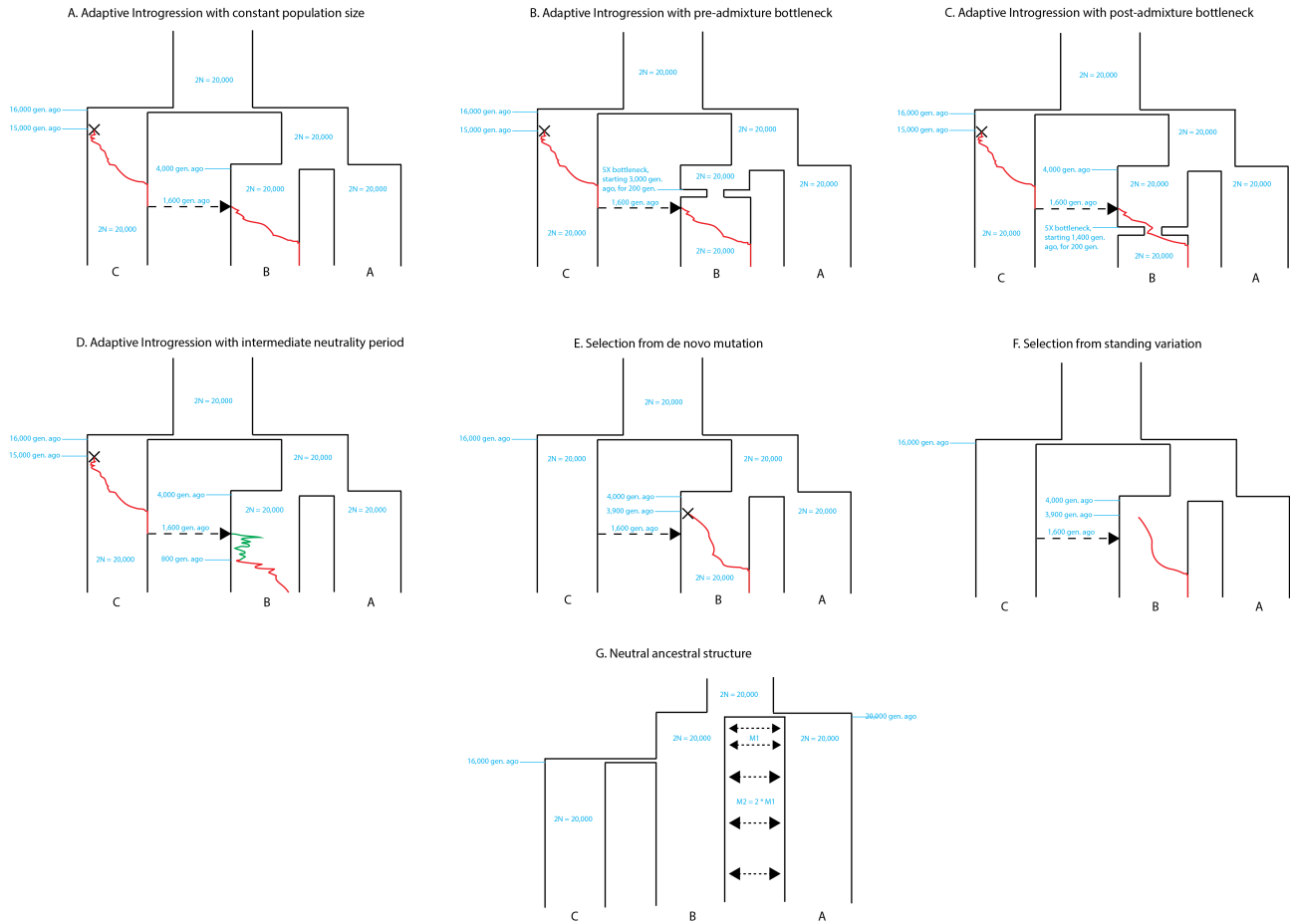


Figure 2: Demographic models described in the main text.

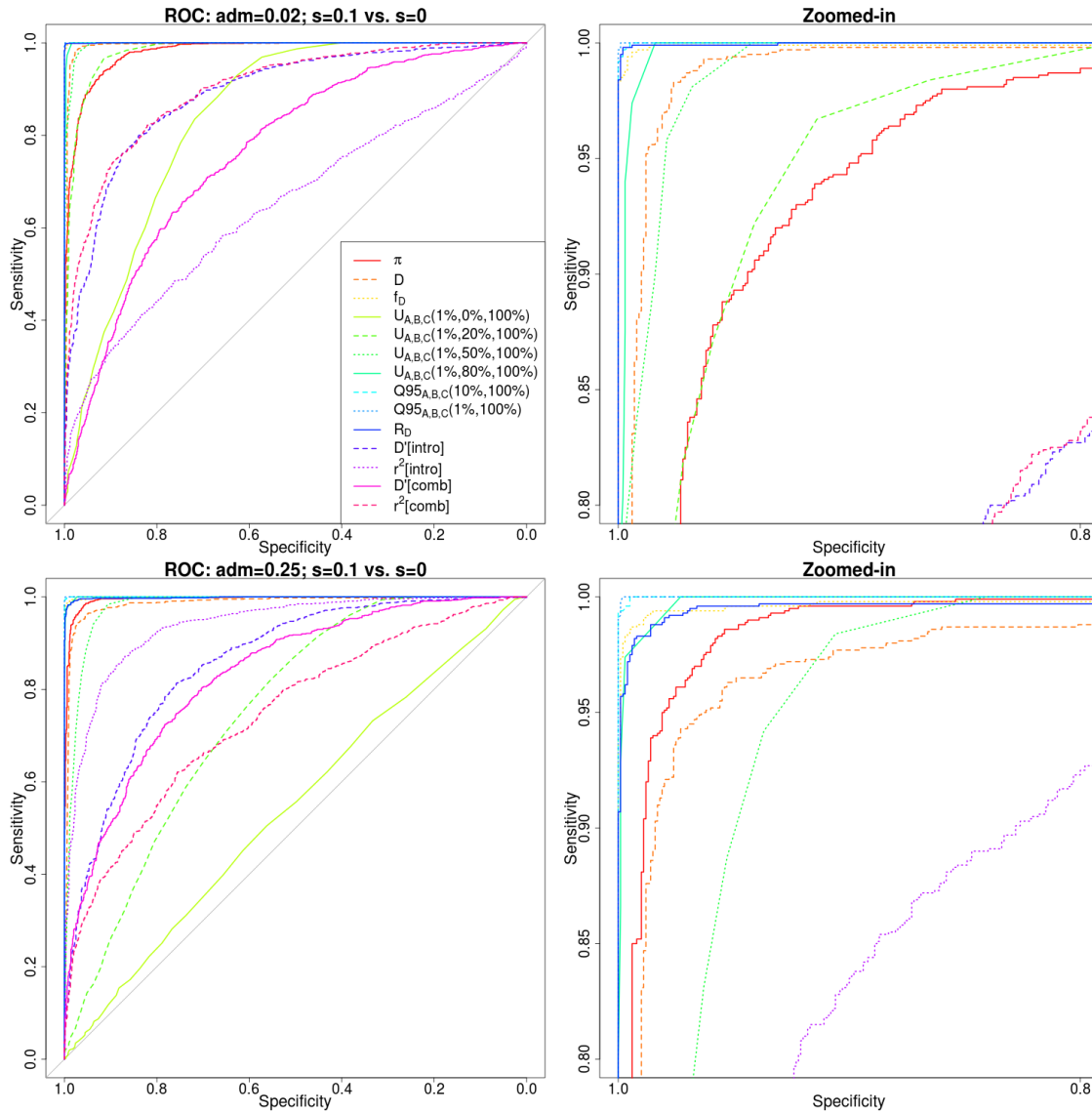


Figure 3: Receiver operating characteristic curves for a scenario of adaptive introgression ( $s=0.1$ ) compared to a scenario of neutrality ( $s=0$ ), using 1,000 simulations for each case. Populations A and B split from each other 4,000 generations ago, and their ancestral population split from population C 16,000 generations ago. Population sizes were constant and set at  $2N = 20,000$ . The admixture event occurred 1,600 generations ago from population C to population B, at rate 2% (top panels) or 25% (bottom panels). The right panels are zoomed-in versions of the left panels.

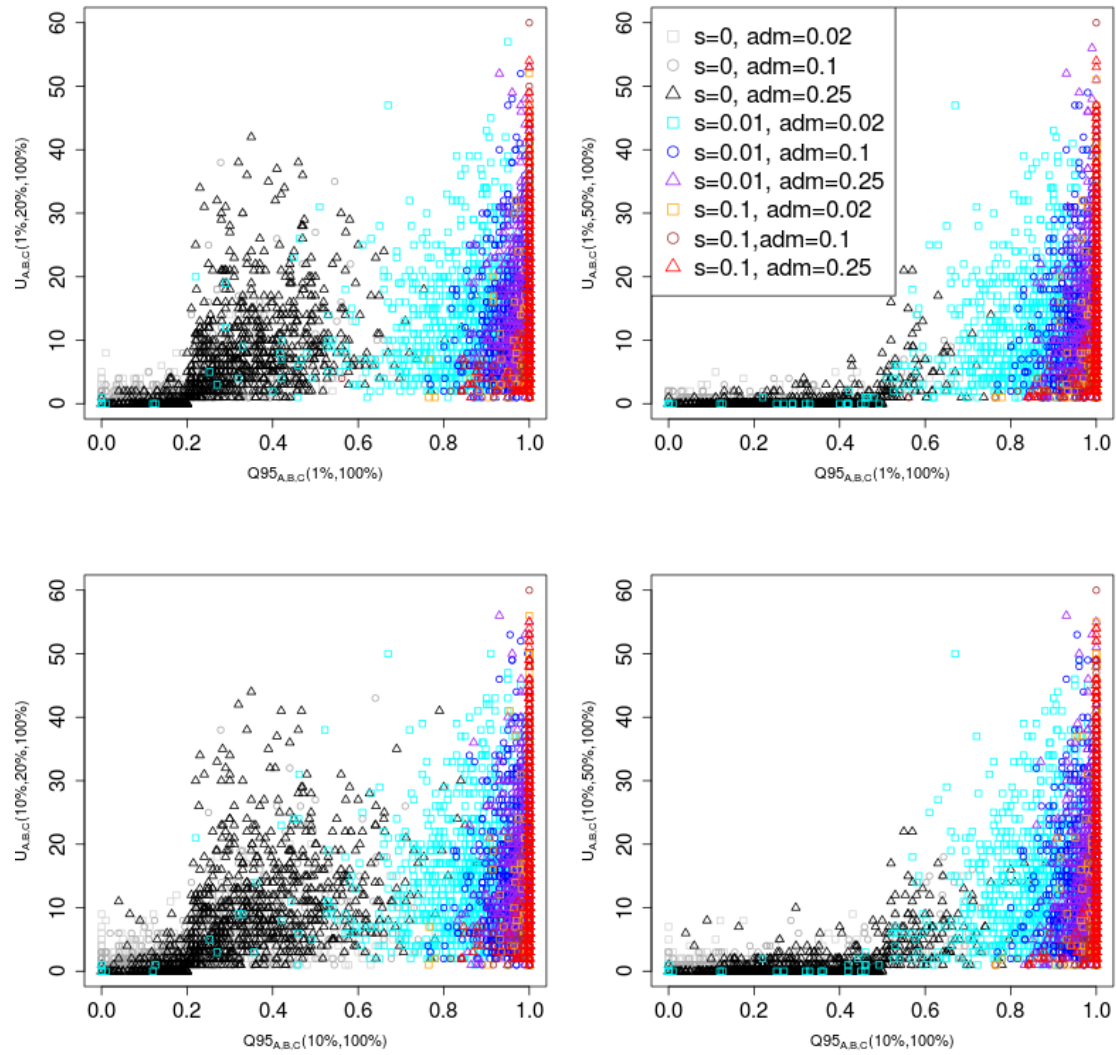


Figure 4: Joint distribution of  $Q95_{A,B,C}(w, y)$  and  $U_{A,B,C}(w, x, y)$  for different choices of  $w$  (1%, 10%) and  $x$  (20%, 50%). We set  $y$  to 100% in all cases. 100 individuals were sampled from panel A, 100 from panel B and 2 from panel C. The demographic parameters were the same as in Figure 3.

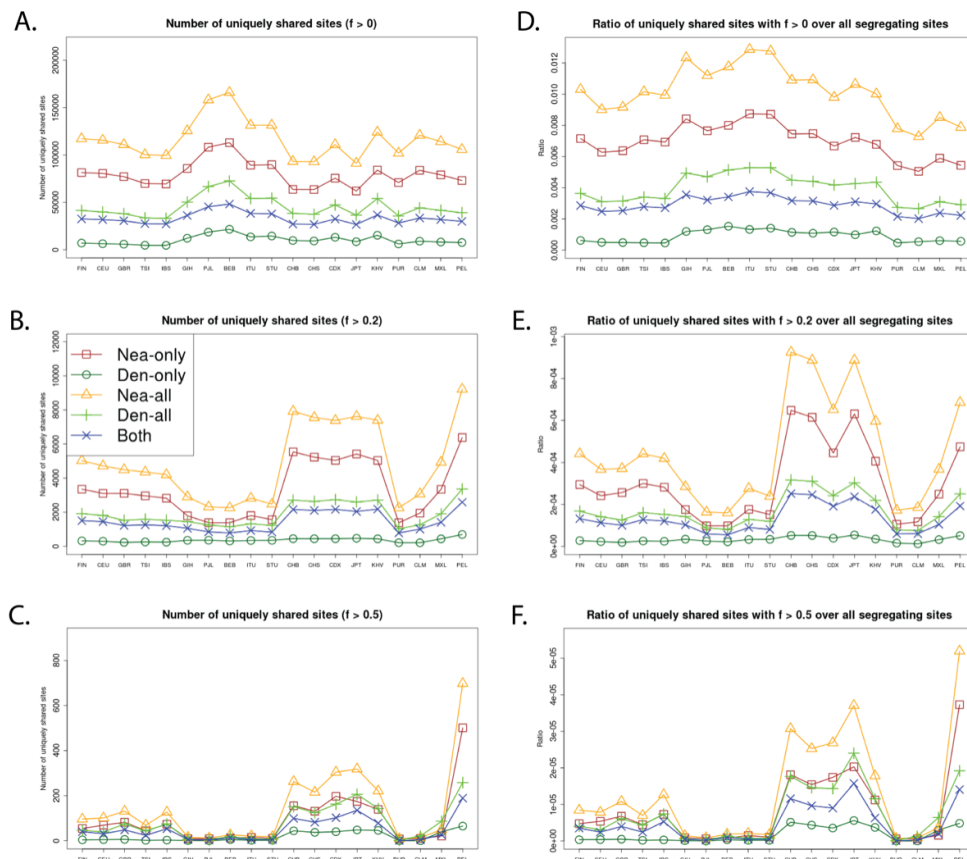


Figure 5: We computed the number of uniquely shared sites in the autosomes and the X chromosome between particular archaic humans and different choices of present-day non-African panels  $X$  (x-axis) from phase 3 of the 1000 Genomes Project. We used a shared frequency cutoff of 0% (A), 20% (B) and 50% (C). Nea-only =  $U_{Afr,X,Nea,Den}(1\%, 20\%, 100\%, 0\%)$ . Den-only =  $U_{Afr,X,Nea,Den}(1\%, 20\%, 0\%, 100\%)$ . Nea-all =  $U_{Afr,X,Nea}(1\%, 20\%, 100\%)$ . Den-all =  $U_{Afr,X,Den}(1\%, 20\%, 100\%)$ . Both =  $U_{Afr,X,Nea,Den}(1\%, 20\%, 100\%, 100\%)$ . Finally, we scaled each of the statistics from panels A-C by the number of segregating sites in each 1000 Genomes population panel, yielding panels D-F.

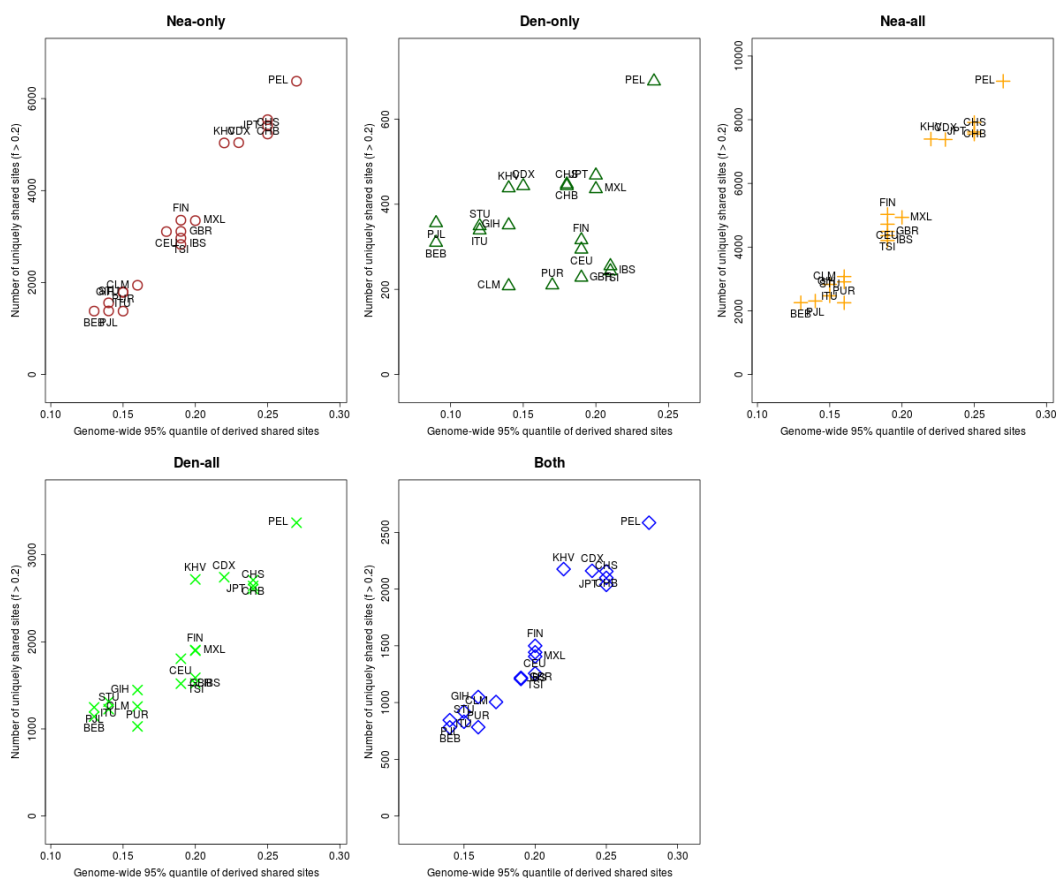


Figure 6: For each population panel from the 1000 Genomes Project, we jointly plotted the  $U$  and  $Q_{95}$  statistics with an archaic frequency cutoff of  $> 20\%$  within each population.  $\text{Nea-only} = U_{Afr,X,Nea,Den}(1\%, 20\%, 100\%, 0\%)$  and  $Q_{95Afr,X,Nea,Den}(1\%, 100\%, 0\%)$ .  $\text{Den-only} = U_{Afr,X,Nea,Den}(1\%, 20\%, 0\%, 100\%)$  and  $Q_{95Afr,X,Nea,Den}(1\%, 0\%, 100\%)$ .  $\text{Nea-all} = U_{Afr,X,Nea}(1\%, 20\%, 100\%)$  and  $Q_{95Afr,X,Nea}(1\%, 100\%)$ .  $\text{Den-all} = U_{Afr,X,Den}(1\%, 20\%, 100\%)$  and  $Q_{95Afr,X,Den}(1\%, 100\%)$ .  $\text{Both} = U_{Afr,X,Nea,Den}(1\%, 20\%, 100\%, 100\%)$  and  $Q_{95Afr,X,Nea,Den}(1\%, 100\%, 100\%)$ .

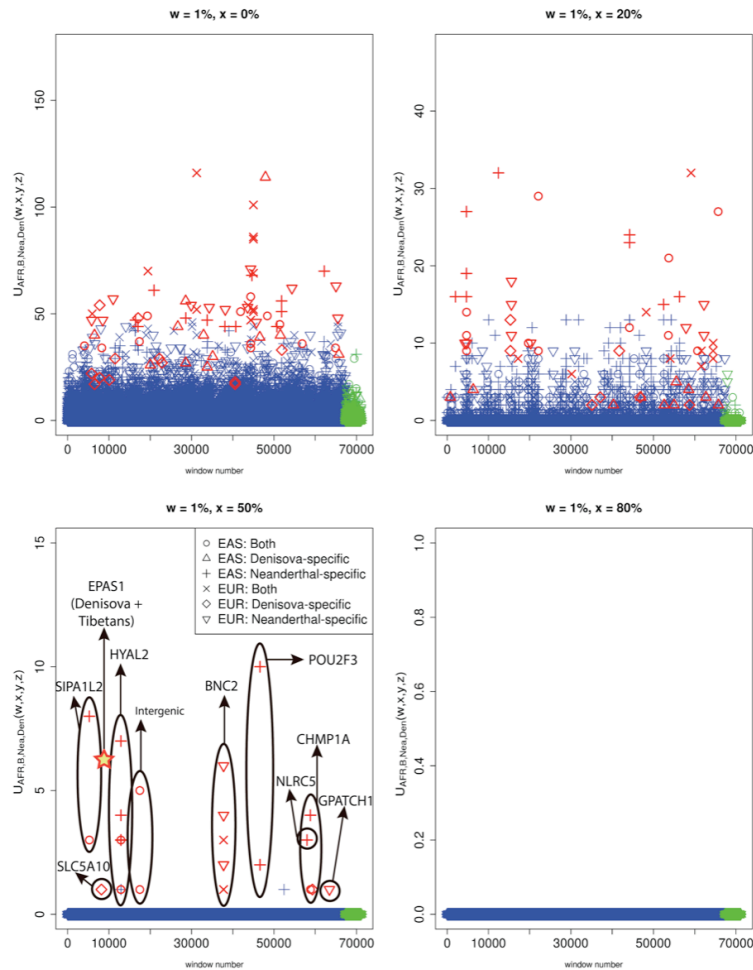


Figure 7: We partitioned the genome into non-overlapping windows of 40kb. Within each window, we computed  $U_{EUR, Out, Nea, Den}(1\%, x, y, z)$  and  $U_{EAS, Out, Nea, Den}(1\%, x, y, z)$ , where Out=EAS+AFR for EUR as the target introgressed population, and Out=EUR+AFR for EAS as the target introgressed population. We searched for Neanderthal-specific alleles ( $y = 100\%$ ,  $z = 0\%$ ), Denisovan-specific alleles ( $y = 0\%$ ,  $z = 100\%$ ) and alleles present in both archaic genomes ( $y = 100\%$ ,  $z = 100\%$ ) that were uniquely shared with either EUR or EAS at frequencies above different cutoffs ( $x=0\%$ ,  $x=20\%$ ,  $x=50\%$  and  $x=80\%$ ). Windows that fall within the upper tail of the distribution for each modern-archaic population pair are colored in red ( $P < 0.001 / \text{number of pairs tested}$ ) and those that do not are colored in blue, except for those in the X chromosome, which are in green. Ovals drawn around multiple points contain multiple windows with uniquely shared alleles that are contiguous. For comparison, the number of high frequency uniquely shared sites between Denisova and Tibetans is also shown [18], although Tibetans are not included in the 1000 Genomes data and the region is 32 kb long, so this may be an underestimate.

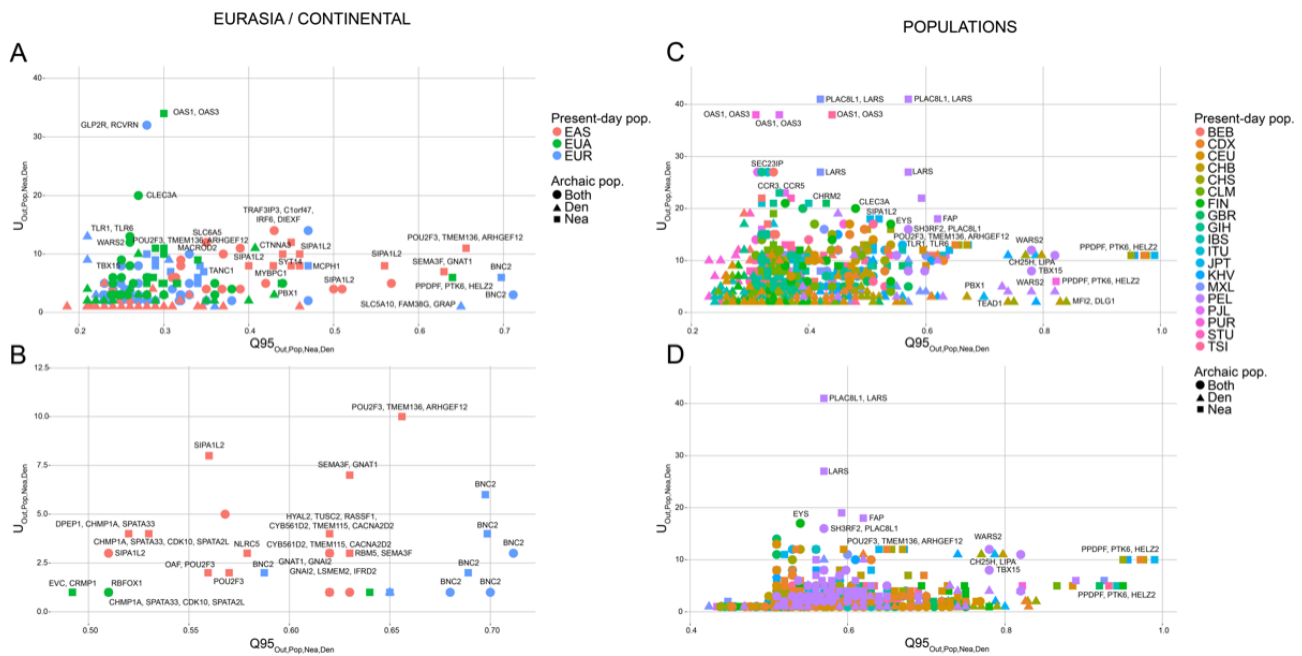


Figure 8: We plotted the 40kb regions in the 99.9% highest quantiles of both the  $Q95_{Out,Pop,Nea,Den}(1\%, y, z)$  and  $U_{Out,Pop,Nea,Den}(1\%, x, y, z)$  statistics for different choices of target introgressed population (Pop) and outgroup non-introgressed population (Out), and different archaic allele frequency cutoffs within the target population (x). A) We plotted the extreme regions for continental populations EUR (Out=EAS+AFR), EAS (Out=EUR+AFR) and Eurasians (EUA, Out=AFR), using a target population archaic allele frequency cutoff x of 20%. B) We plotted the extreme regions from the same statistics as in panel A, but with a more stringent target population archaic allele frequency cutoff x of 50%. C) We plotted the extreme regions for individual non-African populations within the 1000 Genomes data, using all African populations (excluding African-Americans) as the outgroup, and a cutoff x of 20%. D) We plotted the extreme regions from the same statistics as in panel C, but with a more stringent target population archaic allele frequency cutoff x of 50%. Nea-only =  $U_{Out,Pop,Nea,Den}(1\%, x, 100\%, 0\%)$  and  $Q95_{Out,Pop,Nea,Den}(1\%, 100\%, 0\%)$ . Den-only =  $U_{Out,Pop,Nea,Den}(1\%, x, 0\%, 100\%)$  and  $Q95_{Out,Pop,Nea,Den}(1\%, 0\%, 100\%)$ . Both =  $U_{Out,Pop,Nea,Den}(1\%, x, 100\%, 100\%)$  and  $Q95_{Out,Pop,Nea,Den}(1\%, 100\%, 100\%)$ .

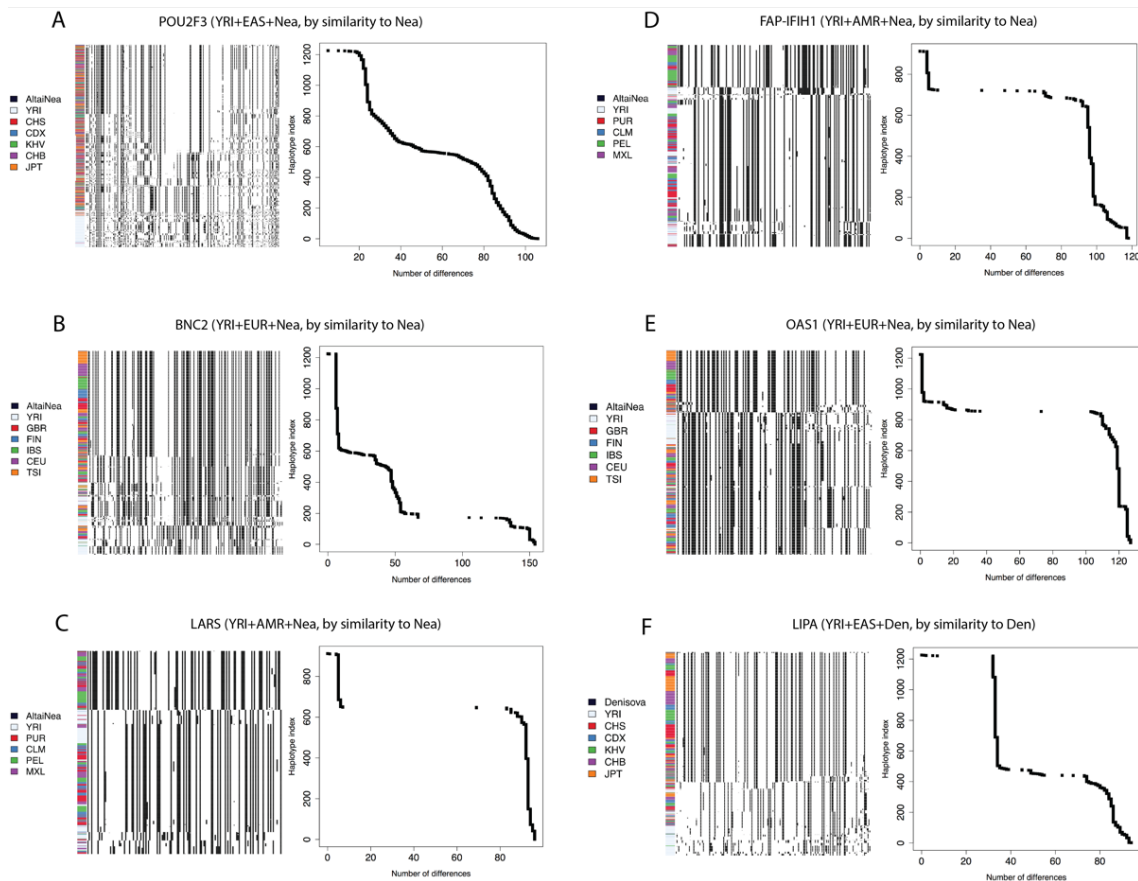


Figure 9: We explored the haplotype structure of six candidate regions with strong evidence for AI. For each region, we applied a clustering algorithm to the haplotypes of particular human populations and then ordered the clusters by decreasing similarity to the archaic human genome with the larger number of uniquely shared sites (see Methods Section). We also plotted the number of differences to the archaic genome for each human haplotype and sorted them simply by decreasing similarity. In the latter case, no clustering was performed, so the rows in the cumulative difference plots do not necessarily correspond to the rows in the adjacent haplotype structure plots. *POU2F3*: chr11:120120001-120200000. *BNC2*: chr9:16720001-16760000. *LARS*: chr5:145480001-145520000. *FAP/IFIH1*: chr2:163040001-163120000. *OAS1*: chr12:113360001-113400000. *LIPA*: chr10:90920001-90980000.



## Supplementary Tables

Table S1: 95% quantiles of the  $U_{A,B,C}$  statistic in a 40 kb window, under different demographic scenarios and archaic allele frequency cutoffs in the outgroup (A) and target (B) population panels. The demographic scenarios correspond to scenarios A, B, C and G from Figure 2. The bottlenecks were 5X and lasted 200 generations.

Max. outgroup freq.	Min. target freq.	Scenario	95% quantile under neutrality
0.01	0.8	Admixture (2%)	0
0.01	0.8	Admixture (10%)	0
0.01	0.8	Admixture (25%)	0
0.01	0.8	Ancestral Structure (strong mig.)	0
0.01	0.8	Ancestral Structure (medium mig.)	1
0.01	0.8	Ancestral Structure (weak mig.)	18
0.01	0.8	Admixture (2%), then bottleneck	0
0.01	0.8	Admixture (10%), then bottleneck	0
0.01	0.8	Admixture (25%), then bottleneck	0.05
0.01	0.8	Bottleneck, then admixture (2%)	0
0.01	0.8	Bottleneck, then admixture (10%)	0
0.01	0.8	Bottleneck, then admixture (25%)	0
0.01	0.5	Admixture (2%)	2
0.01	0.5	Admixture (10%)	2
0.01	0.5	Admixture (25%)	5
0.01	0.5	Ancestral Structure (strong mig.)	0
0.01	0.5	Ancestral Structure (medium mig.)	5
0.01	0.5	Ancestral Structure (weak mig.)	22
0.01	0.5	Admixture (2%), then bottleneck	2
0.01	0.5	Admixture (10%), then bottleneck	2
0.01	0.5	Admixture (25%), then bottleneck	8
0.01	0.5	Bottleneck, then admixture (2%)	2
0.01	0.5	Bottleneck, then admixture (10%)	2
0.01	0.5	Bottleneck, then admixture (25%)	6
0.01	0.2	Admixture (2%)	6
0.01	0.2	Admixture (10%)	13
0.01	0.2	Admixture (25%)	29.05
0.01	0.2	Ancestral Structure (strong mig.)	0
0.01	0.2	Ancestral Structure (medium mig.)	9.05
0.01	0.2	Ancestral Structure (weak mig.)	25
0.01	0.2	Admixture (2%), then bottleneck	6
0.01	0.2	Admixture (10%), then bottleneck	17
0.01	0.2	Admixture (25%), then bottleneck	30
0.01	0.2	Bottleneck, then admixture (2%)	8
0.01	0.2	Bottleneck, then admixture (10%)	13.05
0.01	0.2	Bottleneck, then admixture (25%)	29
0.01	0	Admixture (2%)	24
0.01	0	Admixture (10%)	37
0.01	0	Admixture (25%)	39
0.01	0	Ancestral Structure (strong mig.)	3
0.01	0	Ancestral Structure (medium mig.)	12.05
0.01	0	Ancestral Structure (weak mig.)	27
0.01	0	Admixture (2%), then bottleneck	21
0.01	0	Admixture (10%), then bottleneck	34
0.01	0	Admixture (25%), then bottleneck	38
0.01	0	Bottleneck, then admixture (2%)	28
0.01	0	Bottleneck, then admixture (10%)	34.05
0.01	0	Bottleneck, then admixture (25%)	37.05
0.1	0.8	Admixture (2%)	0
0.1	0.8	Admixture (10%)	2
0.1	0.8	Admixture (25%)	2
0.1	0.8	Ancestral Structure (strong mig.)	0
0.1	0.8	Ancestral Structure (medium mig.)	11
0.1	0.8	Ancestral Structure (weak mig.)	23.05

0.1	0.8	Admixture (2%), then bottleneck	0
0.1	0.8	Admixture (10%), then bottleneck	2
0.1	0.8	Admixture (25%), then bottleneck	2
0.1	0.8	Bottleneck, then admixture (2%)	1
0.1	0.8	Bottleneck, then admixture (10%)	2
0.1	0.8	Bottleneck, then admixture (25%)	2
<hr/>			
0.1	0.5	Admixture (2%)	5
0.1	0.5	Admixture (10%)	6
0.1	0.5	Admixture (25%)	12
0.1	0.5	Ancestral Structure (strong mig.)	0
0.1	0.5	Ancestral Structure (medium mig.)	17
0.1	0.5	Ancestral Structure (weak mig.)	29
0.1	0.5	Admixture (2%), then bottleneck	6
0.1	0.5	Admixture (10%), then bottleneck	7
0.1	0.5	Admixture (25%), then bottleneck	12
0.1	0.5	Bottleneck, then admixture (2%)	6
0.1	0.5	Bottleneck, then admixture (10%)	6.05
0.1	0.5	Bottleneck, then admixture (25%)	12
<hr/>			
0.1	0.2	Admixture (2%)	12
0.1	0.2	Admixture (10%)	18.05
0.1	0.2	Admixture (25%)	35
0.1	0.2	Ancestral Structure (strong mig.)	4
0.1	0.2	Ancestral Structure (medium mig.)	21
0.1	0.2	Ancestral Structure (weak mig.)	32.05
0.1	0.2	Admixture (2%), then bottleneck	14
0.1	0.2	Admixture (10%), then bottleneck	22
0.1	0.2	Admixture (25%), then bottleneck	37
0.1	0.2	Bottleneck, then admixture (2%)	14
0.1	0.2	Bottleneck, then admixture (10%)	20
0.1	0.2	Bottleneck, then admixture (25%)	37
<hr/>			
0.1	0	Admixture (2%)	29
0.1	0	Admixture (10%)	44
0.1	0	Admixture (25%)	45
0.1	0	Ancestral Structure (strong mig.)	11
0.1	0	Ancestral Structure (medium mig.)	25
0.1	0	Ancestral Structure (weak mig.)	34
0.1	0	Admixture (2%), then bottleneck	28
0.1	0	Admixture (10%), then bottleneck	40
0.1	0	Admixture (25%), then bottleneck	44
0.1	0	Bottleneck, then admixture (2%)	35
0.1	0	Bottleneck, then admixture (10%)	41
0.1	0	Bottleneck, then admixture (25%)	45

Table S2: 95% quantiles of the  $Q_{95A,B,C}$  statistic in a 40 kb window, under different demographic scenarios and archaic allele frequency cutoffs in the outgroup (A) population panel. The demographic scenarios correspond to scenarios A, B, C and G from Figure 2.

Max. outgroup freq.	Scenario	95% quantile under neutrality
0.01	Admixture (2%)	0.28
0.01	Admixture (10%)	0.37
0.01	Admixture (25%)	0.54
0.01	Ancestral Structure (strong mig.)	0.04
0.01	Ancestral Structure (medium mig.)	0.67
0.01	Ancestral Structure (weak mig.)	1
0.01	Admixture (2%), then bottleneck	0.31
0.01	Admixture (10%), then bottleneck	0.44
0.01	Admixture (25%), then bottleneck	0.6
0.01	Bottleneck, then admixture (2%)	0.28
0.01	Bottleneck, then admixture (10%)	0.42
0.01	Bottleneck, then admixture (25%)	0.55
0.1	Admixture (2%)	0.47
0.1	Admixture (10%)	0.51
0.1	Admixture (25%)	0.63
0.1	Ancestral Structure (strong mig.)	0.25
0.1	Ancestral Structure (medium mig.)	0.91
0.1	Ancestral Structure (weak mig.)	1
0.1	Admixture (2%), then bottleneck	0.53
0.1	Admixture (10%), then bottleneck	0.58
0.1	Admixture (25%), then bottleneck	0.67
0.1	Bottleneck, then admixture (2%)	0.47
0.1	Bottleneck, then admixture (10%)	0.53
0.1	Bottleneck, then admixture (25%)	0.66

Table S3: 40 kb windows that lie in the highest 99.9% quantile of both  $U_{A,B,Nea,Den}$  and  $Q95_{A,B,Nea,Den}$  for various outgroup panels A and target panels B, using an outgroup maximum frequency cutoff of 1%, and using different target allele frequency cutoffs (20%, 50%). For each region, we also show other statistics indicative of AI for reference. We partitioned the 1000 Genomes panels into outgroup panel A and target panel B in different ways (column "Mode"), depending on the signals we were looking for. These modes of partitioning are as follows. "Populations" = outgroup panel was the combination of all the populations that were not the target panel. "PopulationsB" = outgroup panel was the combination of all African panels (excluding admixed African-Americans), while target panel was one of the non-African panels. "Continents" = target panel was either the EUR continental panel (in which case the outgroup was AFR+EAS) or the EAS continental panel (in which case the outgroup was AFR+EUR). "ContinentsB" = target panel was the EUR continental panel (in which case the outgroup was AFR+EAS+SAS) or the EAS continental panel (in which case the outgroup was AFR+EUR+SAS) or the SAS continental panel (in which case the outgroup was AFR+EUR+EAS). "Eurasia" = target panel was EUR+EAS, while outgroup panel was AFR.

[https://www.dropbox.com/s/p9k94i2c50rincq/Extreme\\_gene\\_table.xlsx?dl=0](https://www.dropbox.com/s/p9k94i2c50rincq/Extreme_gene_table.xlsx?dl=0)

## Supplementary Figures

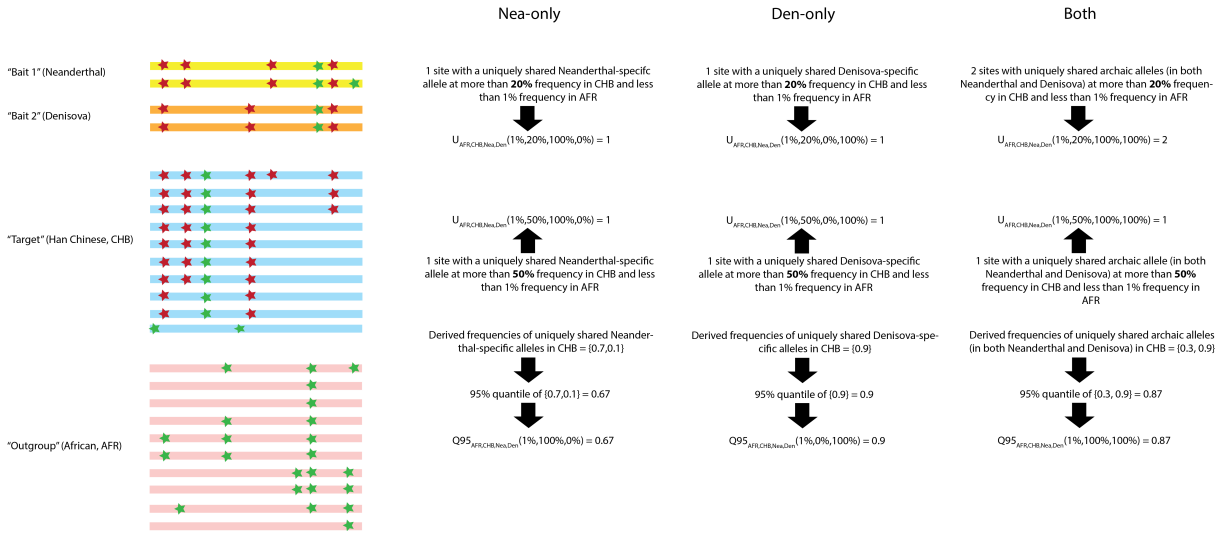


Figure S1: Schematic illustration of the way the  $U_{A,B,C,D}$  and  $Q95_{A,B,C,D}$  statistics are calculated.

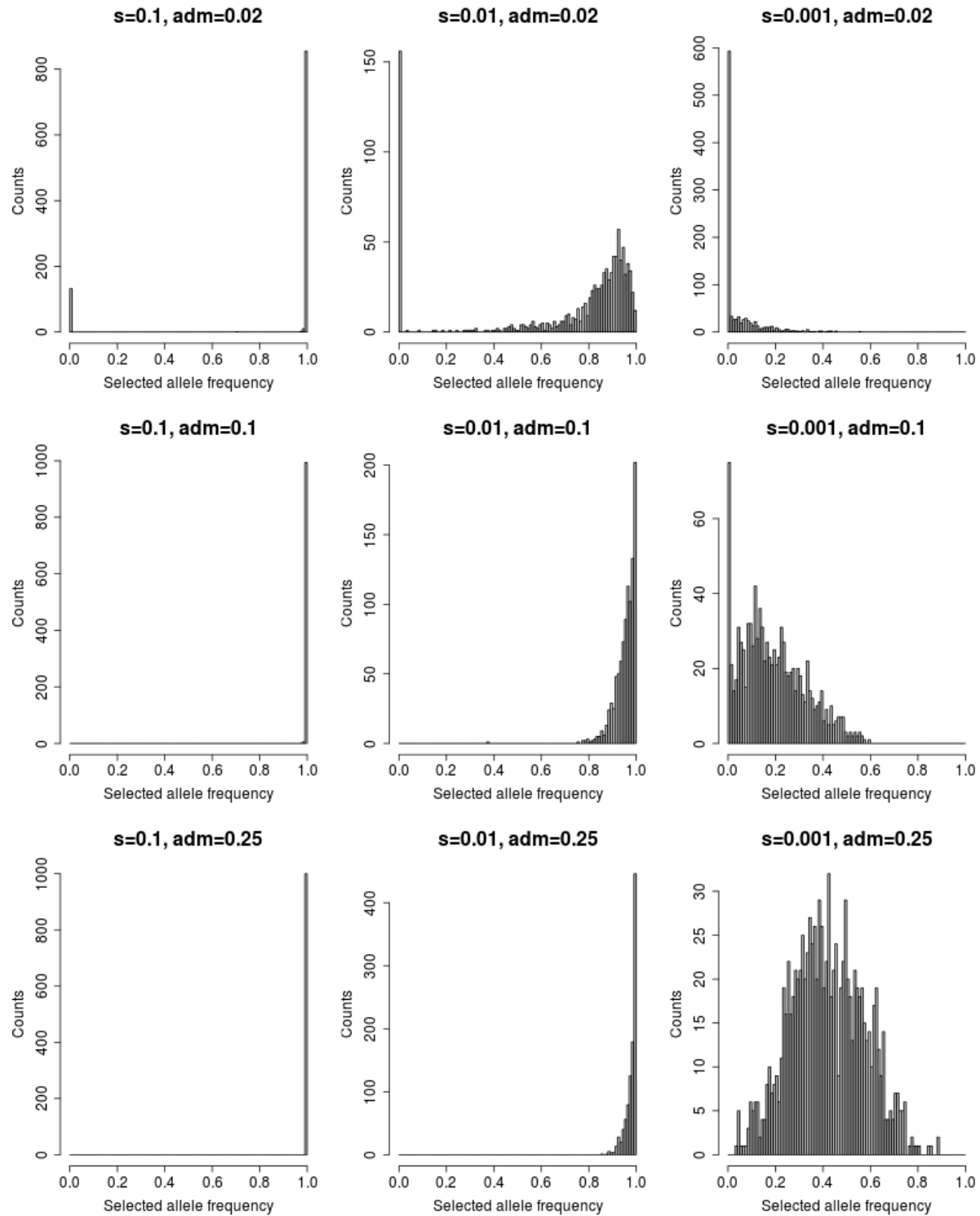


Figure S2: Histograms of the frequencies of the selected allele in the introgressed population in the present, for each AI scenario under constant population sizes.

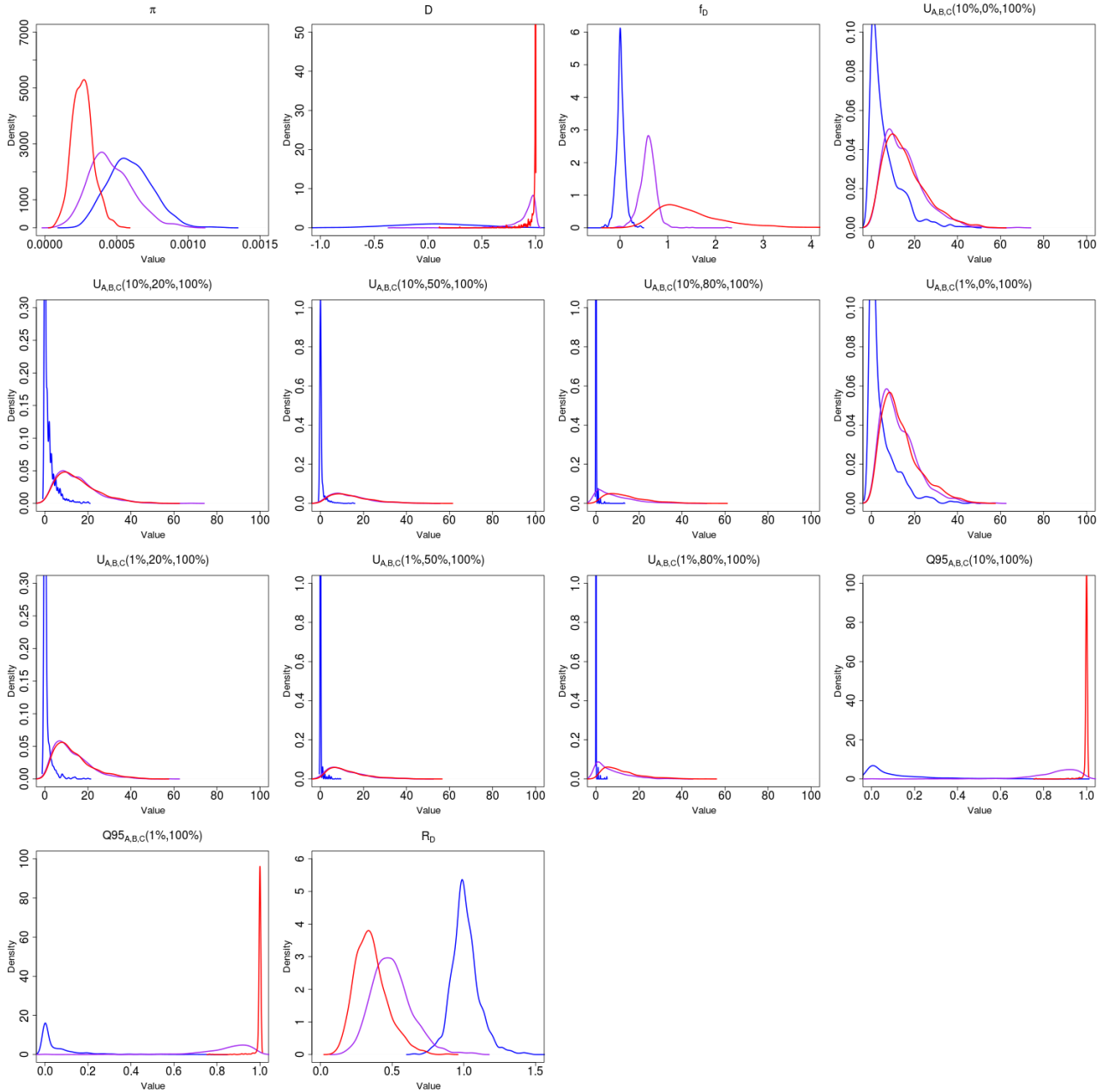


Figure S3: Density of various statistics meant to detect genetic patterns left by adaptive introgression, for three scenarios: neutrality ( $s=0$ ) in blue, weak adaptive introgression ( $s=0.01$ ) in purple and strong adaptive introgression ( $s=0.1$ ) in red. The demography was the same as in Figure 3 and the admixture rate was set at 2%. See Table 1 for a definition of the statistics shown.

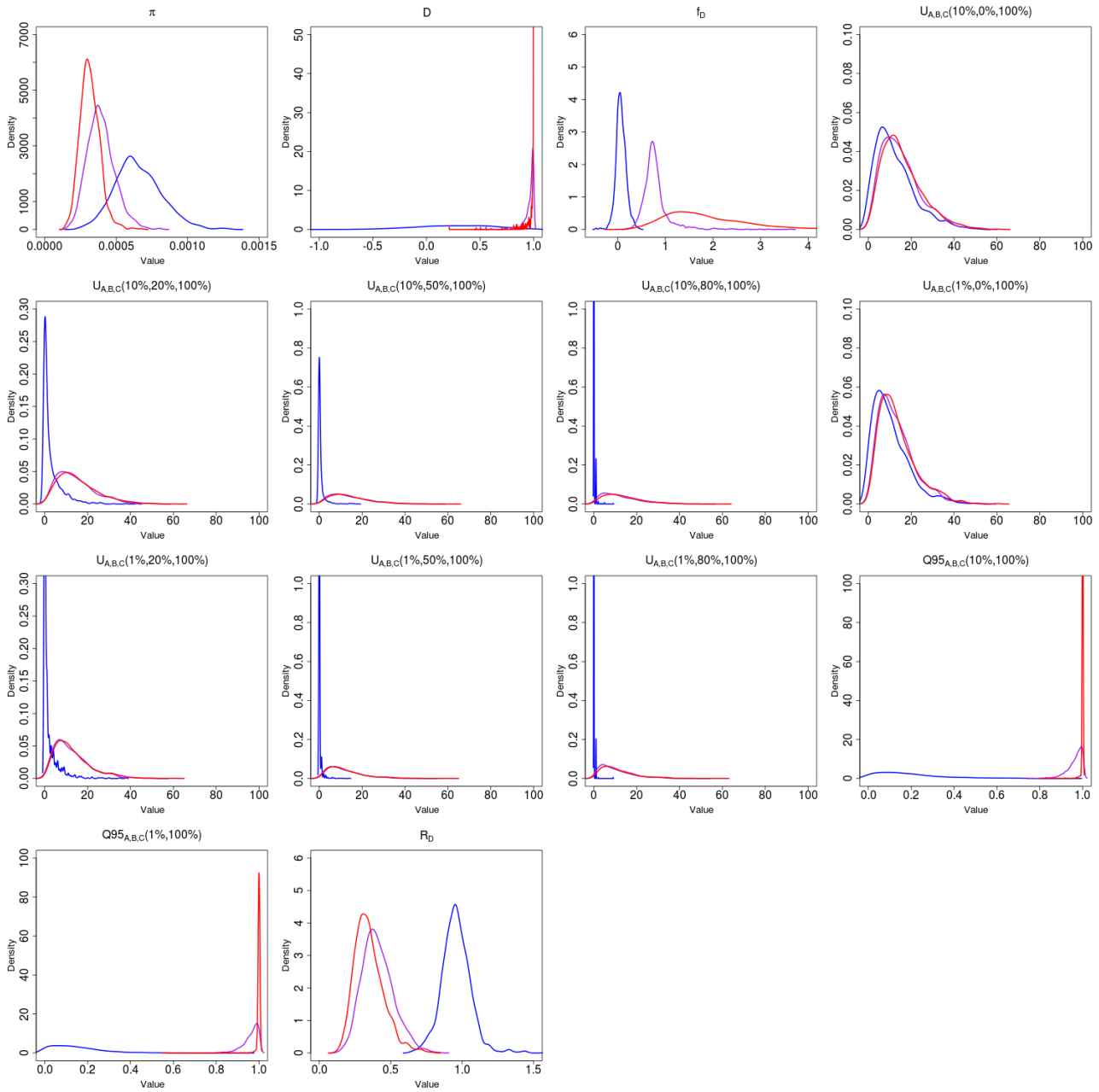


Figure S4: Density of various statistics meant to detect genetic patterns left by adaptive introgression, for three scenarios: neutrality ( $s=0$ ) in blue, weak adaptive introgression ( $s=0.01$ ) in purple and strong adaptive introgression ( $s=0.1$ ) in red. The demography was the same as in Figure 3 and the admixture rate was set at 10%. See Table 1 for a definition of the statistics shown.



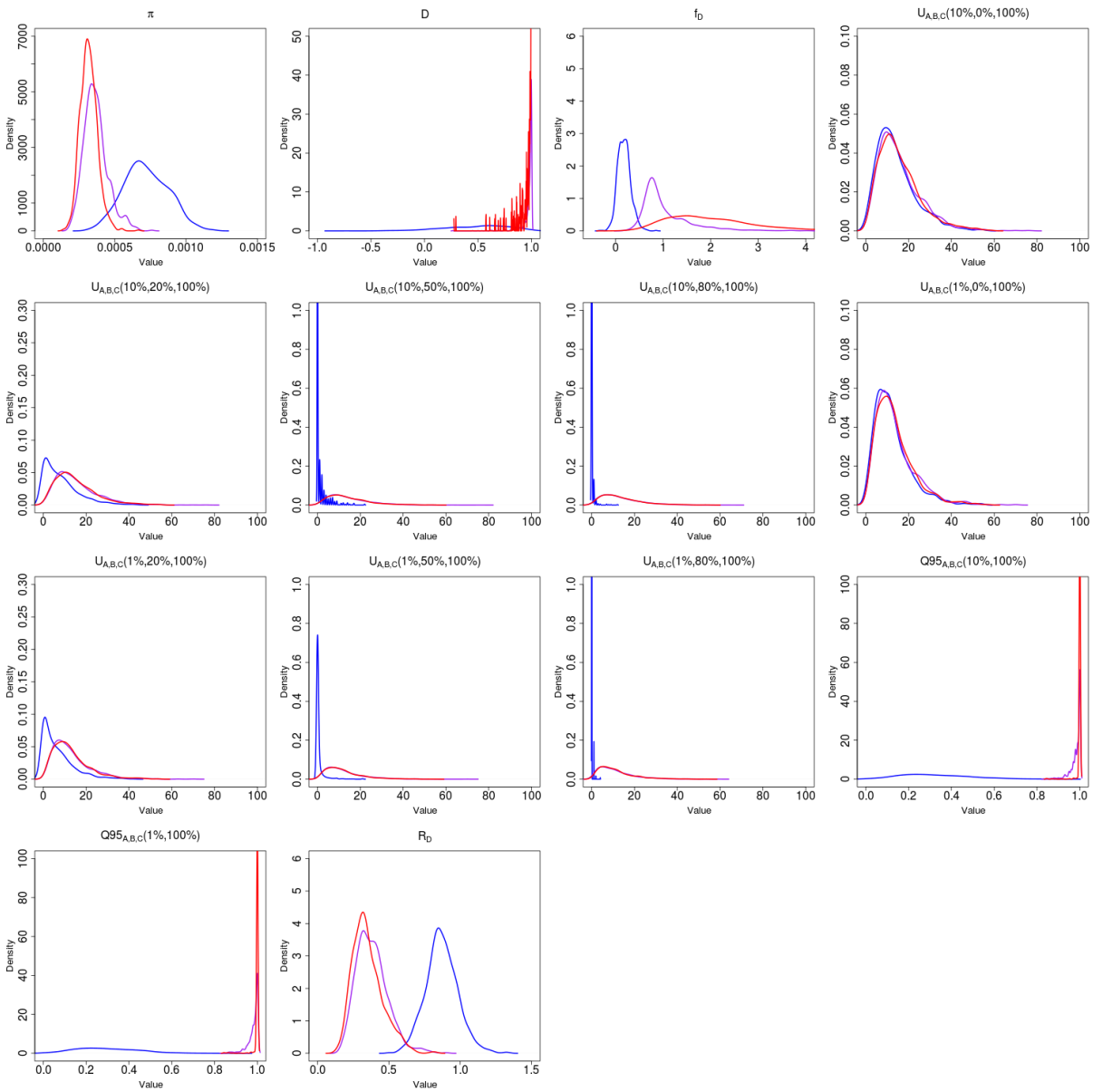


Figure S5: Density of various statistics meant to detect genetic patterns left by adaptive introgression, for three scenarios: neutrality ( $s=0$ ) in blue, weak adaptive introgression ( $s=0.01$ ) in purple and strong adaptive introgression ( $s=0.1$ ) in red. The demography was the same as in Figure 3 and the admixture rate was set at 25%. See Table 1 for a definition of the statistics shown.

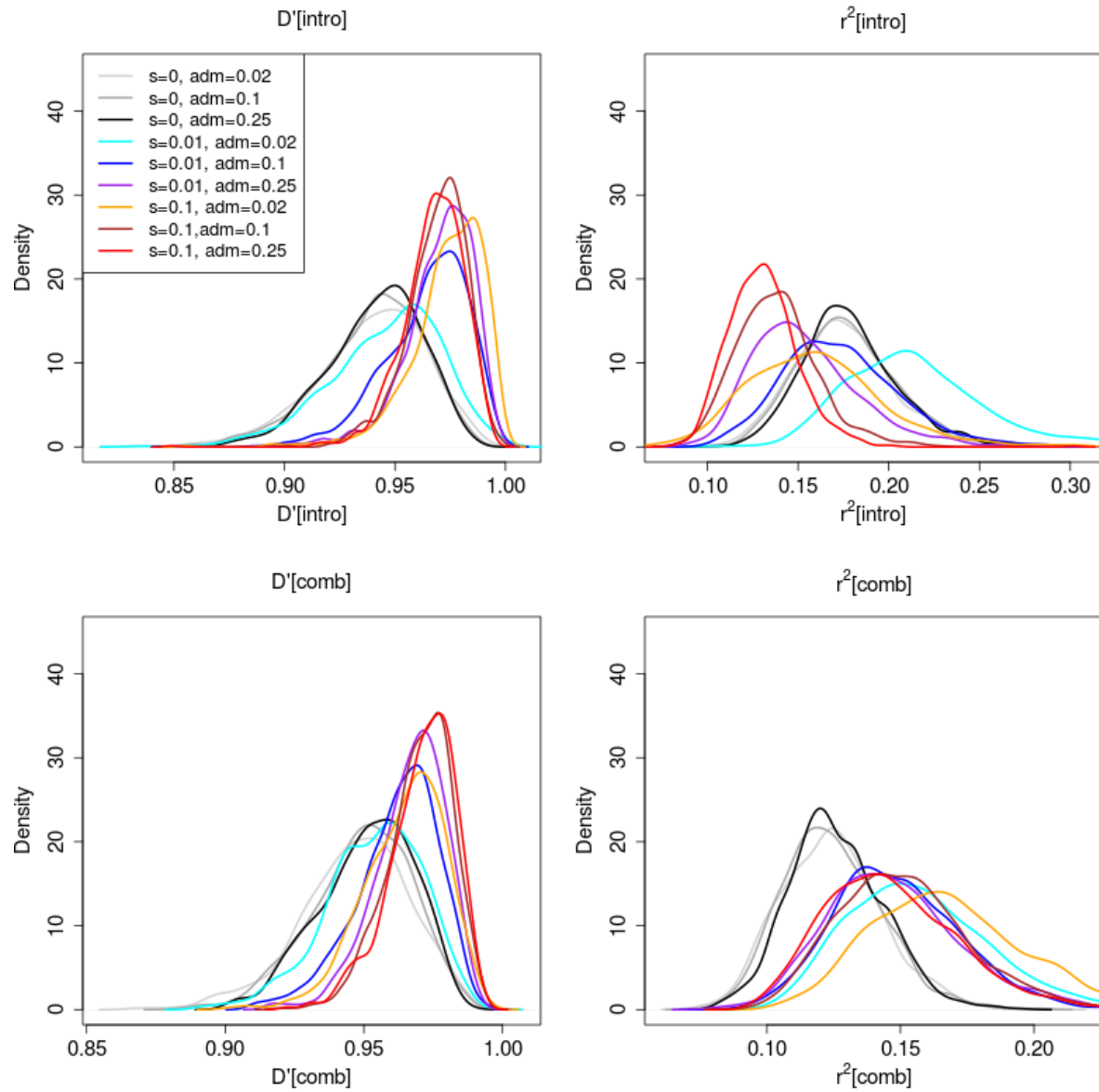


Figure S6: Density of statistics that detect patterns of linkage disequilibrium for various neutral and adaptive introgression scenarios. See Table 1 for a definition of the statistics shown.

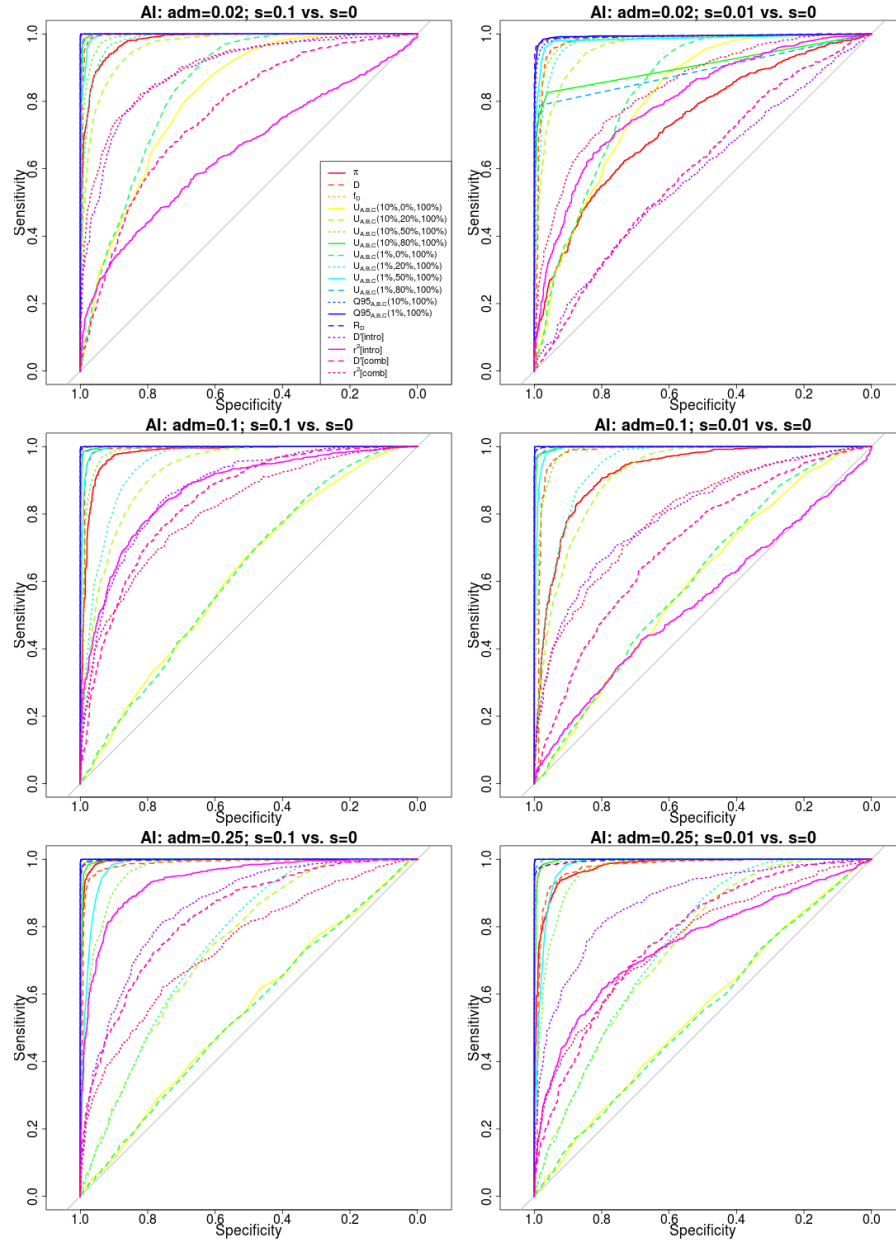


Figure S7: Receiver operating characteristic curves for adaptive introgression with constant population size, using 1,000 simulations of adaptive introgression, under various selection ( $s=0.1$ ,  $s=0.01$ ) and admixture rate (2%, 10%, 25%) regimes. Populations A and B split from each other 4,000 generations ago, and their ancestral population split from population C 16,000 generations ago. Population sizes were set at  $2N = 20,000$ . The admixture event occurred 1,600 generations ago from population C into population B,

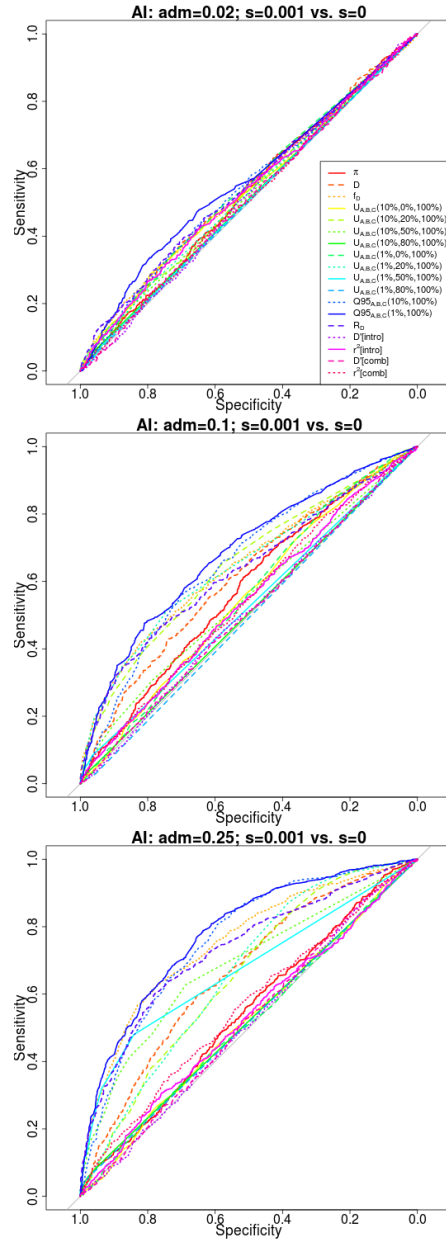


Figure S8: Receiver operating characteristic curves for adaptive introgression with constant population size, using 1,000 simulations of adaptive introgression, under weak selection ( $s=0.001$ ) and different admixture rate (2%, 10%, 25%) regimes. Populations A and B split from each other 4,000 generations ago, and their ancestral population split from population C 16,000 generations ago. Population sizes were set at  $2N = 20,000$ . The admixture event occurred 1,600 generations ago from population C into population B,

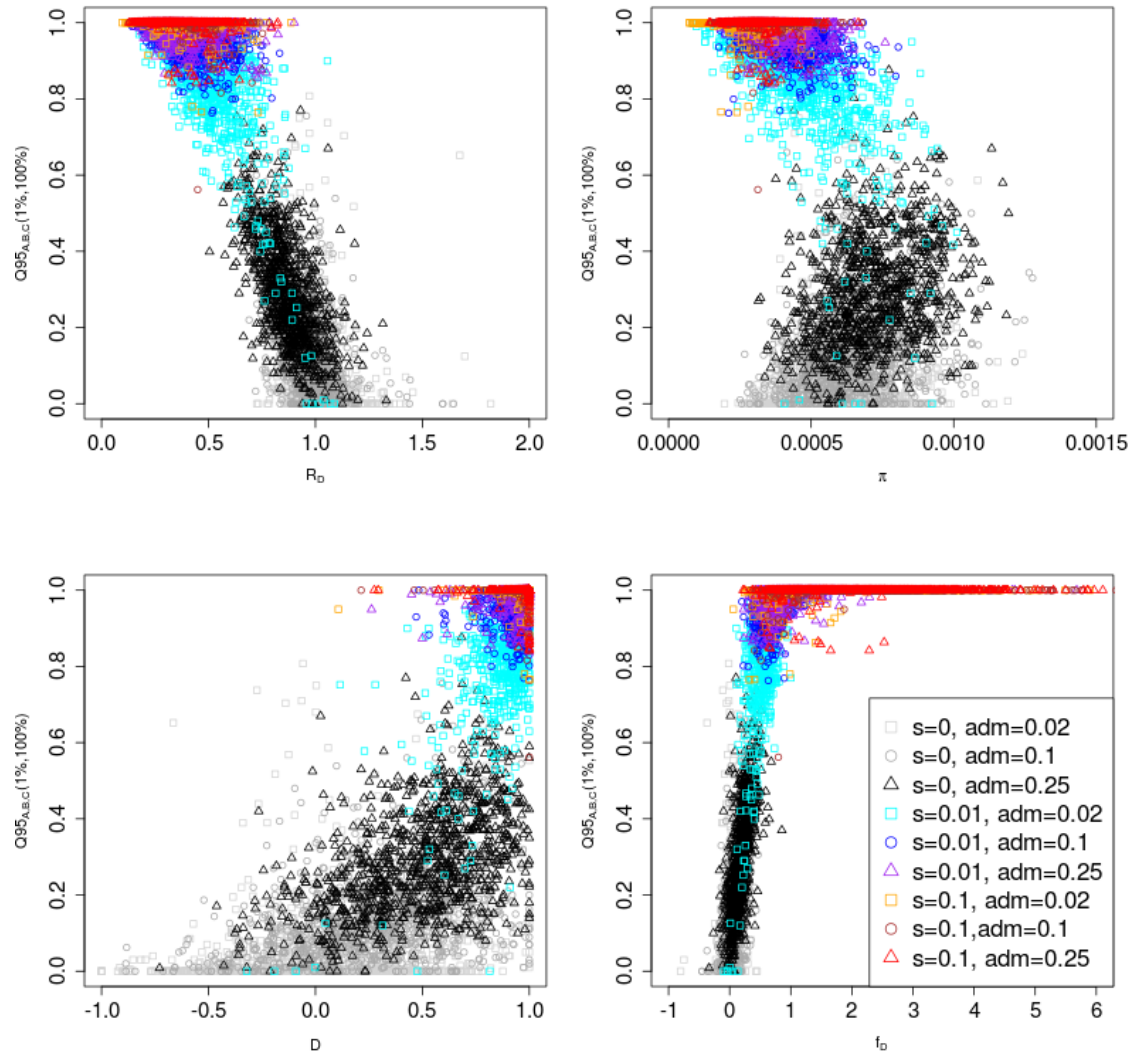


Figure S9: Joint distribution of  $Q95_{A,B,C}(1\%, 100\%)$  and other statistics ( $R_D$ ,  $\pi$ ,  $D$  and  $f_D$ ). 100 individuals were sampled from panel A, 100 from panel B and 2 from panel C. The demographic parameters were the same as in Figure 3.

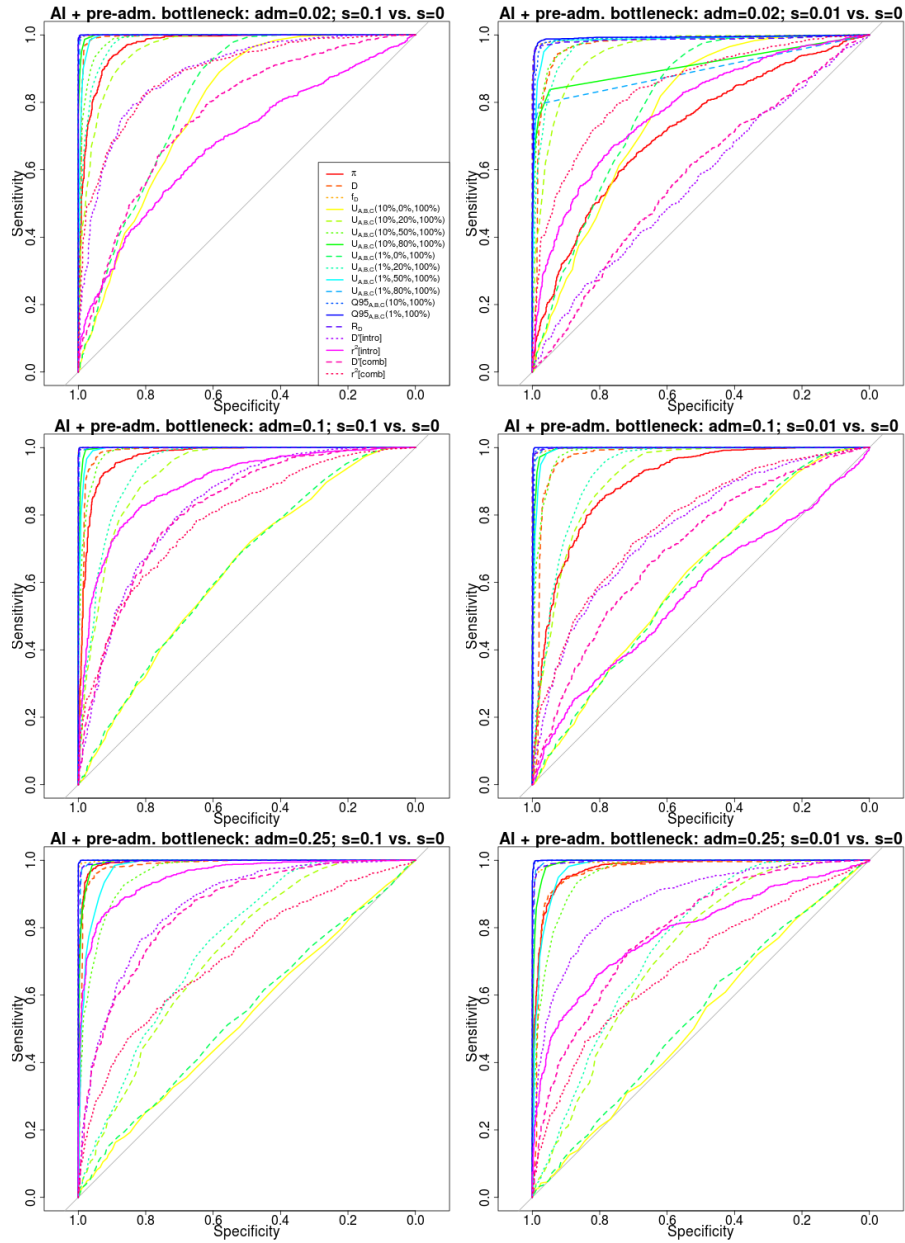


Figure S10: Receiver operating characteristic curves for adaptive introgression with a pre-admixture bottleneck, using 1,000 simulations under adaptive introgression. We simulated the same demography as in Figure 3, but also included a 5X bottleneck in population  $B$  before the introgression event, starting 3,000 generations ago and finishing 2,800 generations ago.

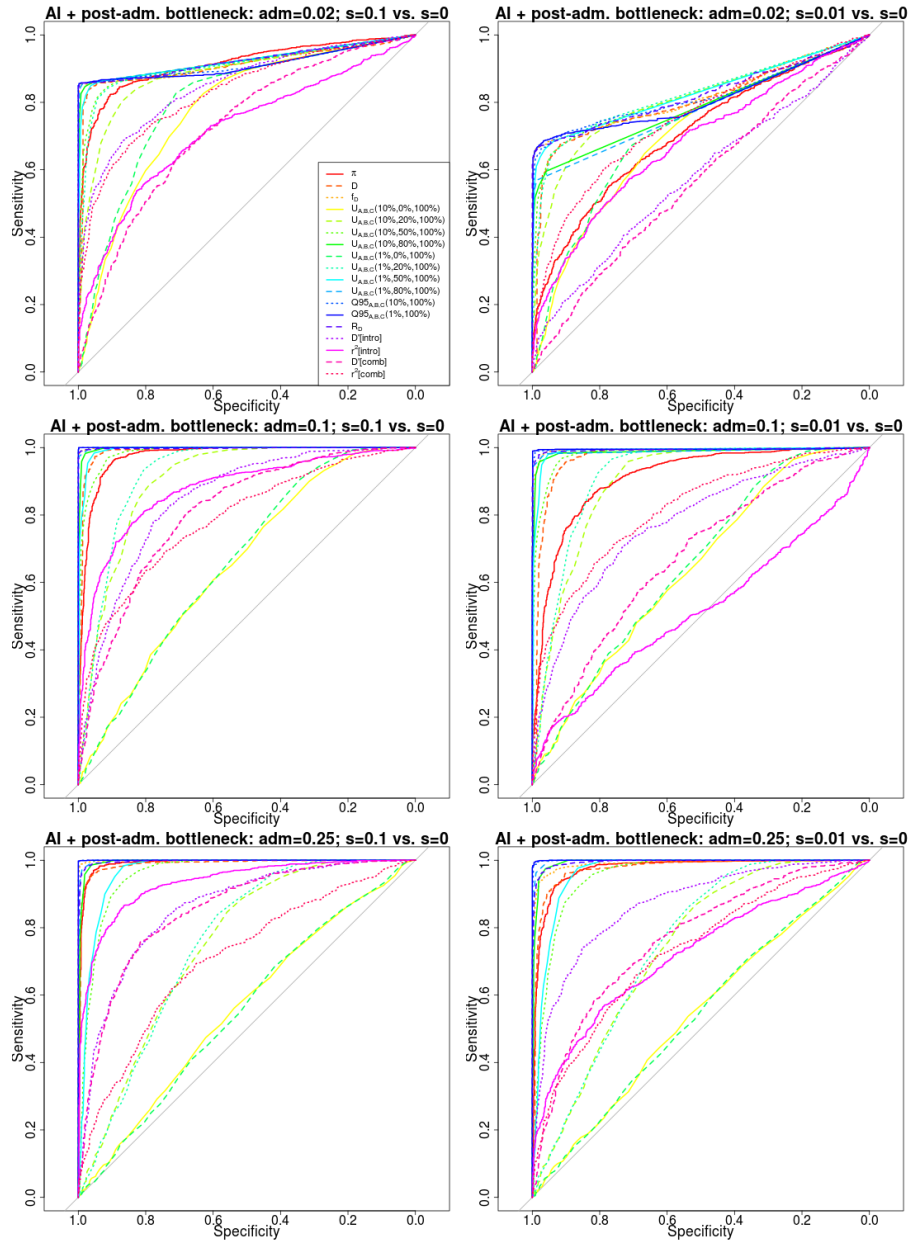


Figure S11: Receiver operating characteristic curves for adaptive introgression with a post-admixture bottleneck, using 1,000 simulations under adaptive introgression. We simulated the same demography as in Figure 3, but also included a 5X bottleneck in population  $B$  after the introgression event, starting 1,400 generations ago and finishing 1,200 generations ago.

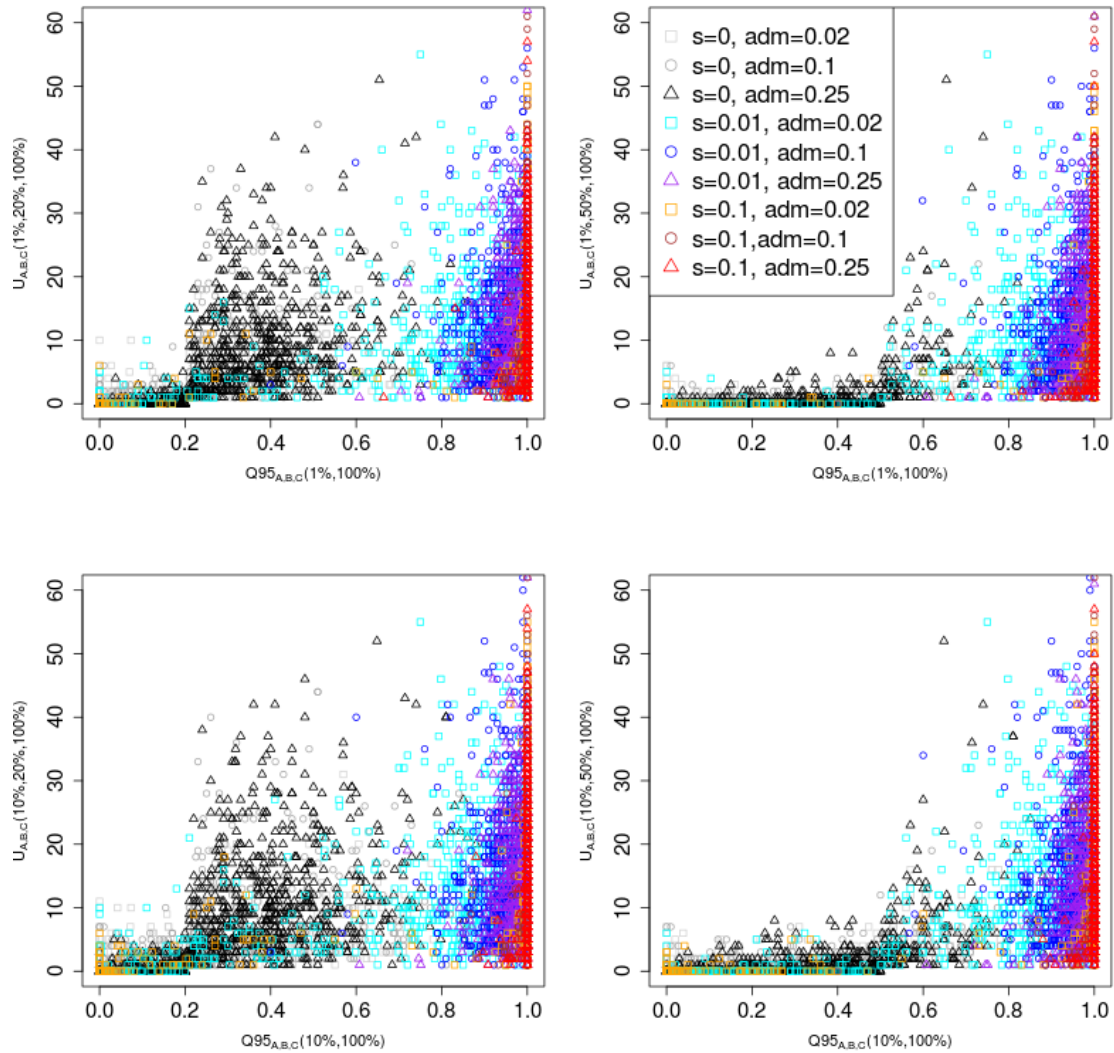


Figure S12: Joint distribution of  $Q95_{A,B,C}(w, y)$  and  $U_{A,B,C}(w, x, y)$  for different choices of  $w$  (1%, 10%) and  $x$  (20%, 50%). We set  $y$  to 100% in all cases. 100 individuals were sampled from panel A, 100 from panel B and 2 from panel C. In this case, we included a 5X bottleneck in population  $B$  after the introgression event, starting 1,400 generations ago and finishing 1,200 generations ago.



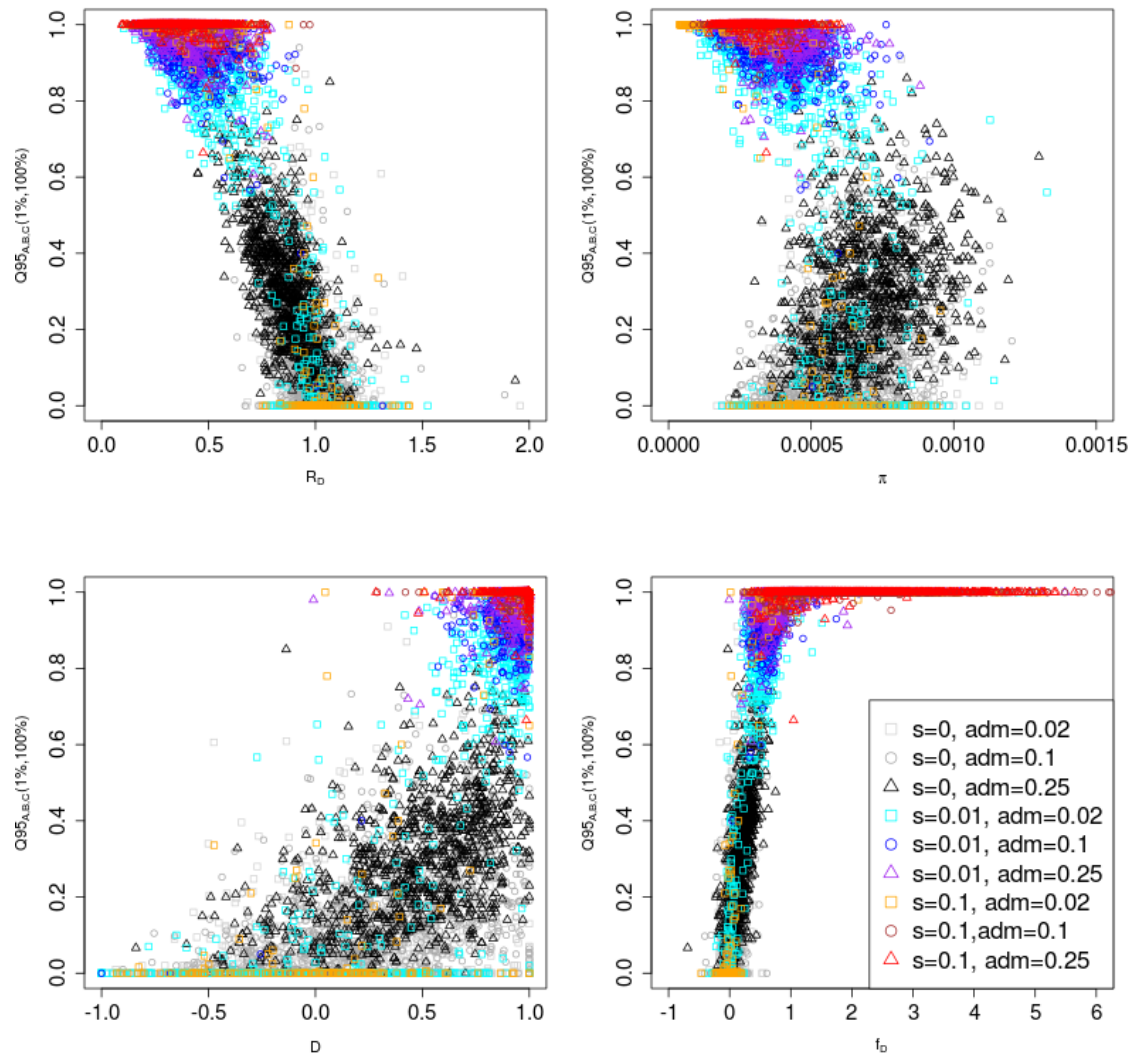


Figure S13: Joint distribution of  $Q95_{A,B,C}(1\%, 100\%)$  and other statistics ( $R_D$ ,  $\pi$ ,  $D$  and  $f_D$ ). 100 individuals were sampled from panel A, 100 from panel B and 2 from panel C. In this case, we included a 5X bottleneck in population  $B$  after the introgression event, starting 1,400 generations ago and finishing 1,200 generations ago.

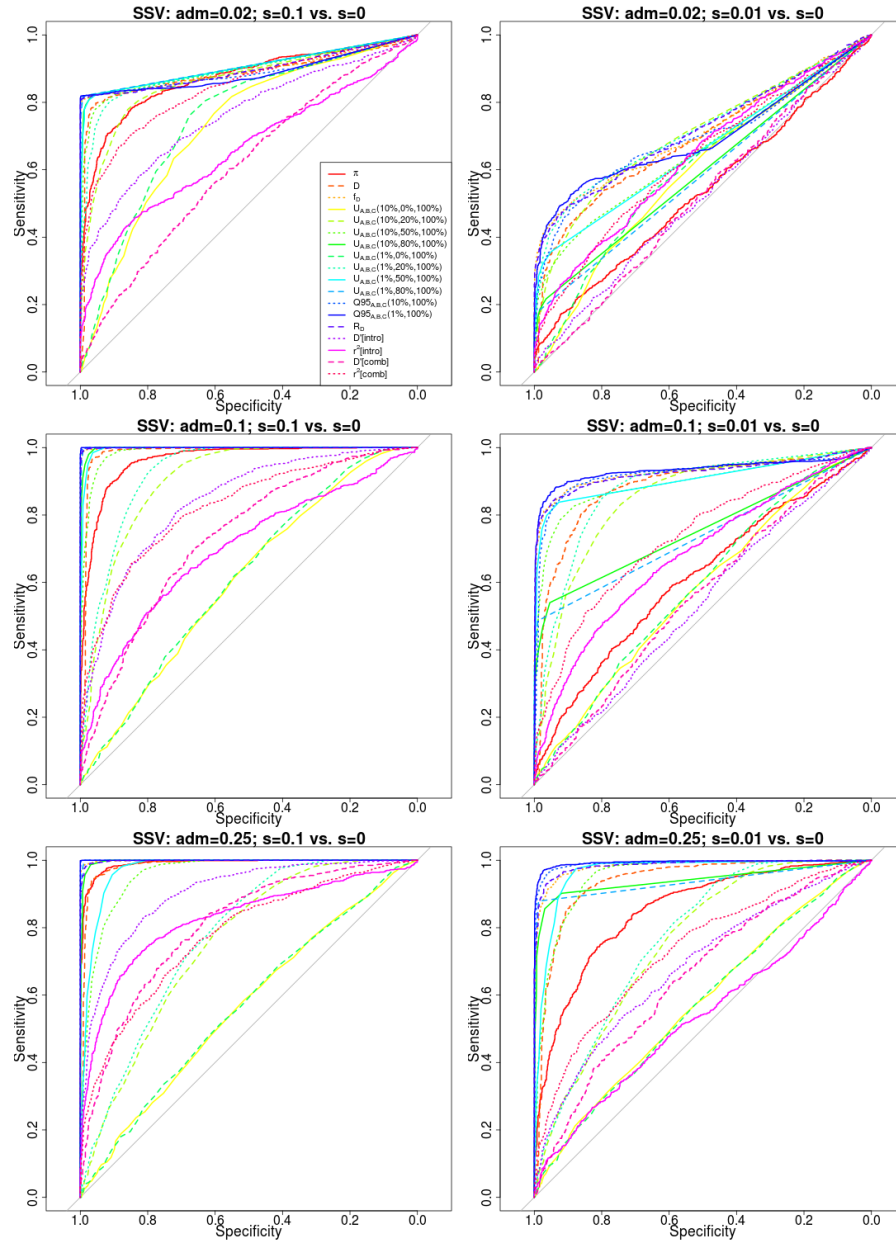


Figure S14: Receiver operating characteristic curves for adaptive introgression with an intermediate neutrality period. We simulated the same demography as in Figure 3, but changed the selection coefficient of the beneficial variant to be 0 right after the introgression event (1,600 generations ago). If still present in population  $B$ , the variant regained its original coefficient 800 generations ago.

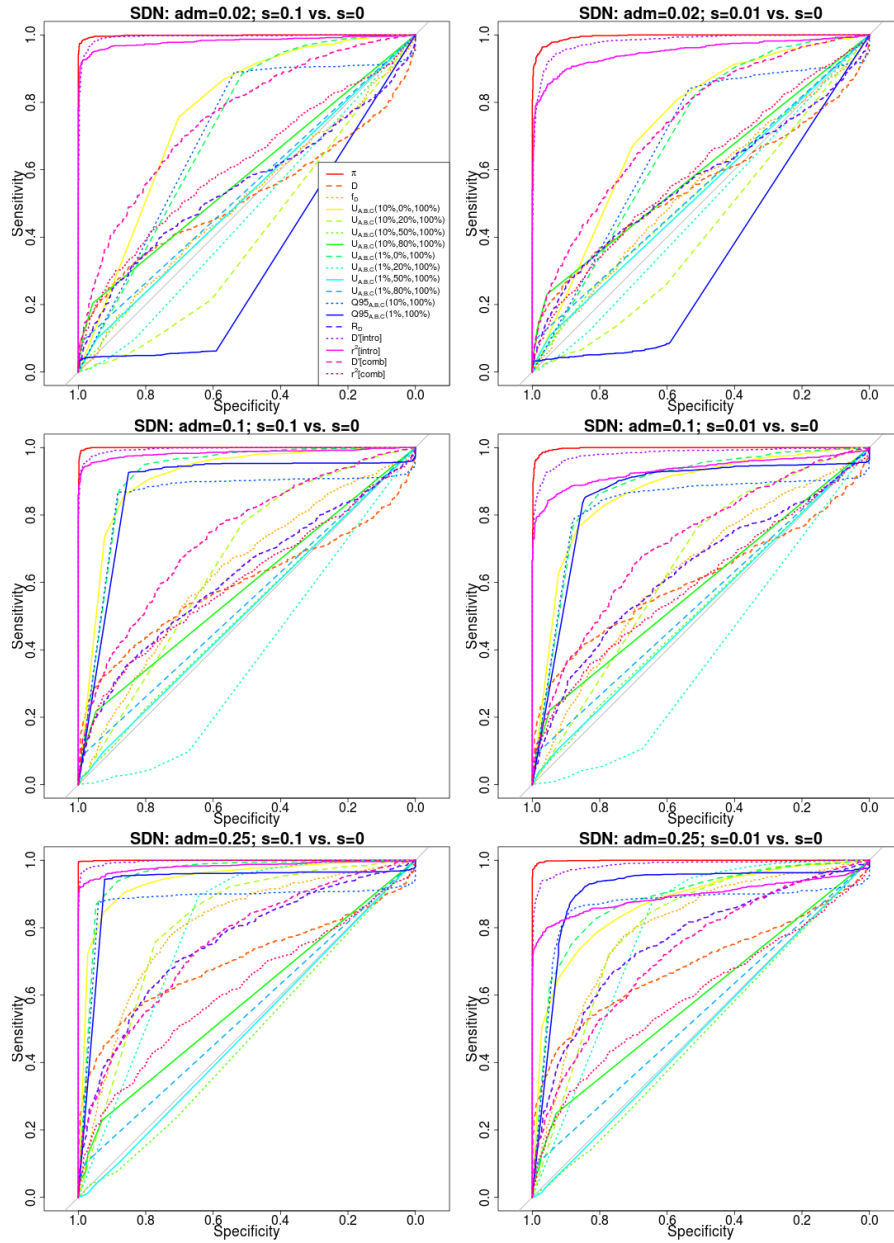


Figure S15: Receiver operating characteristic curves for a selective sweep from de novo mutation. We simulated the same demography as in Figure 3, but rather than introducing the beneficial variant in the introgressed population via admixture from an archaic population, we introduced it by mutation in the introgressed population ( $B$ ) 3,900 generations ago.

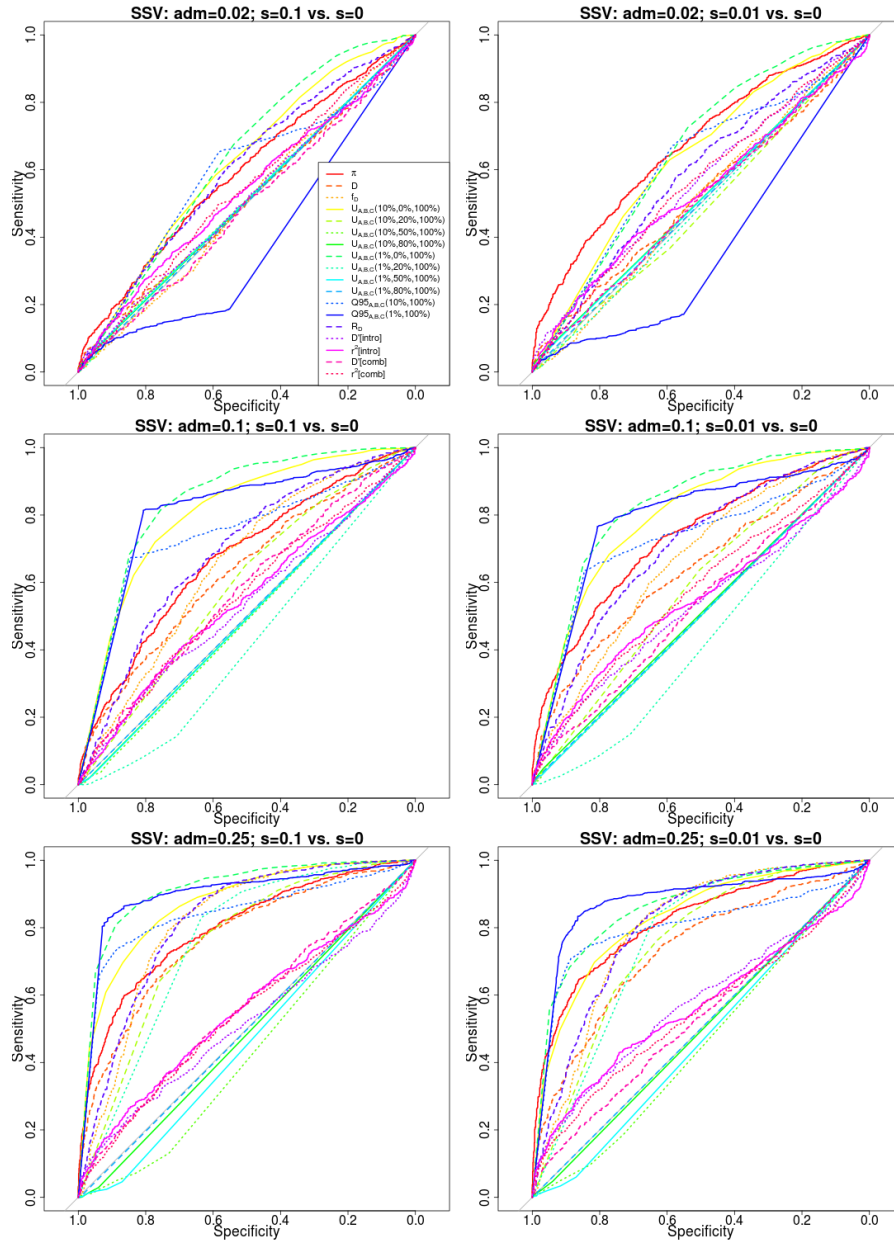


Figure S16: Receiver operating characteristic curves for selection from standing variation. We simulated the same demography as in Figure 3, but rather than introducing the beneficial variant in the introgressed population via admixture from an archaic population, we introduced it with a starting frequency of 20% in the introgressed population ( $B$ ) 3,900 generations ago.

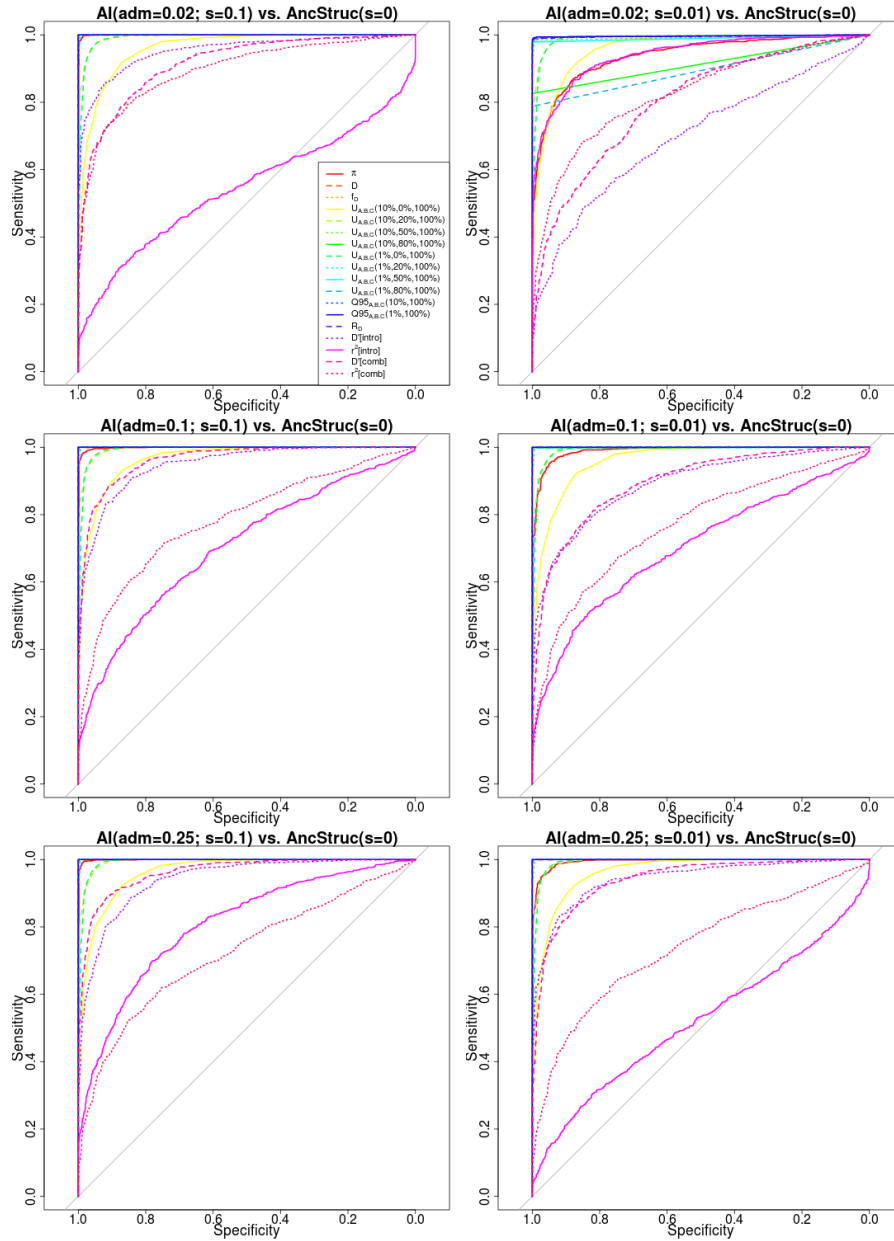


Figure S17: Receiving operating characteristic curves for adaptive introgression against a neutral ancestral structure model with strong migration rates. The demographic scenario for adaptive introgression was the same as in Figure 3. For a description of the ancestral structure model, see main text.

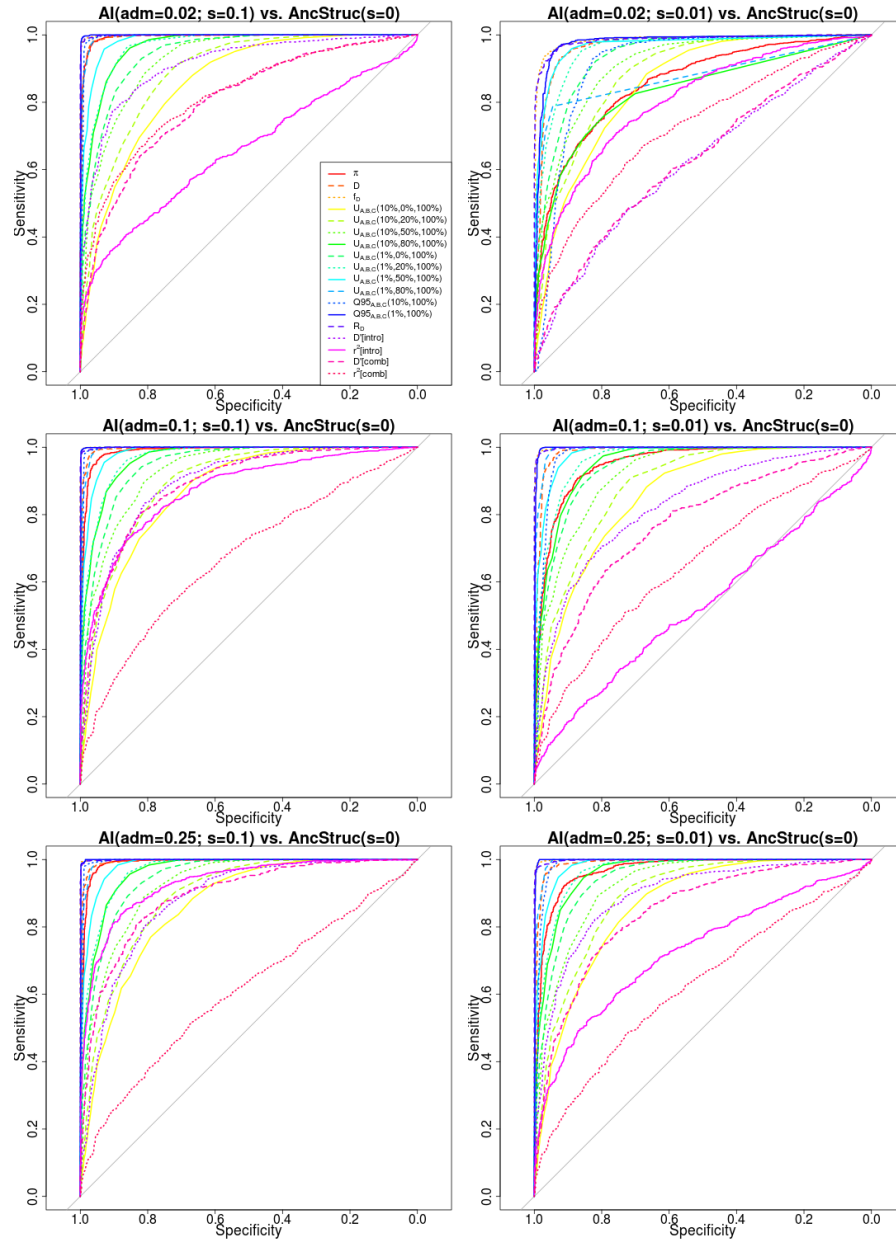


Figure S18: Receiving operating characteristic curves for adaptive introgression against a neutral ancestral structure model with intermediate migration rates. The demographic scenario for adaptive introgression was the same as in Figure 3. For a description of the ancestral structure model, see main text.

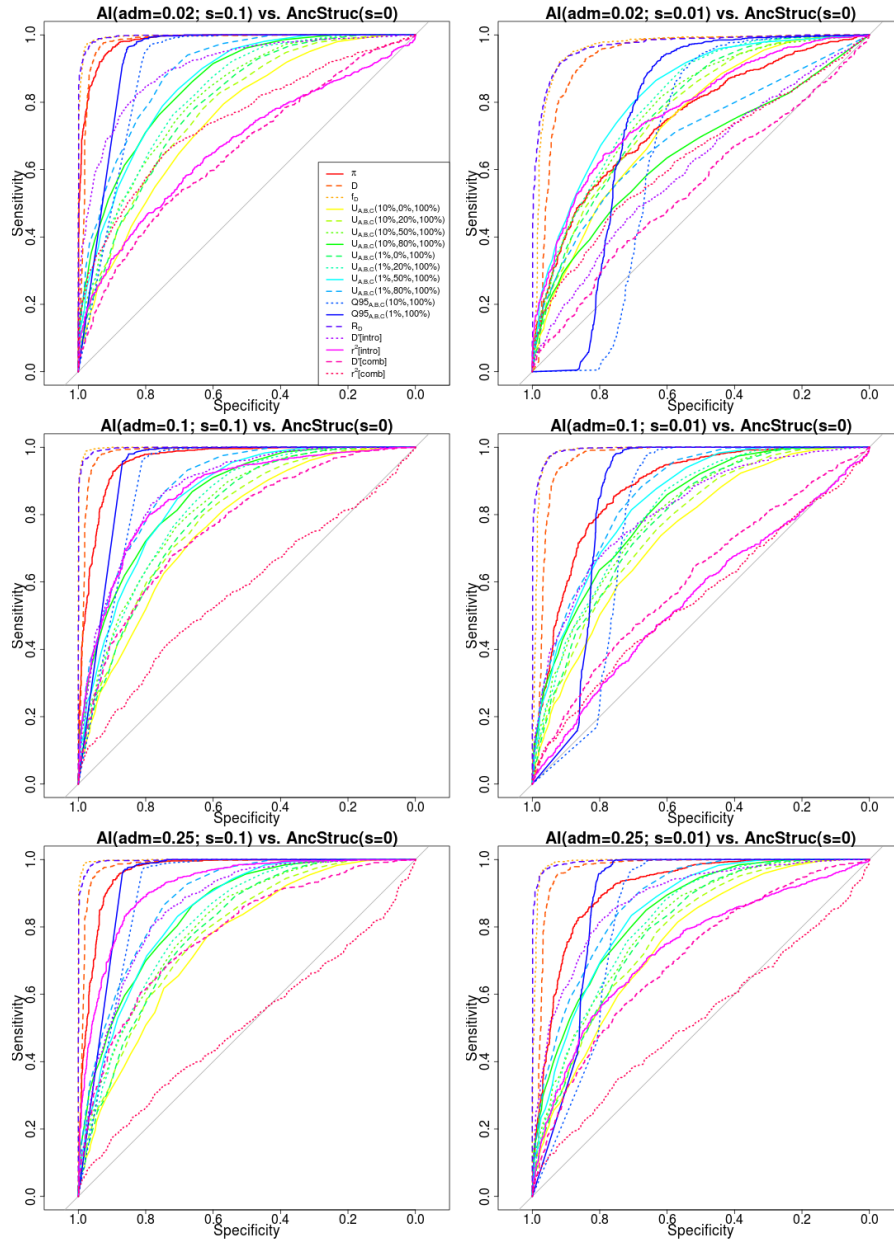


Figure S19: Receiving operating characteristic curves for adaptive introgression against a neutral ancestral structure model with weak migration rates. The demographic scenario for adaptive introgression was the same as in Figure 3. For a description of the ancestral structure model, see main text.

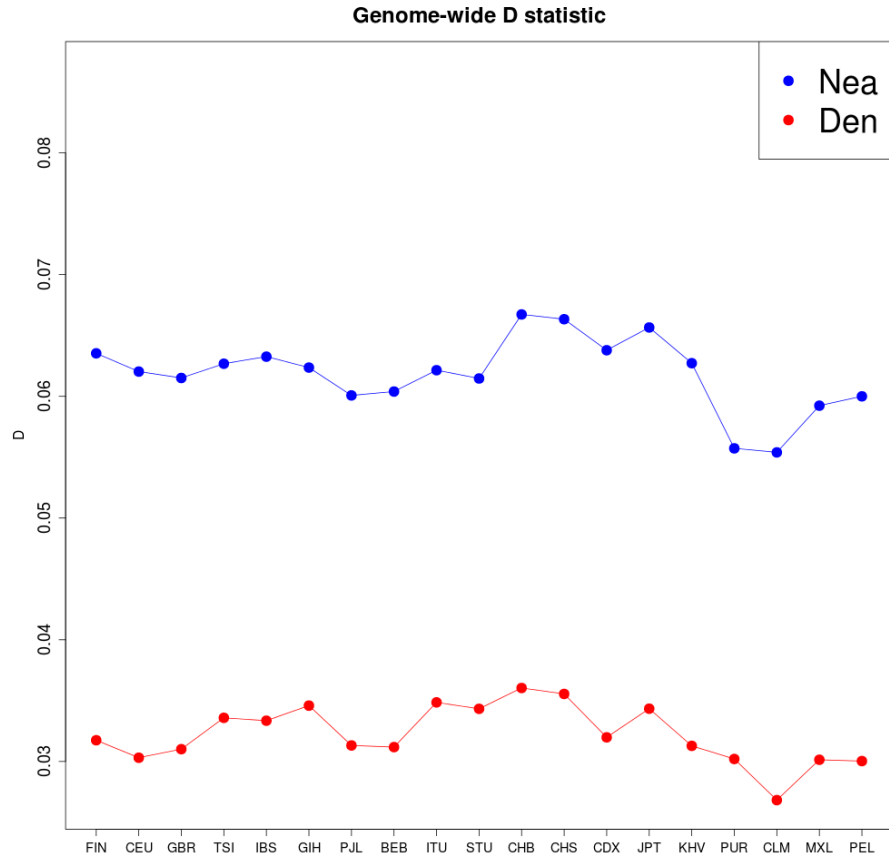


Figure S20: We computed  $D(X, YRI, Y, \text{Chimpanzee})$  for different choices of present-day human panels  $X$  (x-axis) from phase 3 of the 1000 Genomes Project, and for two high-coverage archaic human genomes  $Y$ : Altai Neanderthal (blue) and Denisova (red). The low value of the right-most panel is due to that panel being composed of African-Americans, which have a higher proportion of African ancestry than the other panels.



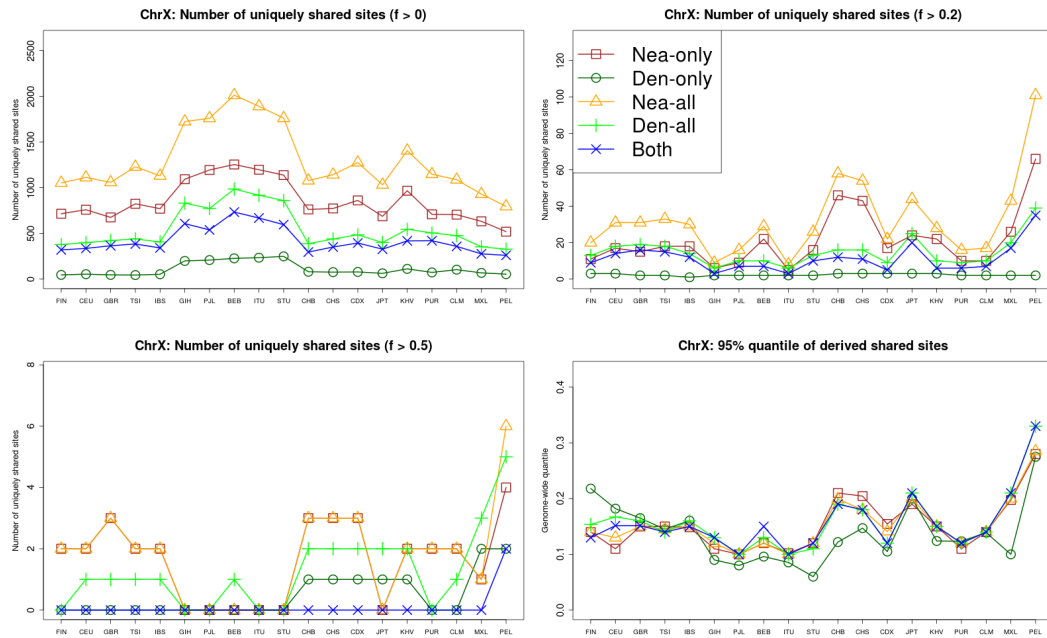


Figure S21: We computed the number of uniquely shared sites in the X chromosome between particular archaic humans genomes and different choices of present-day non-African human panels X (x-axis) from phase 3 of the 1000 Genomes Project, using a shared frequency cutoff of 0% (top-left panel), 20% (top-right panel) and 50% (bottom-left panel). Nea-only =  $U_{Afr,X,Nea,Den}(1\%, 20\%, 100\%, 0\%)$ . Den-only =  $U_{Afr,X,Nea,Den}(1\%, 20\%, 0\%, 100\%)$ . Nea-all =  $U_{Afr,X,Nea}(1\%, 20\%, 100\%)$ . Den-all =  $U_{Afr,X,Den}(1\%, 20\%, 100\%)$ . Both =  $U_{Afr,X,Nea,Den}(1\%, 20\%, 100\%, 100\%)$ . We also computed the quantile statistics Q95 for different choices of present-day non-African human panels (x-axis) from phase 3 of the 1000 Genomes Project (bottom-right panel). Nea-only =  $Q95_{Afr,X,Nea,Den}(1\%, 100\%, 0\%)$ . Den-only =  $Q95_{Afr,X,Nea,Den}(1\%, 0\%, 100\%)$ . Nea-all =  $Q95_{Afr,X,Nea}(1\%, 100\%)$ . Den-all =  $Q95_{Afr,X,Den}(1\%, 50\%, 100\%)$ . Both =  $Q95_{Afr,X,Nea,Den}(1\%, 100\%, 100\%)$ .

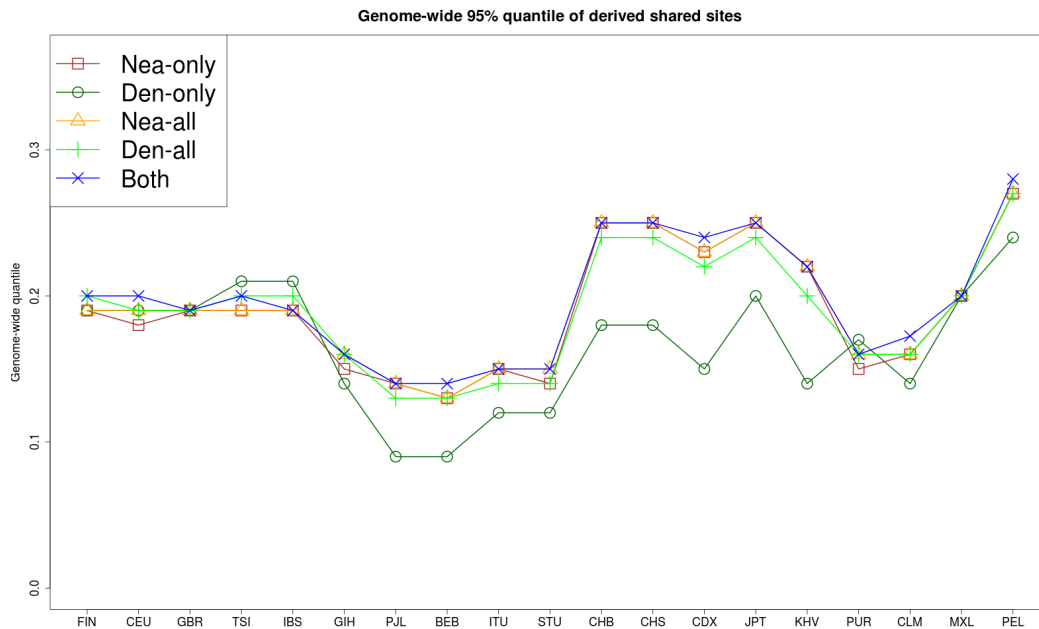


Figure S22: We computed the quantile statistics  $Q95$  for different choices of present-day non-African human panels (x-axis) from phase 3 of the 1000 Genomes Project (D). Nea-only =  $Q95_{Afr,X,Nea,Den}(1\%, 100\%, 0\%)$ . Den-only =  $Q95_{Afr,X,Nea,Den}(1\%, 0\%, 100\%)$ . Nea-all =  $Q95_{Afr,X,Nea}(1\%, 100\%)$ . Den-all =  $Q95_{Afr,X,Den}(1\%, 100\%)$ . Both =  $Q95_{Afr,X,Nea,Den}(1\%, 100\%, 100\%)$ .

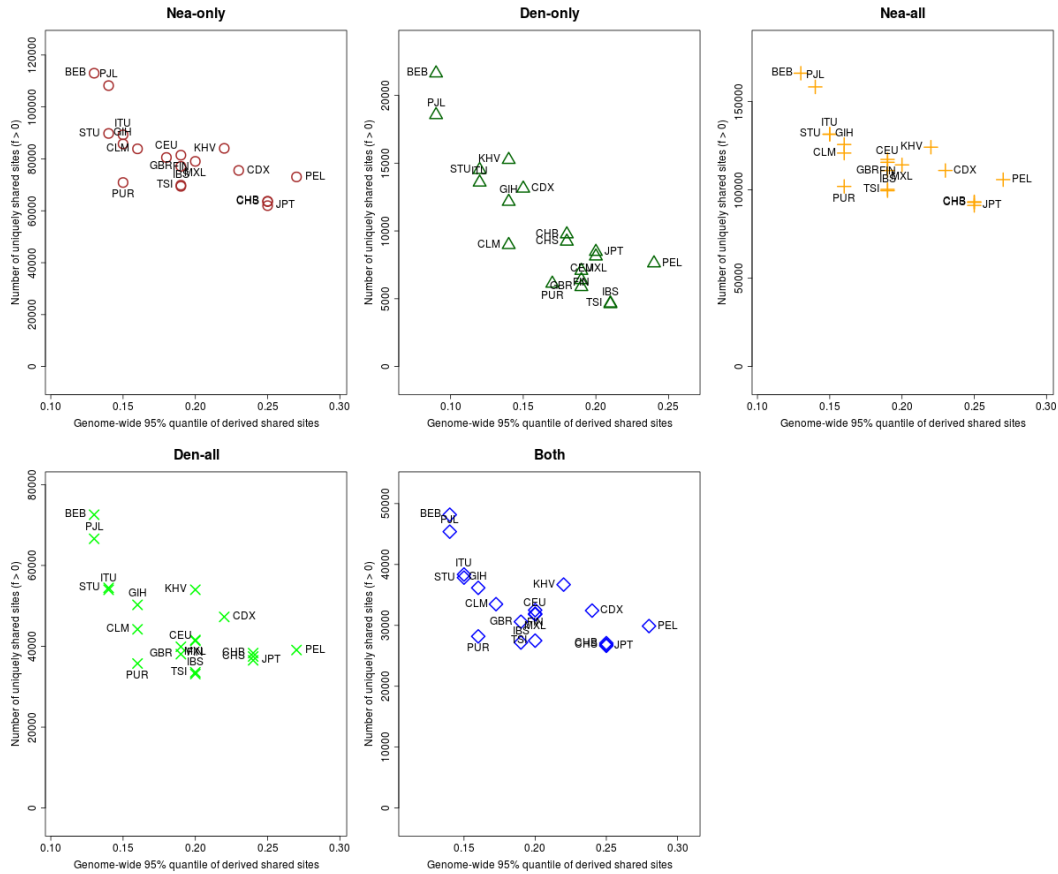


Figure S23: For each population panel from the 1000 Genomes Project, we jointly plotted the  $U$  and  $Q_{95}$  statistics with an archaic frequency cutoff of  $> 0\%$  within each population. Nea-only =  $U_{Afr,X,Nea,Den}(1\%, 0\%, 100\%, 0\%)$  and  $Q_{95Afr,X,Nea,Den}(1\%, 100\%, 0\%)$ . Den-only =  $U_{Afr,X,Nea,Den}(1\%, 0\%, 0\%, 100\%)$  and  $Q_{95Afr,X,Nea,Den}(1\%, 0\%, 100\%)$ . Nea-all =  $U_{Afr,X,Nea}(1\%, 0\%, 100\%)$  and  $Q_{95Afr,X,Nea}(1\%, 100\%)$ . Den-all =  $U_{Afr,X,Den}(1\%, 0\%, 100\%)$  and  $Q_{95Afr,X,Den}(1\%, 100\%)$ . Both =  $U_{Afr,X,Nea,Den}(1\%, 0\%, 100\%, 100\%)$  and  $Q_{95Afr,X,Nea,Den}(1\%, 100\%, 100\%)$ .

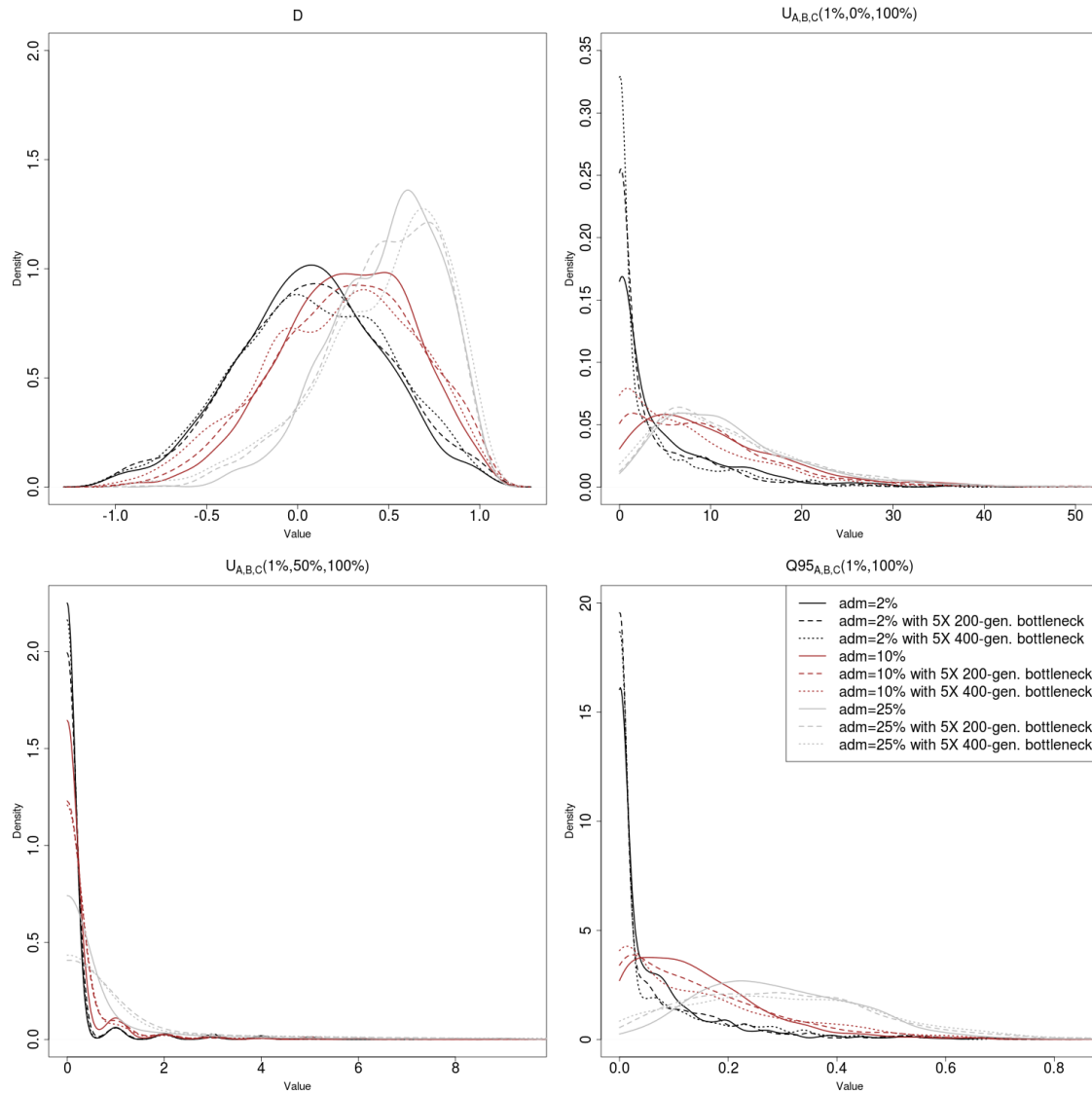


Figure S24: Effect of bottlenecks after the admixture event on the distribution of various statistics under introgression and neutrality.

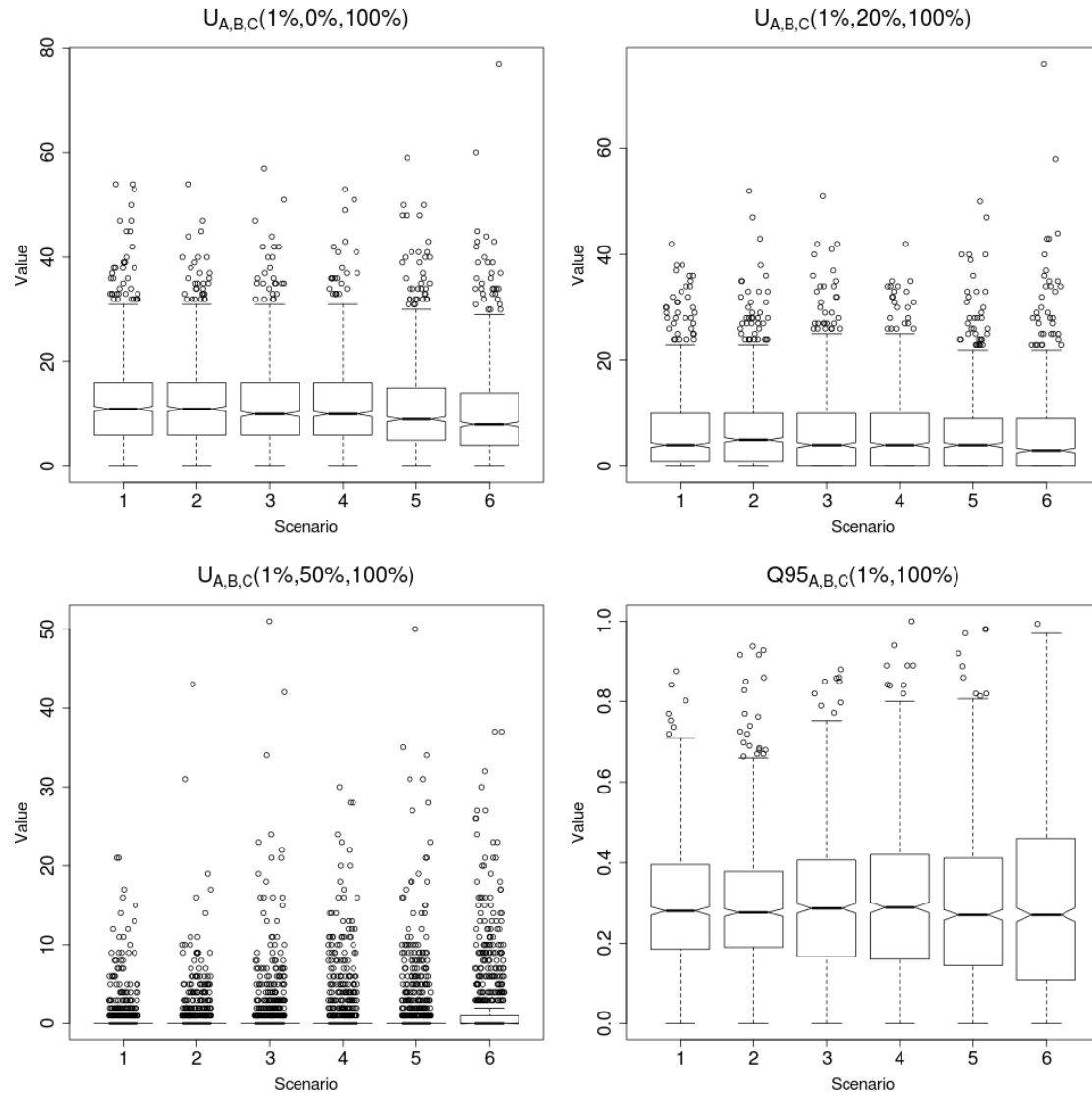


Figure S25: Boxplots showing the effect of different types of bottlenecks on the distribution of  $U$  and  $Q_{95}$  under neutrality. We performed 1,000 simulations for each of 6 different 3-population scenarios with 25% admixture from population C into population B, following the models described in Figure 2. Scenario 1: Constant population size (Figure 2.A). Scenario 2: Pre-admixture 5X bottleneck for 200 generations (Figure 2.B). Scenario 3: Post-admixture 5X bottleneck for 200 generations (Figure 2.C). Scenario 4: Post-admixture 5X bottleneck for 400 generations. Scenario 5: Post-admixture 10X bottleneck for 200 generations. Scenario 6: Post-admixture 10X bottleneck for 400 generations.

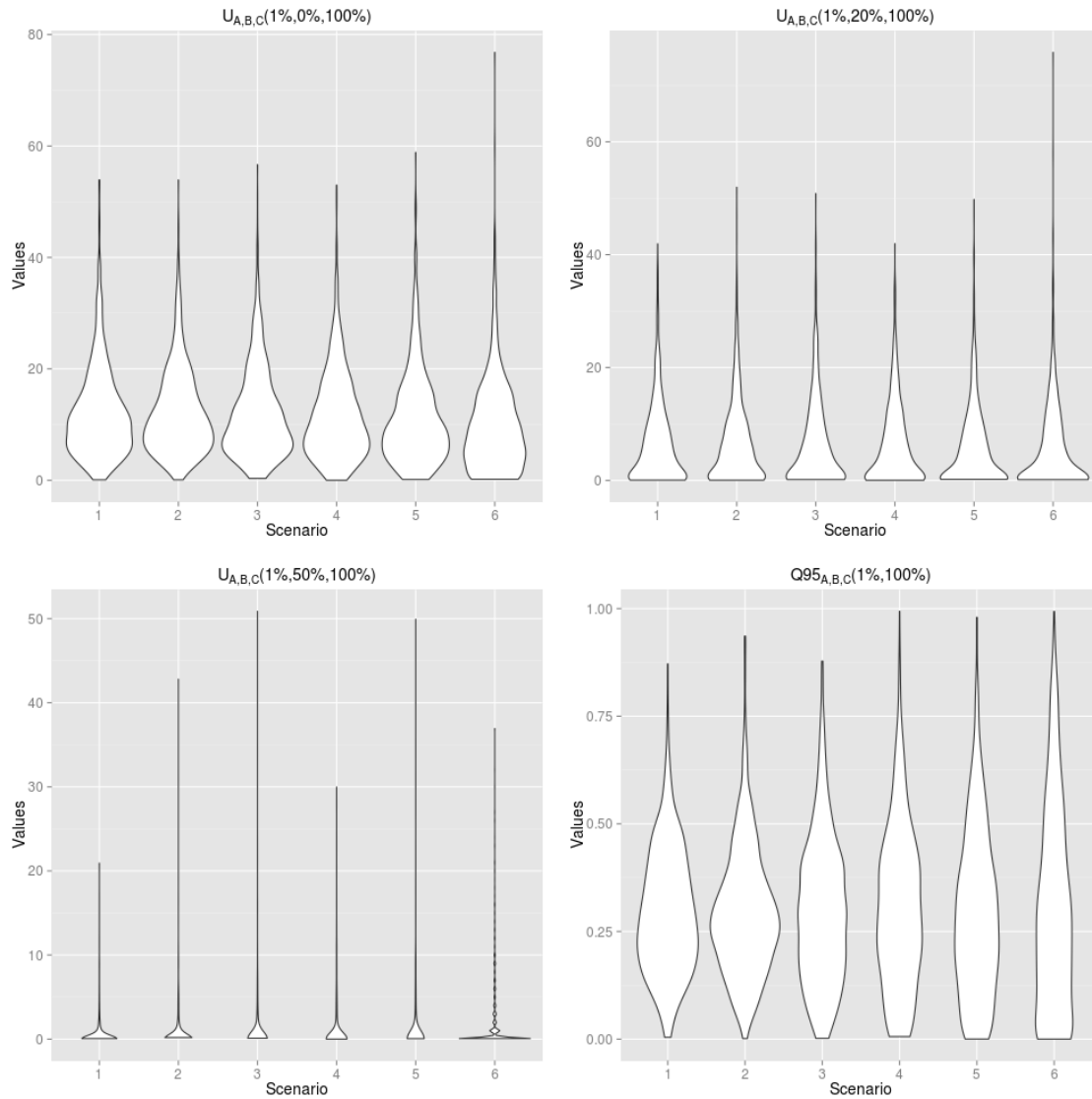


Figure S26: Violin plots showing the effect of different types of bottlenecks on the distribution of  $U$  and  $Q95$  under neutrality (this is the same data as Figure S25). We performed 1,000 simulations for each of 6 different 3-population scenarios with 25% admixture from population C into population B, following the models described in Figure 2. Scenario 1: Constant population size (Figure 2.A). Scenario 2: Pre-admixture 5X bottleneck for 200 generations (Figure 2.B). Scenario 3: Post-admixture 5X bottleneck for 200 generations (Figure 2.C). Scenario 4: Post-admixture 5X bottleneck for 400 generations. Scenario 5: Post-admixture 10X bottleneck for 200 generations. Scenario 6: Post-admixture 10X bottleneck for 400 generations.

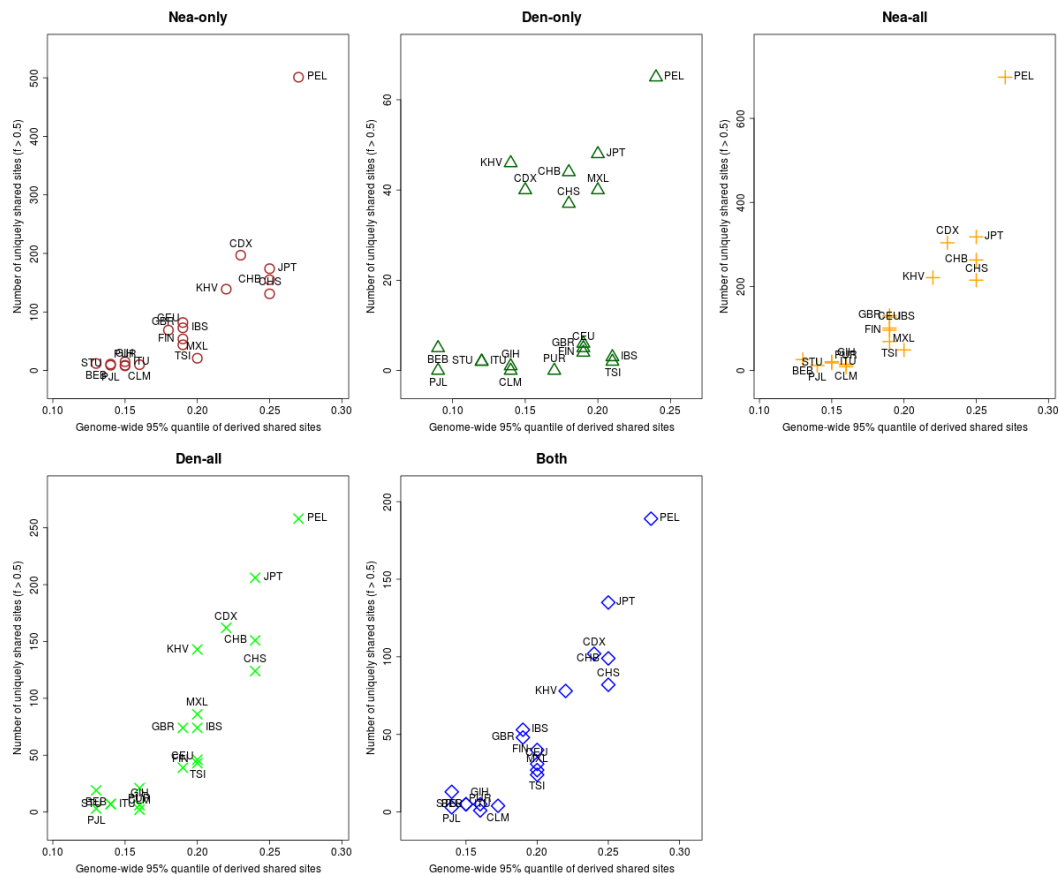


Figure S27: For each population panel from the 1000 Genomes Project, we jointly plotted the  $U$  and  $Q_{95}$  statistics with an archaic frequency cutoff of  $> 50\%$  within each population. Nea-only =  $U_{Afr,X,Nea,Den}(1\%, 50\%, 100\%, 0\%)$  and  $Q_{95Afr,X,Nea,Den}(1\%, 100\%, 0\%)$ . Den-only =  $U_{Afr,X,Nea,Den}(1\%, 50\%, 0\%, 100\%)$  and  $Q_{95Afr,X,Nea,Den}(1\%, 0\%, 100\%)$ . Nea-all =  $U_{Afr,X,Nea}(1\%, 50\%, 100\%)$  and  $Q_{95Afr,X,Nea}(1\%, 100\%)$ . Den-all =  $U_{Afr,X,Den}(1\%, 50\%, 100\%)$  and  $Q_{95Afr,X,Den}(1\%, 100\%)$ . Both =  $U_{Afr,X,Nea,Den}(1\%, 50\%, 100\%, 100\%)$  and  $Q_{95Afr,X,Nea,Den}(1\%, 100\%, 100\%)$ .

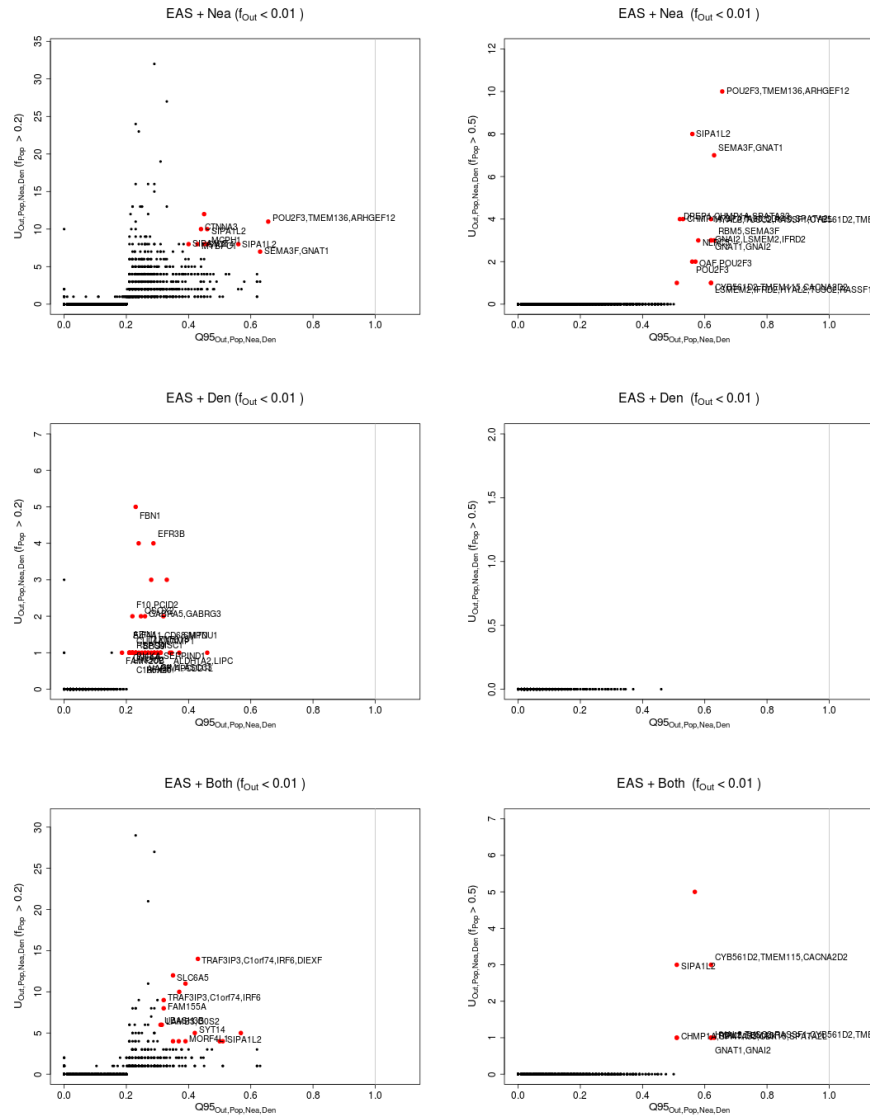


Figure S28: Uniquely shared archaic alleles in an East Asian (EAS) panel. Joint distribution of  $Q95_{EUR+AFR,EAS,Nea,Den}(1\%,y,z)$  and  $U_{EUR+AFR,EAS,Nea,Den}(1\%,x,y,z)$ , for 40kb non-overlapping regions along the genome, using two choices of  $x$  (20% in left column panels, 50% in right column panels). Red dots refer to regions that are in the 99.9% quantiles for both statistics. Neanderthal-specific shared alleles are displayed in the top panels, Denisovan-specific shared alleles are displayed in the middle-row panels, and alleles shared with both archaic human genome are displayed in the bottom panels.

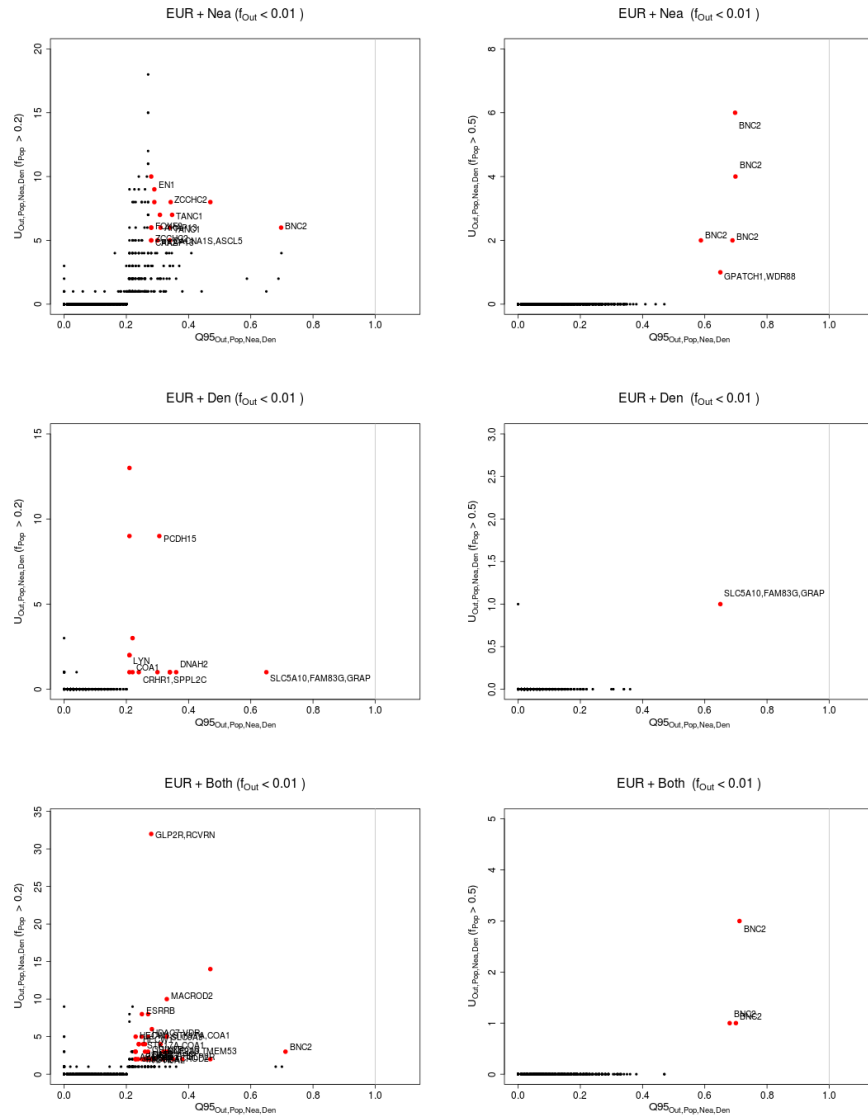


Figure S29: Uniquely shared archaic alleles in an European (EUR) panel. Joint distribution of  $Q95_{EAS+AFR, EUR, Nea, Den}(1\%, y, z)$  and  $U_{EAS+AFR, EUR, Nea, Den}(1\%, x, y, z)$ , for 40kb non-overlapping regions along the genome, using two choices of  $x$  (20% in left column panels, 50% in right column panels). Red dots refer to regions that are in the 99.9th quantiles for both statistics. Neanderthal-specific shared alleles are displayed in the top panels, Denisovan-specific shared alleles are displayed in the middle-row panels, and alleles shared with both archaic human genome are displayed in the bottom panels.



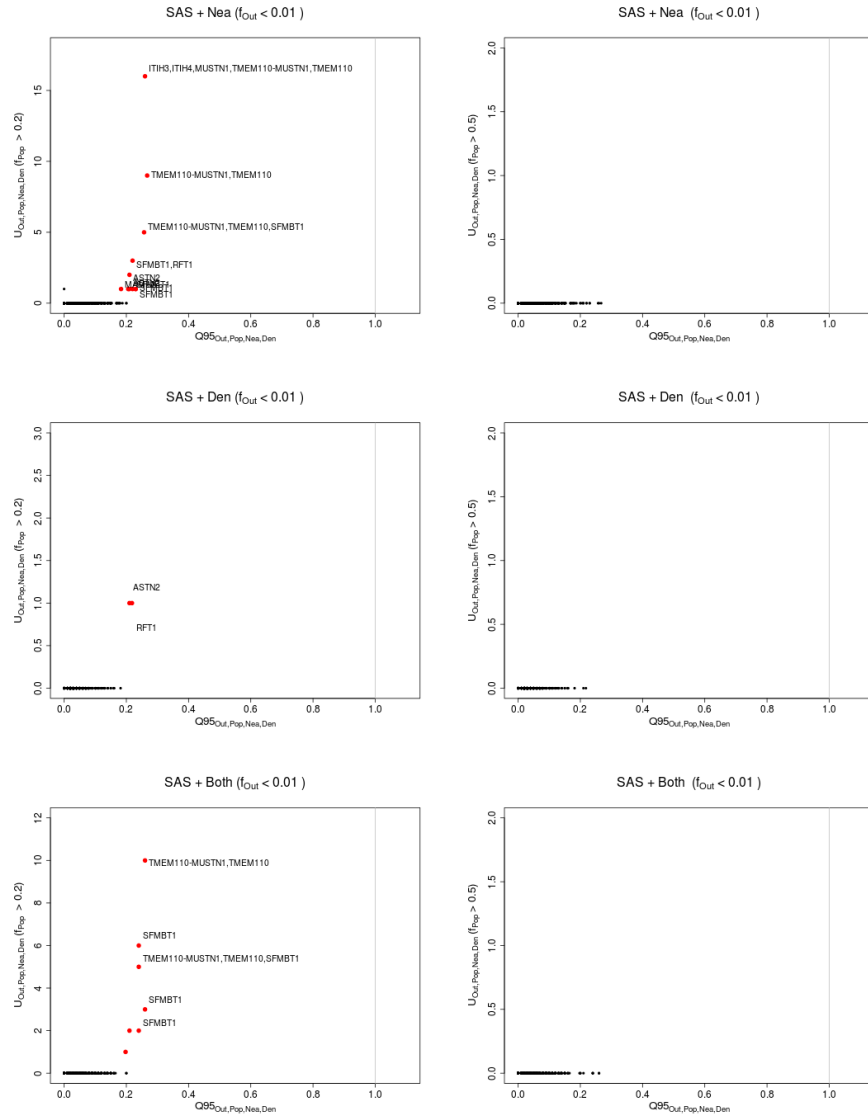


Figure S30: Uniquely shared archaic alleles in a South Asian (SAS) panel. Joint distribution of  $Q95_{EAS+EUR+AFR,SAS,Nea,Den}(1\%, y, z)$  and  $U_{EAS+EUR+AFR,SAS,Nea,Den}(1\%, x, y, z)$ , for 40kb non-overlapping regions along the genome, using two choices of  $x$  (20% in left column panels, 50% in right column panels). Red dots refer to regions that are in the 99.9% quantiles for both statistics. Neanderthal-specific shared alleles are displayed in the top panels, Denisovan-specific shared alleles are displayed in the middle-row panels, and alleles shared with both archaic human genome are displayed in the bottom panels.

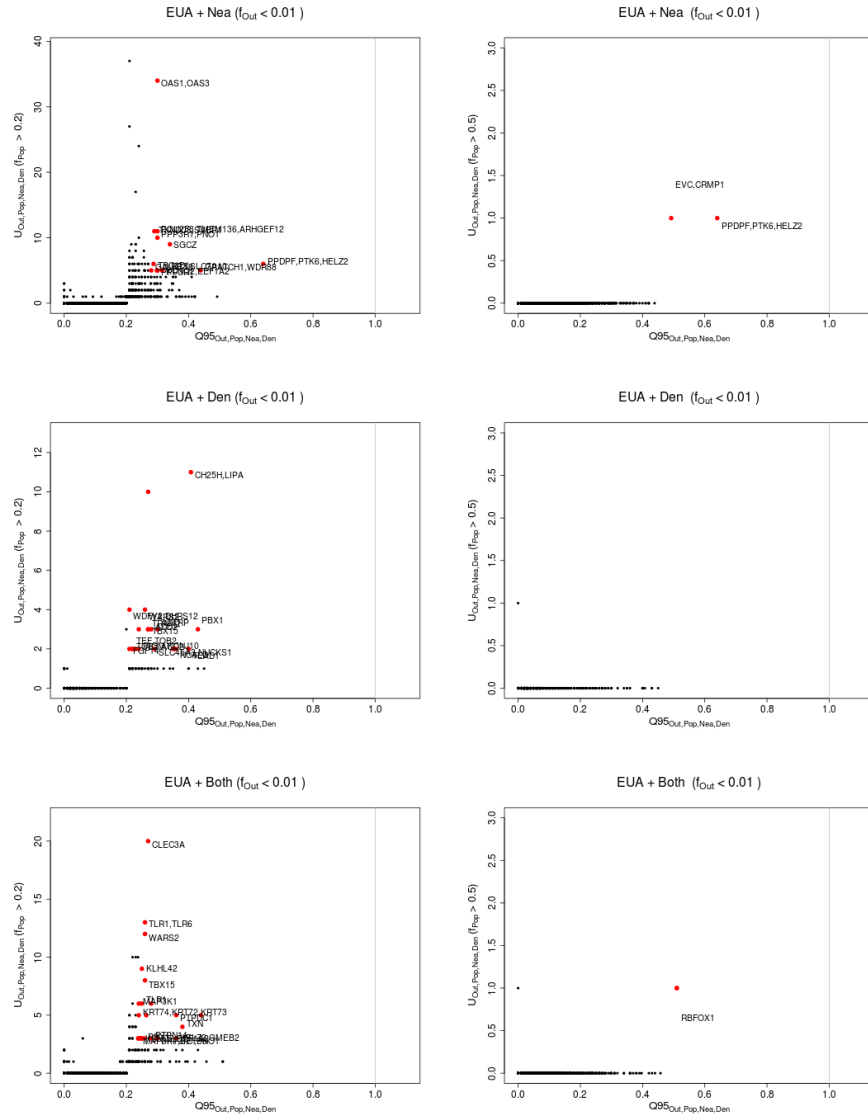


Figure S31: Uniquely shared archaic alleles in a Eurasian (EUA=EUR+SAS+EAS) panel. Joint distribution of  $Q95_{AFR, EUR+SAS+EAS, Nea, Den}(1\%, y, z)$  and  $U_{AFR, EUR+SAS+EAS, Nea, Den}(1\%, x, y, z)$ , for 40kb non-overlapping regions along the genome, using two choices of  $x$  (20% in left column panels, 50% in right column panels). Red dots refer to regions that are in the 99.9% quantiles for both statistics. Neanderthal-specific shared alleles are displayed in the top panels, Denisovan-specific shared alleles are displayed in the middle-row panels, and alleles shared with both archaic human genome are displayed in the bottom panels.

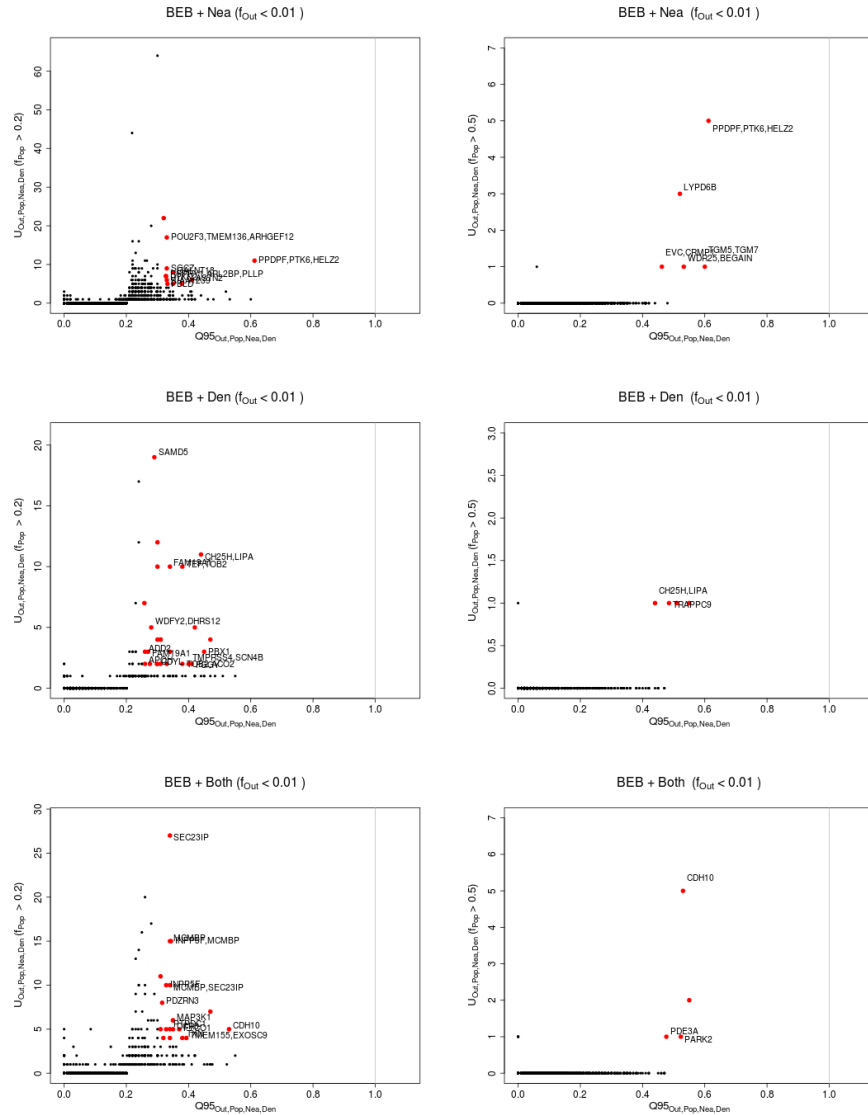


Figure S32: Uniquely shared archaic alleles in a Bengali (BEB) panel. Joint distribution of  $Q95_{AFR,BEB,Nea,Den}(1\%,y,z)$  and  $U_{AFR,BEB,Nea,Den}(1\%,x,y,z)$ , for 40kb non-overlapping regions along the genome, using two choices of  $x$  (20% in left column panels, 50% in right column panels). Red dots refer to regions that are in the 99.9% quantiles for both statistics. Neanderthal-specific shared alleles are displayed in the top panels, Denisovan-specific shared alleles are displayed in the middle-row panels, and alleles shared with both archaic human genome are displayed in the bottom panels.

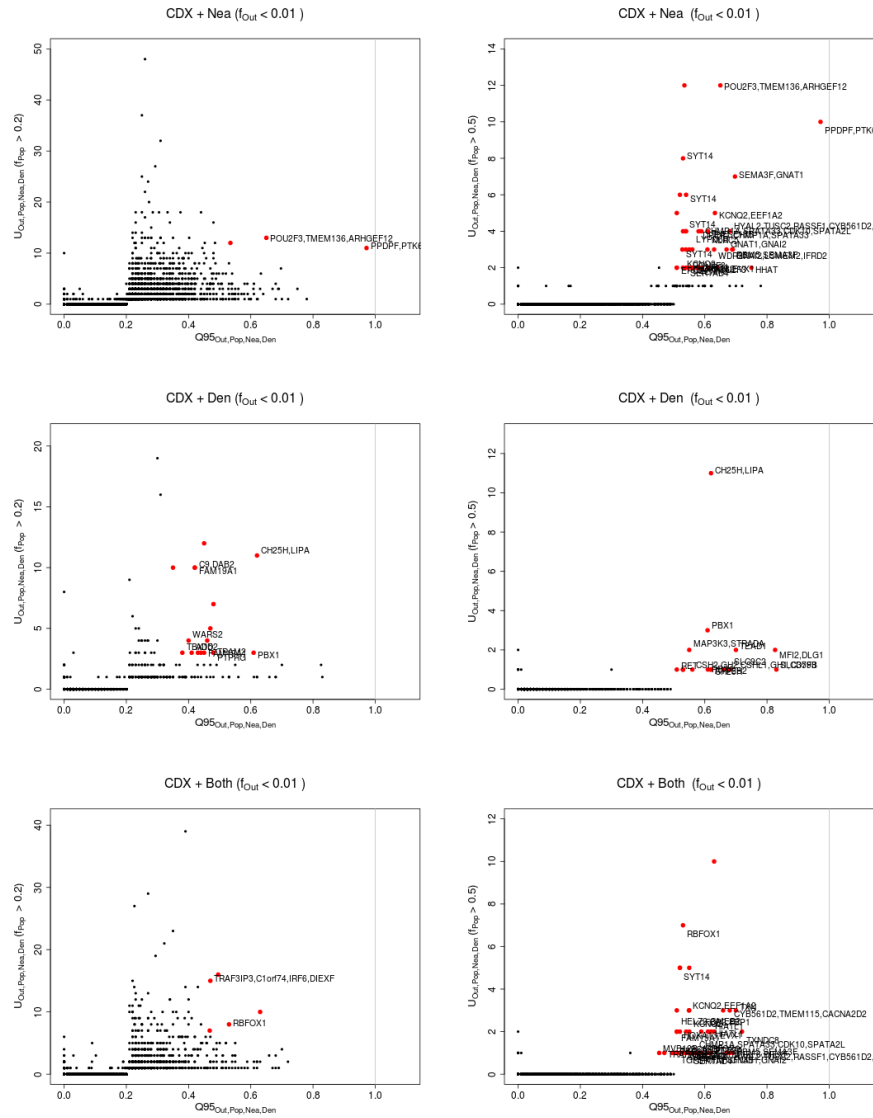


Figure S33: Uniquely shared archaic alleles in a Chinese Dai (CDX) panel. Joint distribution of  $Q95_{AFR,CDX,Nea,Den}(1\%,y,z)$  and  $U_{AFR,CDX,Nea,Den}(1\%,x,y,z)$ , for 40kb non-overlapping regions along the genome, using two choices of  $x$  (20% in left column panels, 50% in right column panels). Red dots refer to regions that are in the 99.9% quantiles for both statistics. Neanderthal-specific shared alleles are displayed in the top panels, Denisovan-specific shared alleles are displayed in the middle-row panels, and alleles shared with both archaic human genome are displayed in the bottom panels.

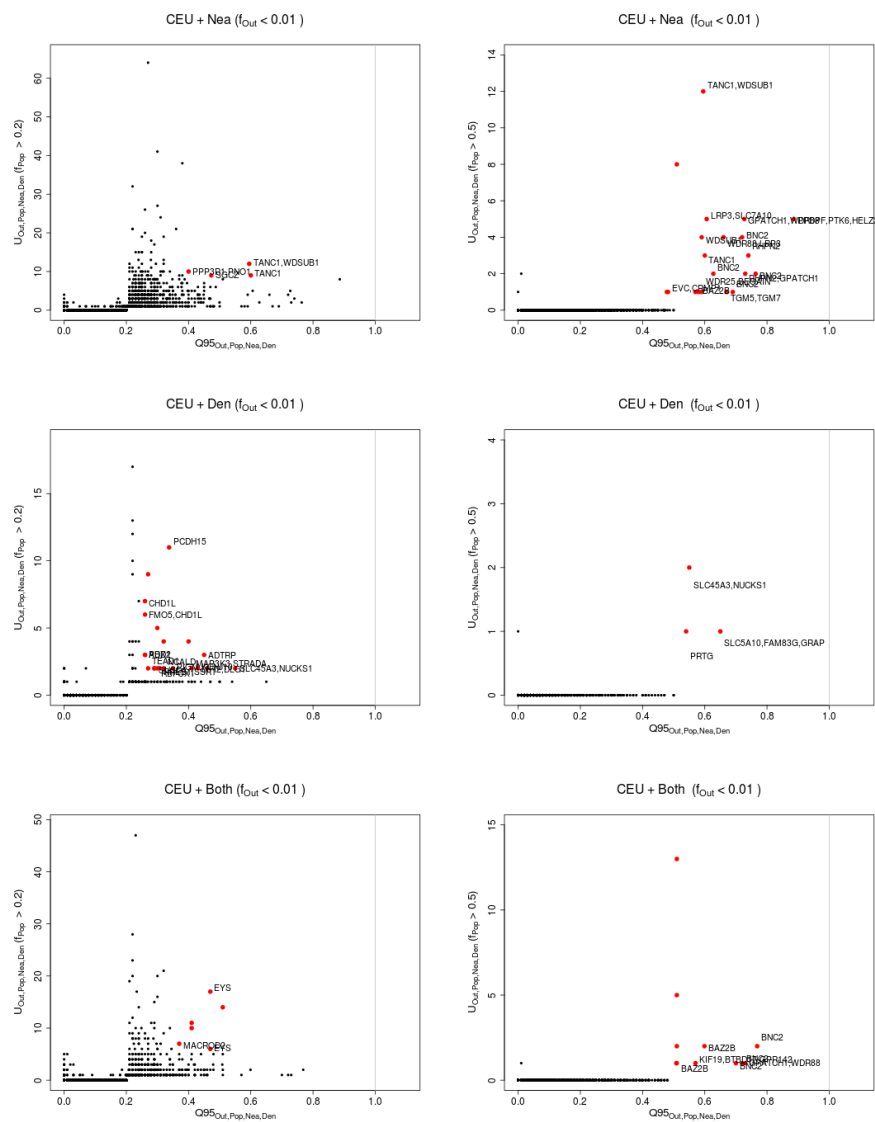


Figure S34: Uniquely shared archaic alleles in a Central European (CEU) panel. Joint distribution of  $Q95_{AFR,CEU,Nea,Den}(1\%,y,z)$  and  $U_{AFR,CEU,Nea,Den}(1\%,x,y,z)$ , for 40kb non-overlapping regions along the genome, using two choices of  $x$  (20% in left column panels, 50% in right column panels). Red dots refer to regions that are in the 99.9% quantiles for both statistics. Neanderthal-specific shared alleles are displayed in the top panels, Denisovan-specific shared alleles are displayed in the middle-row panels, and alleles shared with both archaic human genome are displayed in the bottom panels.

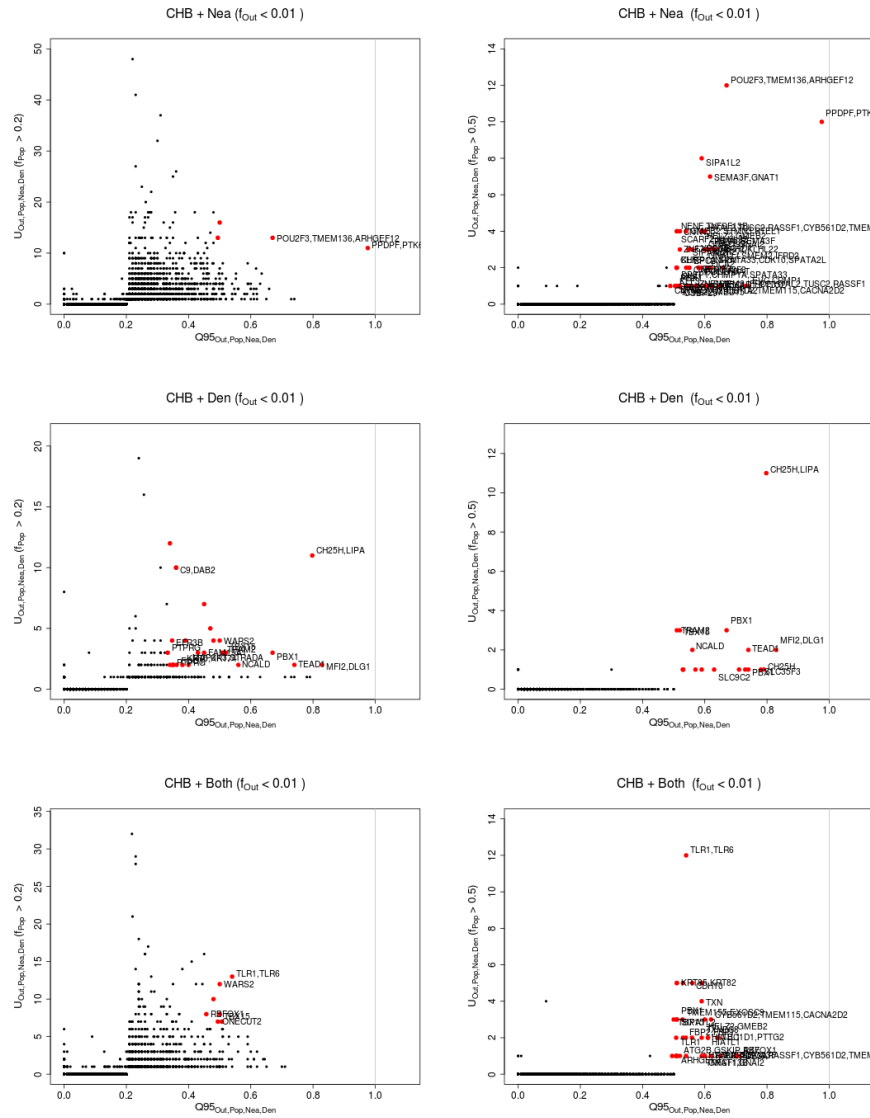


Figure S35: Uniquely shared archaic alleles in a Han Chinese (CHB) panel. Joint distribution of  $Q95_{AFR,CHB,Nea,Den}(1\%, y, z)$  and  $U_{AFR,CHB,Nea,Den}(1\%, x, y, z)$ , for 40kb non-overlapping regions along the genome, using two choices of  $x$  (20% in left column panels, 50% in right column panels). Red dots refer to regions that are in the 99.9% quantiles for both statistics. Neanderthal-specific shared alleles are displayed in the top panels, Denisovan-specific shared alleles are displayed in the middle-row panels, and alleles shared with both archaic human genome are displayed in the bottom panels.

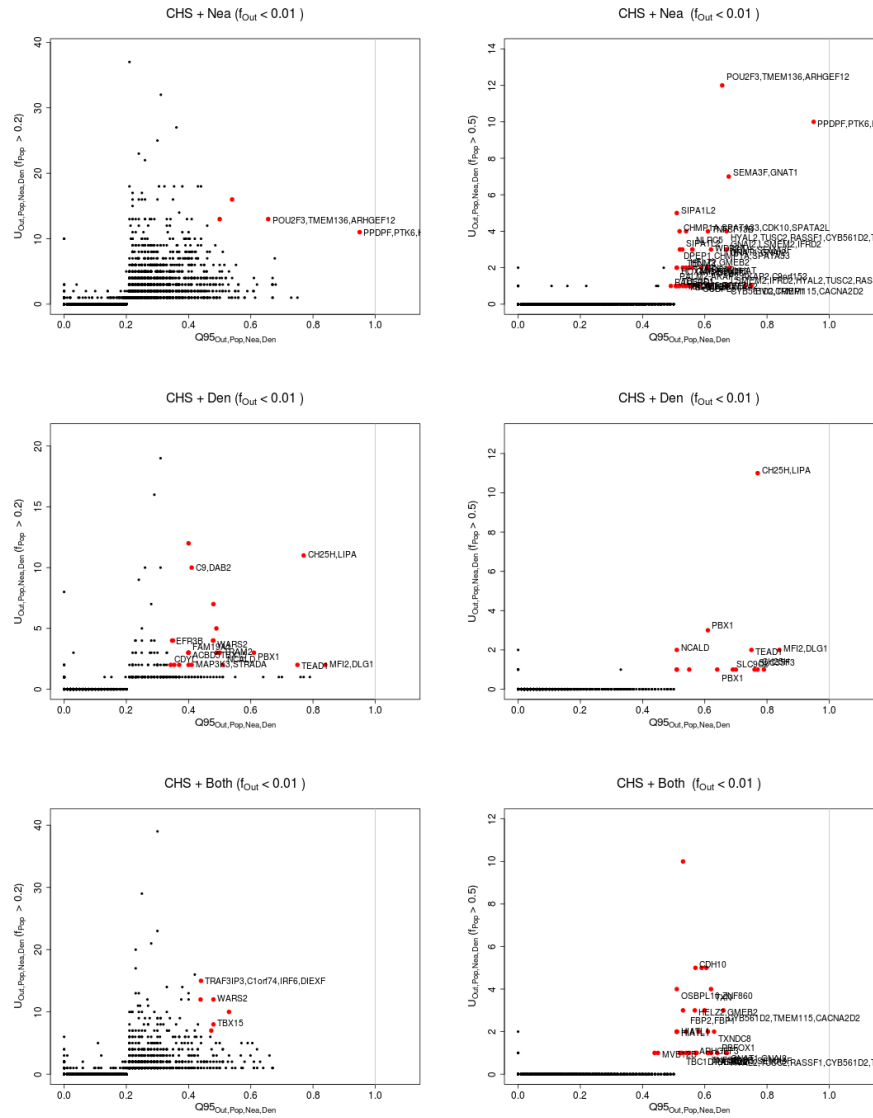


Figure S36: Uniquely shared archaic alleles in a Southern Han Chinese (CHS) panel. Joint distribution of  $Q_{95}^{\text{AFR,BEB,Nea,Den}}(1\%, y, z)$  and  $U_{\text{AFR,CHS,Nea,Den}}(1\%, x, y, z)$ , for 40kb non-overlapping regions along the genome, using two choices of x (20% in left column panels, 50% in right column panels). Red dots refer to regions that are in the 99.9% quantiles for both statistics. Neanderthal-specific shared alleles are displayed in the top panels, Denisovan-specific shared alleles are displayed in the middle-row panels, and alleles shared with both archaic human genome are displayed in the bottom panels.

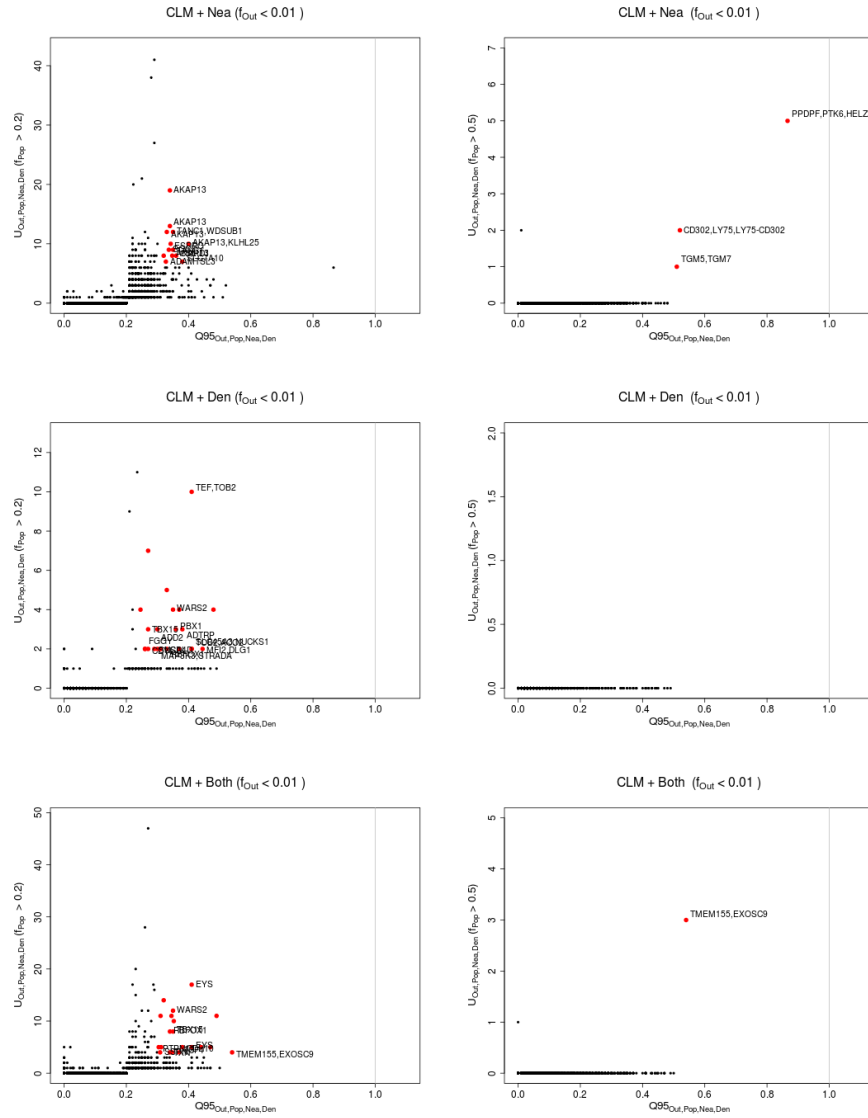


Figure S37: Uniquely shared archaic alleles in a Colombian (CLM) panel. Joint distribution of  $Q95_{AFR,CLM,Nea,Den}(1\%, y, z)$  and  $U_{AFR,CLM,Nea,Den}(1\%, x, y, z)$ , for 40kb non-overlapping regions along the genome, using two choices of  $x$  (20% in left column panels, 50% in right column panels). Red dots refer to regions that are in the 99.9% quantiles for both statistics. Neanderthal-specific shared alleles are displayed in the top panels, Denisovan-specific shared alleles are displayed in the middle-row panels, and alleles shared with both archaic human genome are displayed in the bottom panels.



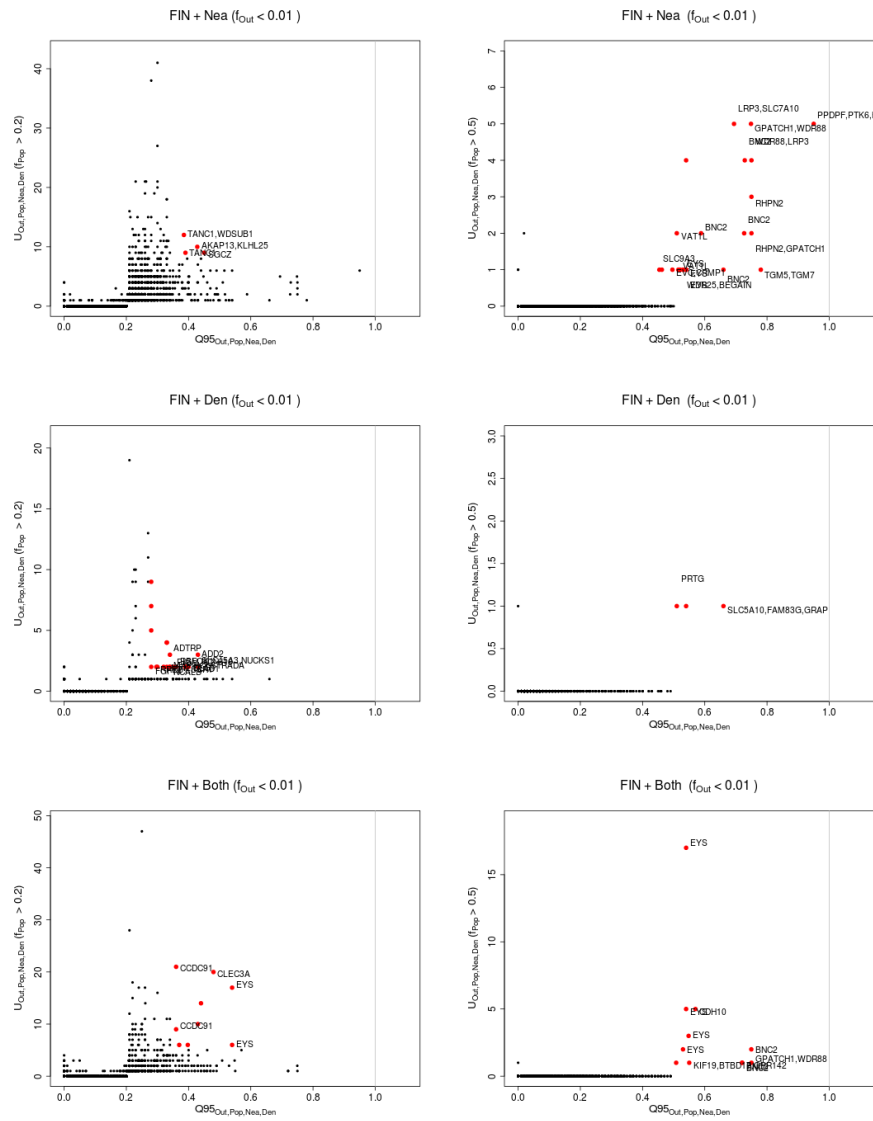


Figure S38: Uniquely shared archaic alleles in a Finnish (FIN) panel. Joint distribution of  $Q95_{AFR,FIN,Nea,Den}(1\%,y,z)$  and  $U_{AFR,FIN,Nea,Den}(1\%,x,y,z)$ , for 40kb non-overlapping regions along the genome, using two choices of  $x$  (20% in left column panels, 50% in right column panels). Red dots refer to regions that are in the 99.9% quantiles for both statistics. Neanderthal-specific shared alleles are displayed in the top panels, Denisovan-specific shared alleles are displayed in the middle-row panels, and alleles shared with both archaic human genome are displayed in the bottom panels.

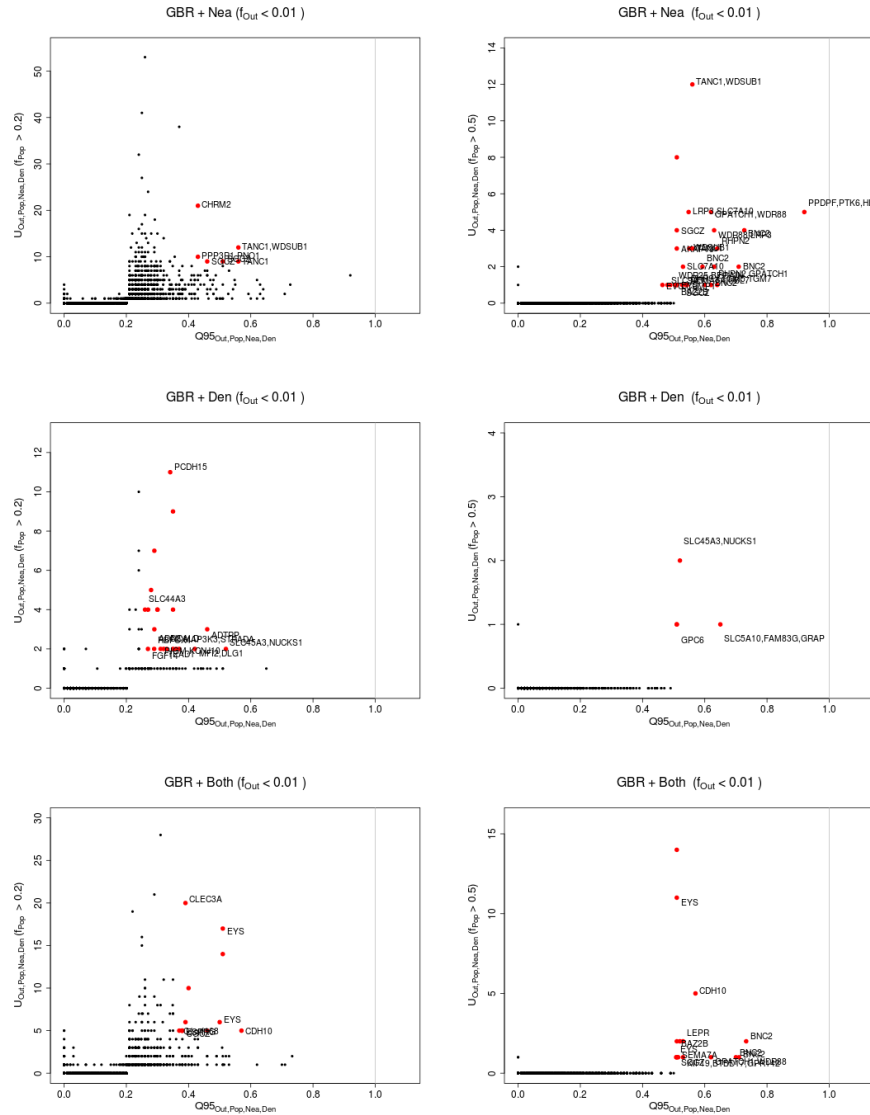


Figure S39: Uniquely shared archaic alleles in a British (GBR) panel. Joint distribution of  $Q95_{AFR,GBR,Nea,Den}(1\%,y,z)$  and  $U_{AFR,GBR,Nea,Den}(1\%,x,y,z)$ , for 40kb non-overlapping regions along the genome, using two choices of  $x$  (20% in left column panels, 50% in right column panels). Red dots refer to regions that are in the 99.9% quantiles for both statistics. Neanderthal-specific shared alleles are displayed in the top panels, Denisovan-specific shared alleles are displayed in the middle-row panels, and alleles shared with both archaic human genome are displayed in the bottom panels.

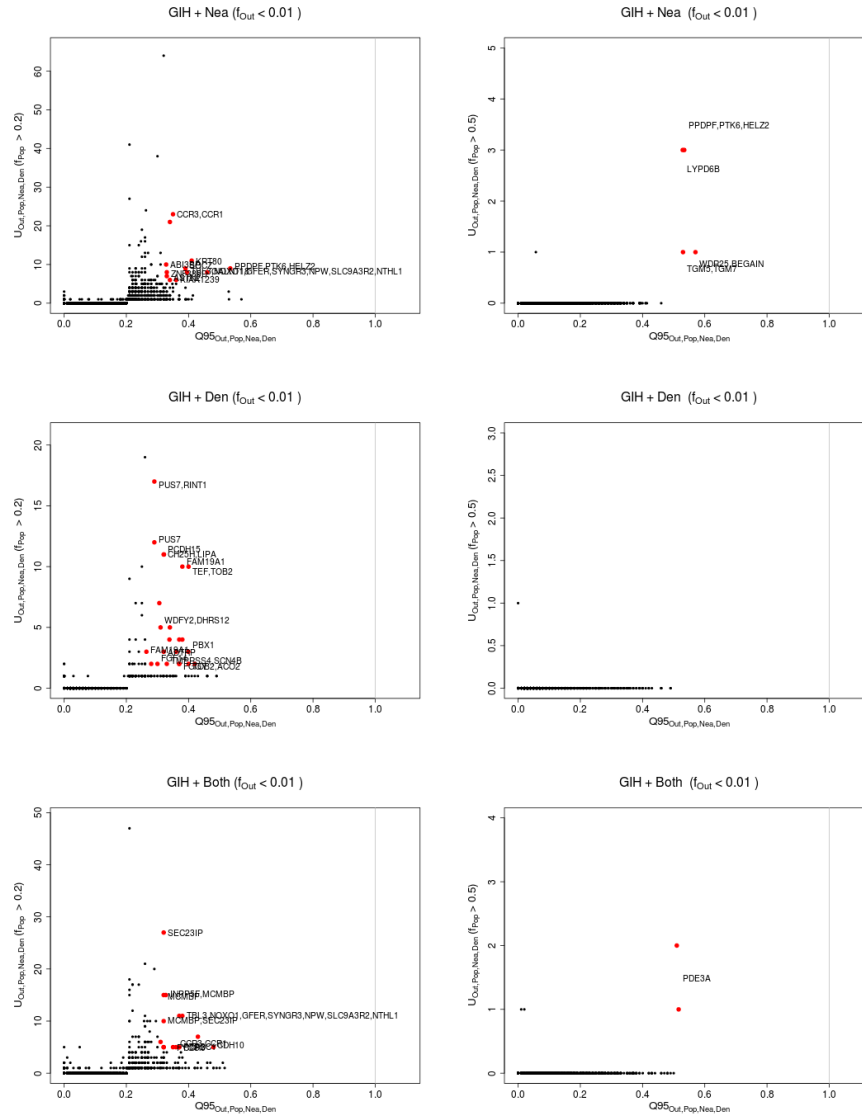


Figure S40: Uniquely shared archaic alleles in a Gujarati Indian (GIH) panel. Joint distribution of  $Q95_{AFR,GIH,Nea,Den}(1\%, y, z)$  and  $U_{AFR,GIH,Nea,Den}(1\%, x, y, z)$ , for 40kb non-overlapping regions along the genome, using two choices of  $x$  (20% in left column panels, 50% in right column panels). Red dots refer to regions that are in the 99.9% quantiles for both statistics. Neanderthal-specific shared alleles are displayed in the top panels, Denisovan-specific shared alleles are displayed in the middle-row panels, and alleles shared with both archaic human genome are displayed in the bottom panels.

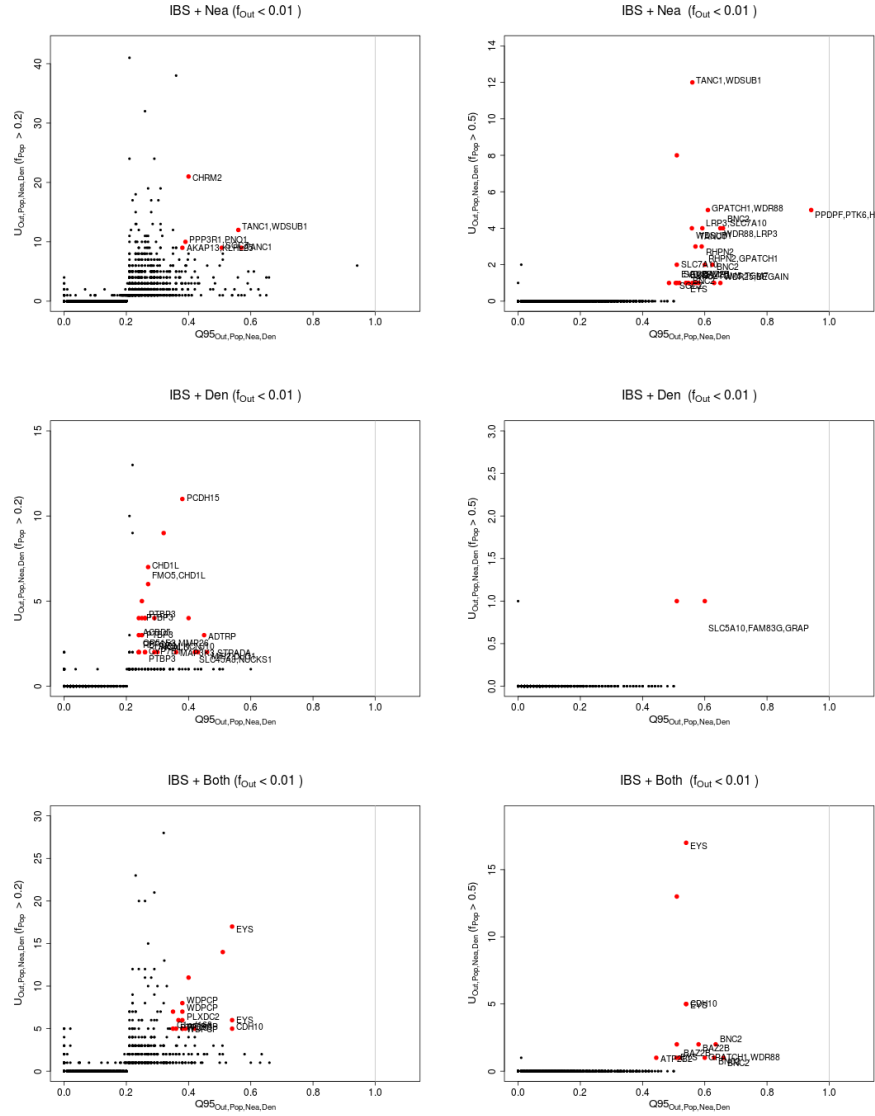


Figure S41: Uniquely shared archaic alleles in an Iberian (IBS) panel. Joint distribution of  $Q95_{AFR,IBS,Nea,Den}(1\%,y,z)$  and  $U_{AFR,IBS,Nea,Den}(1\%,x,y,z)$ , for 40kb non-overlapping regions along the genome, using two choices of  $x$  (20% in left column panels, 50% in right column panels). Red dots refer to regions that are in the 99.9% quantiles for both statistics. Neanderthal-specific shared alleles are displayed in the top panels, Denisovan-specific shared alleles are displayed in the middle-row panels, and alleles shared with both archaic human genome are displayed in the bottom panels.

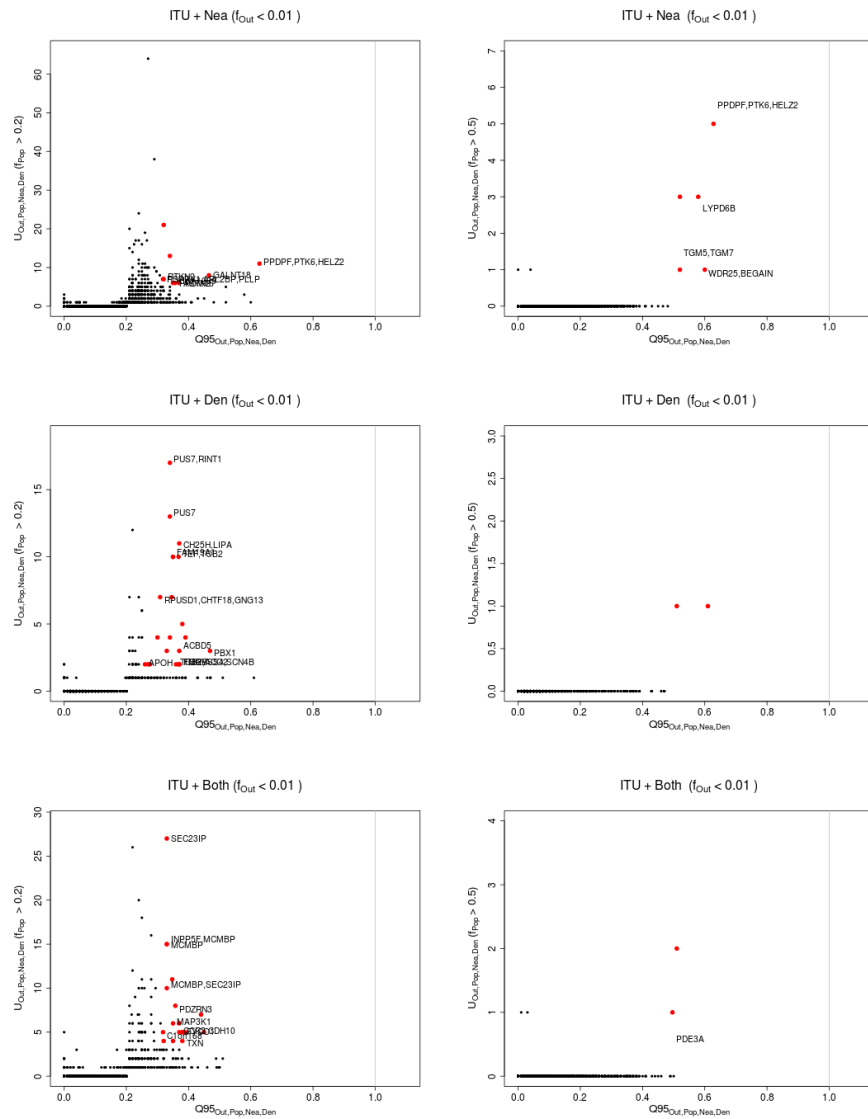


Figure S42: Uniquely shared archaic alleles in an Indian Telugu (ITU) panel. Joint distribution of  $Q95_{AFR,ITU,Nea,Den}(1\%, y, z)$  and  $U_{AFR,ITU,Nea,Den}(1\%, x, y, z)$ , for 40kb non-overlapping regions along the genome, using two choices of  $x$  (20% in left column panels, 50% in right column panels). Red dots refer to regions that are in the 99.9% quantiles for both statistics. Neanderthal-specific shared alleles are displayed in the top panels, Denisovan-specific shared alleles are displayed in the middle-row panels, and alleles shared with both archaic human genome are displayed in the bottom panels.

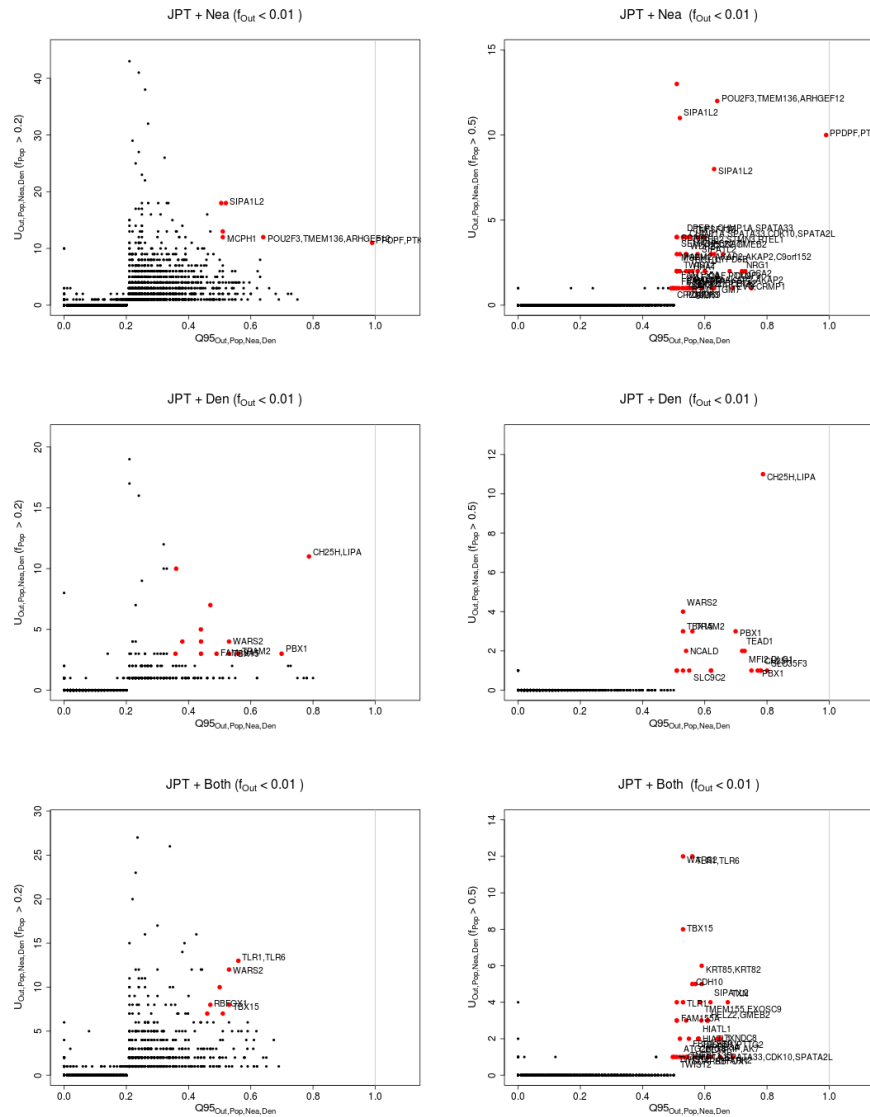


Figure S43: Uniquely shared archaic alleles in a Japanese (JPT) panel. Joint distribution of  $Q95_{AFR,JPT,Nea,Den}(1\%,y,z)$  and  $U_{AFR,JPT,Nea,Den}(1\%,x,y,z)$ , for 40kb non-overlapping regions along the genome, using two choices of  $x$  (20% in left column panels, 50% in right column panels). Red dots refer to regions that are in the 99.9% quantiles for both statistics. Neanderthal-specific shared alleles are displayed in the top panels, Denisovan-specific shared alleles are displayed in the middle-row panels, and alleles shared with both archaic human genome are displayed in the bottom panels.

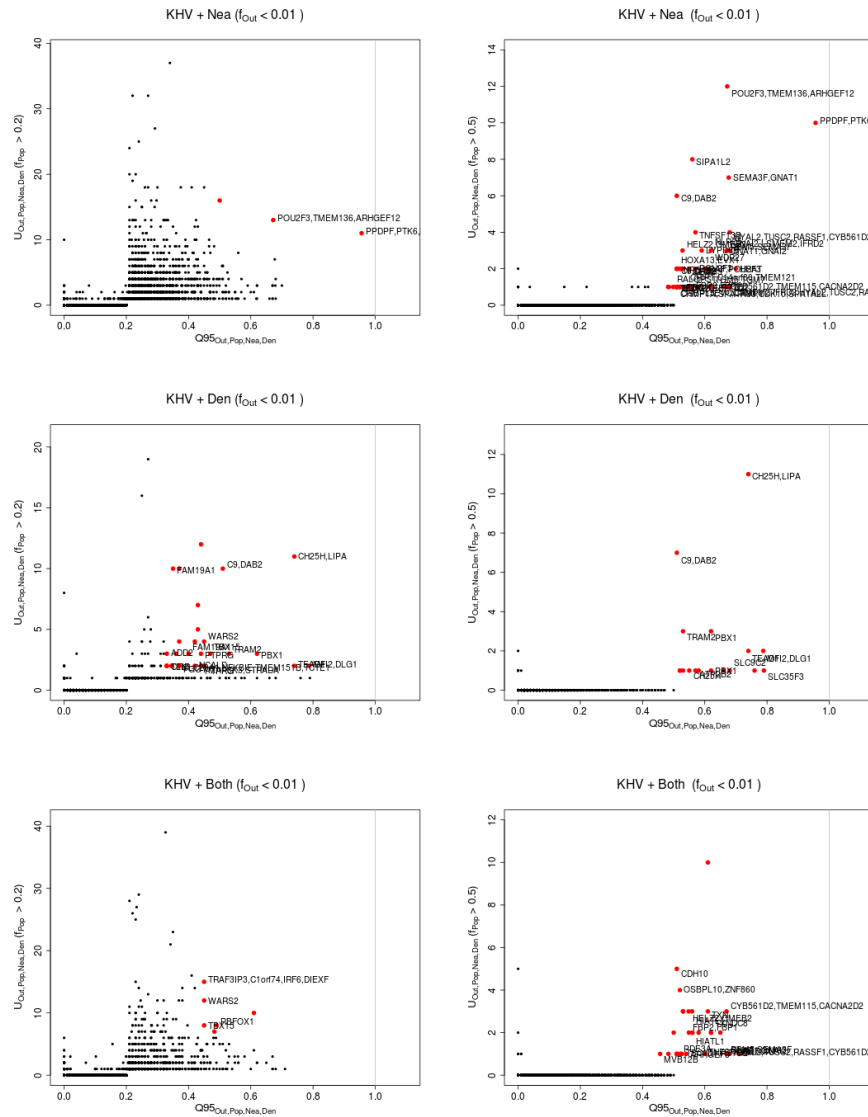


Figure S44: Uniquely shared archaic alleles in a Kinh (KHV) panel. Joint distribution of  $Q95_{AFR,KHV,Nea,Den}(1\%,y,z)$  and  $U_{AFR,KHV,Nea,Den}(1\%,x,y,z)$ , for 40kb non-overlapping regions along the genome, using two choices of  $x$  (20% in left column panels, 50% in right column panels). Red dots refer to regions that are in the 99.9% quantiles for both statistics. Neanderthal-specific shared alleles are displayed in the top panels, Denisovan-specific shared alleles are displayed in the middle-row panels, and alleles shared with both archaic human genome are displayed in the bottom panels.

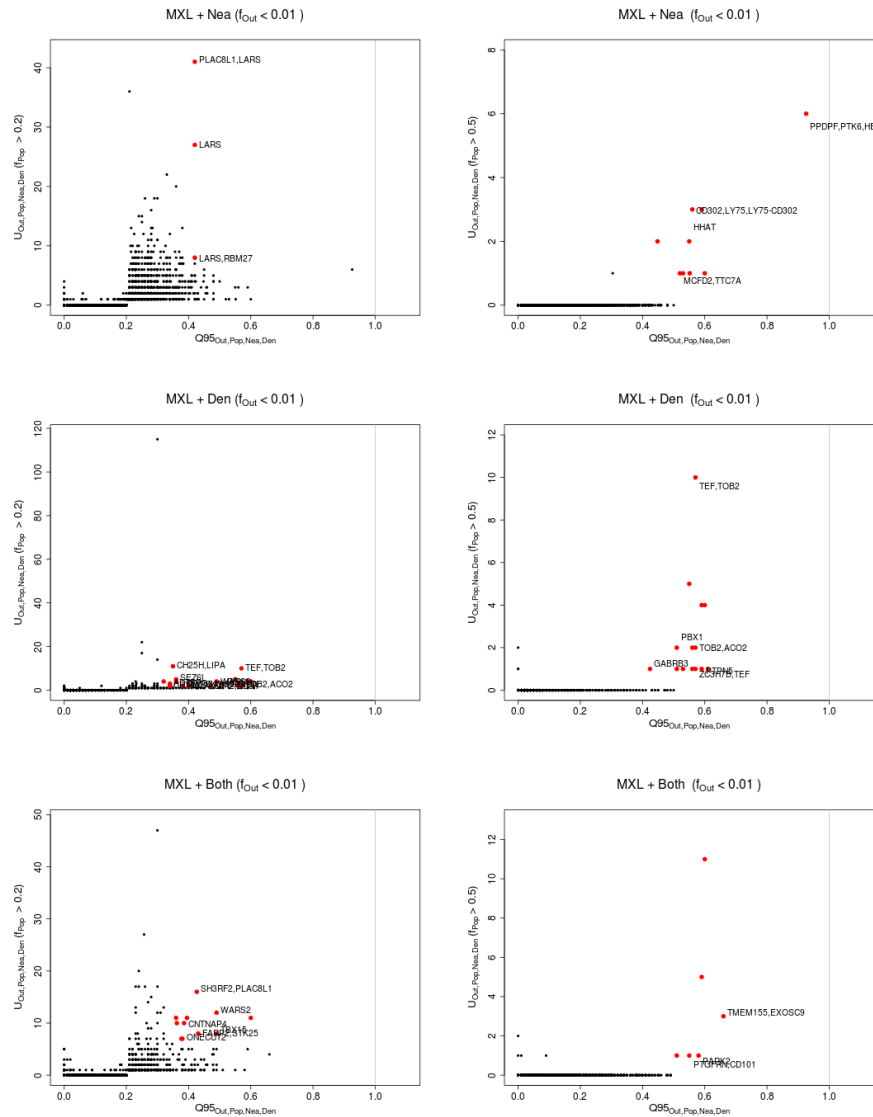


Figure S45: Uniquely shared archaic alleles in a Mexican (MXL) panel. Joint distribution of  $Q95_{AFR, MXL, Nea, Den}(1\%, y, z)$  and  $U_{AFR, MXL, Nea, Den}(1\%, x, y, z)$ , for 40kb non-overlapping regions along the genome, using two choices of  $x$  (20% in left column panels, 50% in right column panels). Red dots refer to regions that are in the 99.9% quantiles for both statistics. Neanderthal-specific shared alleles are displayed in the top panels, Denisovan-specific shared alleles are displayed in the middle-row panels, and alleles shared with both archaic human genome are displayed in the bottom panels.



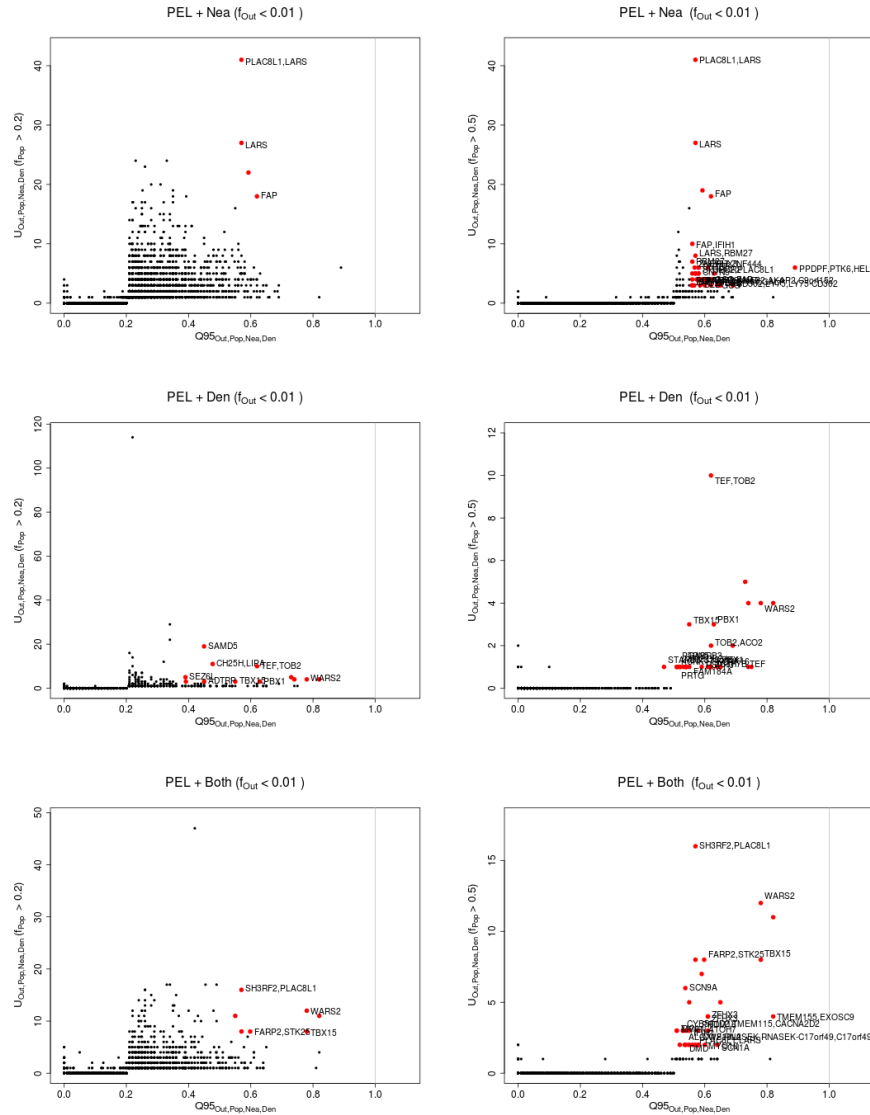


Figure S46: Uniquely shared archaic alleles in a Peruvian (PEL) panel. Joint distribution of  $Q95_{AFR,PEL,Nea,Den}(1\%, y, z)$  and  $U_{AFR,PEL,Nea,Den}(1\%, x, y, z)$ , for 40kb non-overlapping regions along the genome, using two choices of  $x$  (20% in left column panels, 50% in right column panels). Red dots refer to regions that are in the 99.9% quantiles for both statistics. Neanderthal-specific shared alleles are displayed in the top panels, Denisovan-specific shared alleles are displayed in the middle-row panels, and alleles shared with both archaic human genome are displayed in the bottom panels.

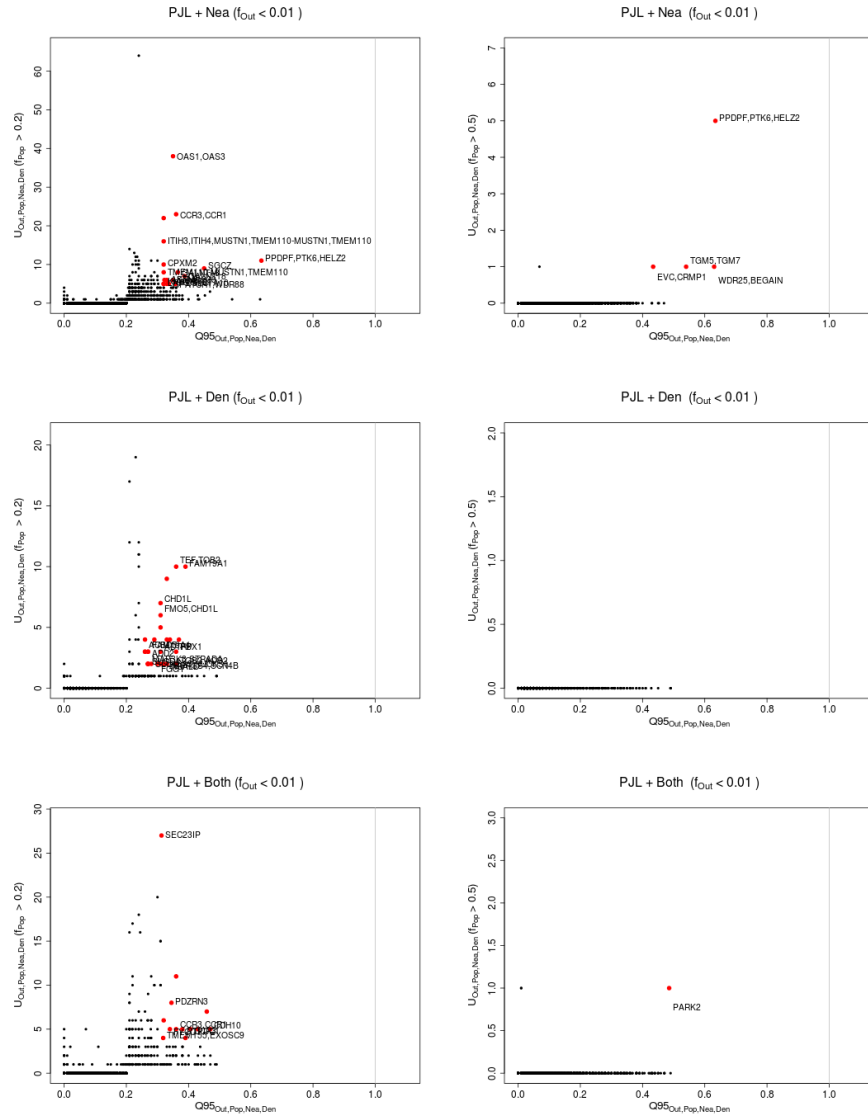


Figure S47: Uniquely shared archaic alleles in a Punjabi (PJI) panel. Joint distribution of  $Q_{95}^{AFR,PJI,Nea,Den}(1\%,y,z)$  and  $U_{AFR,PJI,Nea,Den}(1\%,x,y,z)$ , for 40kb non-overlapping regions along the genome, using two choices of  $x$  (20% in left column panels, 50% in right column panels). Red dots refer to regions that are in the 99.9% quantiles for both statistics. Neanderthal-specific shared alleles are displayed in the top panels, Denisovan-specific shared alleles are displayed in the middle-row panels, and alleles shared with both archaic human genome are displayed in the bottom panels.

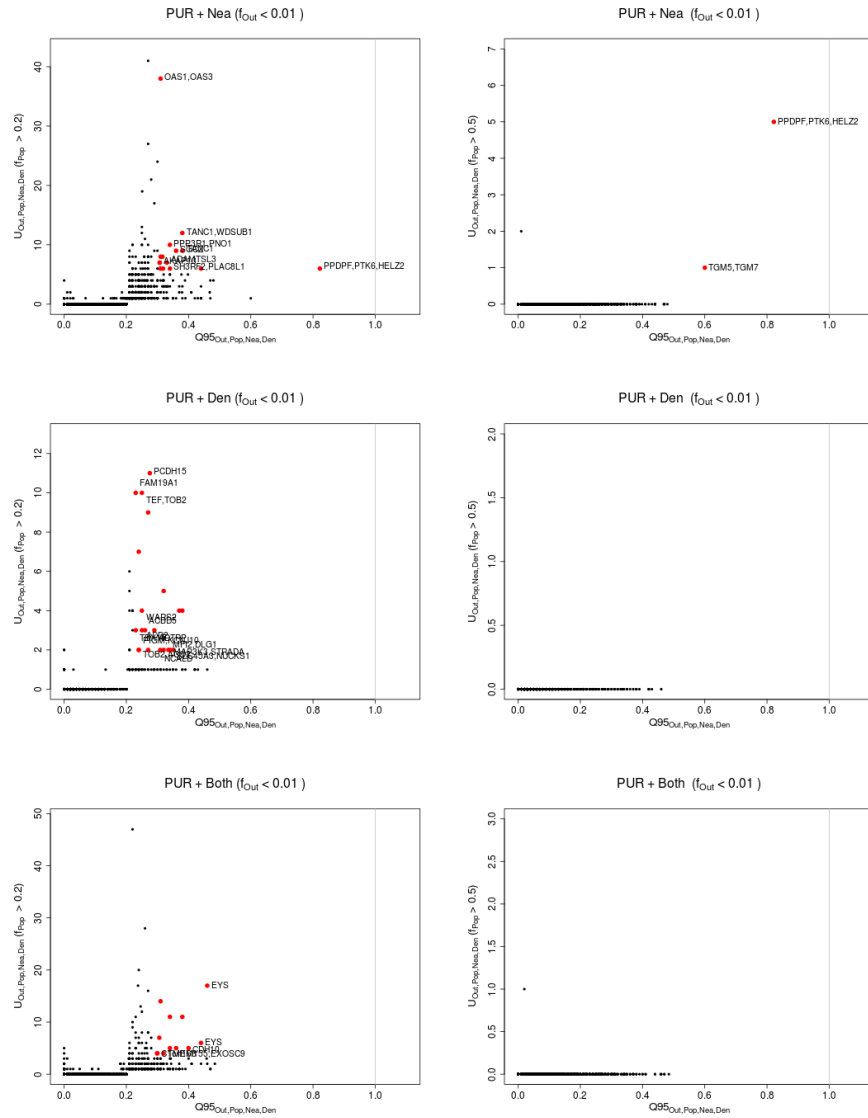


Figure S48: Uniquely shared archaic alleles in a Puerto Rican (PUR) panel. Joint distribution of  $Q95_{AFR,PUR,Nea,Den}(1\%, y, z)$  and  $U_{AFR,PUR,Nea,Den}(1\%, x, y, z)$ , for 40kb non-overlapping regions along the genome, using two choices of  $x$  (20% in left column panels, 50% in right column panels). Red dots refer to regions that are in the 99.9% quantiles for both statistics. Neanderthal-specific shared alleles are displayed in the top panels, Denisovan-specific shared alleles are displayed in the middle-row panels, and alleles shared with both archaic human genome are displayed in the bottom panels.

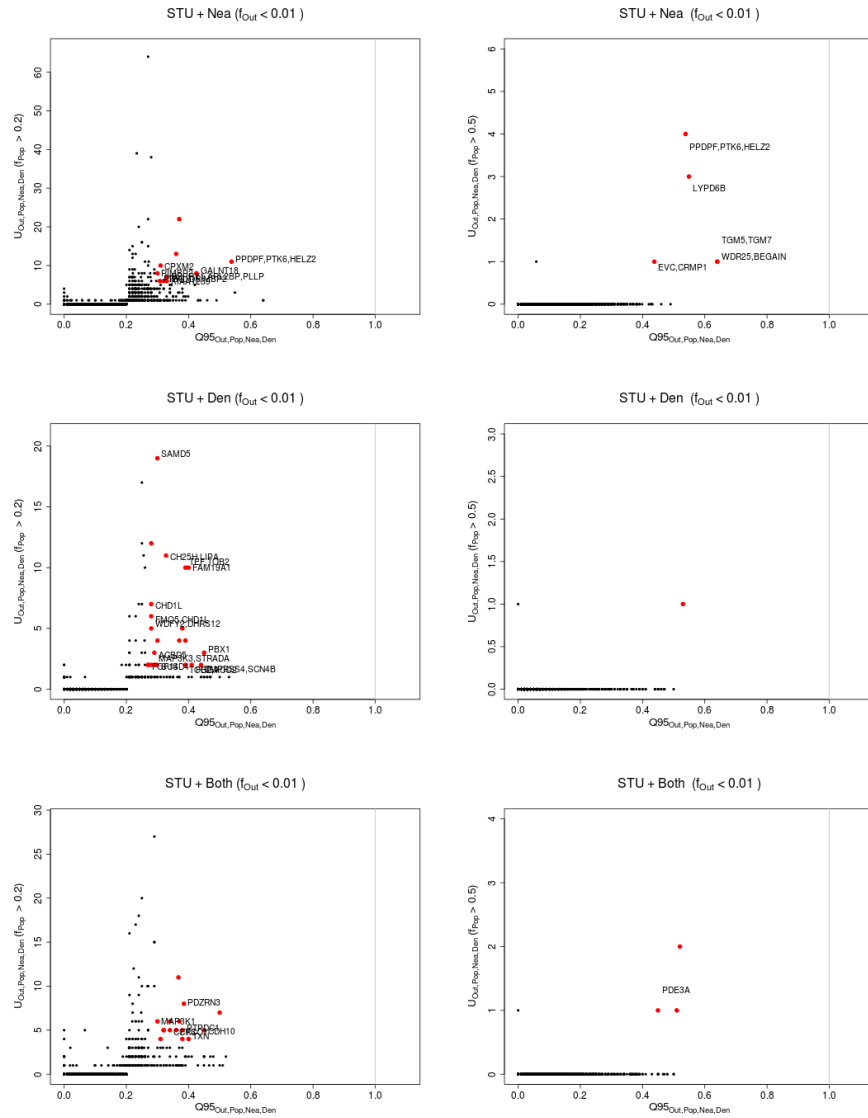


Figure S49: Uniquely shared archaic alleles in a Sri Lankan Tamil (STU) panel. Joint distribution of  $Q95_{AFR,STU,Nea,Den}(1\%,y,z)$  and  $U_{AFR,STU,Nea,Den}(1\%,x,y,z)$ , for 40kb non-overlapping regions along the genome, using two choices of  $x$  (20% in left column panels, 50% in right column panels). Red dots refer to regions that are in the 99.9% quantiles for both statistics. Neanderthal-specific shared alleles are displayed in the top panels, Denisovan-specific shared alleles are displayed in the middle-row panels, and alleles shared with both archaic human genome are displayed in the bottom panels.

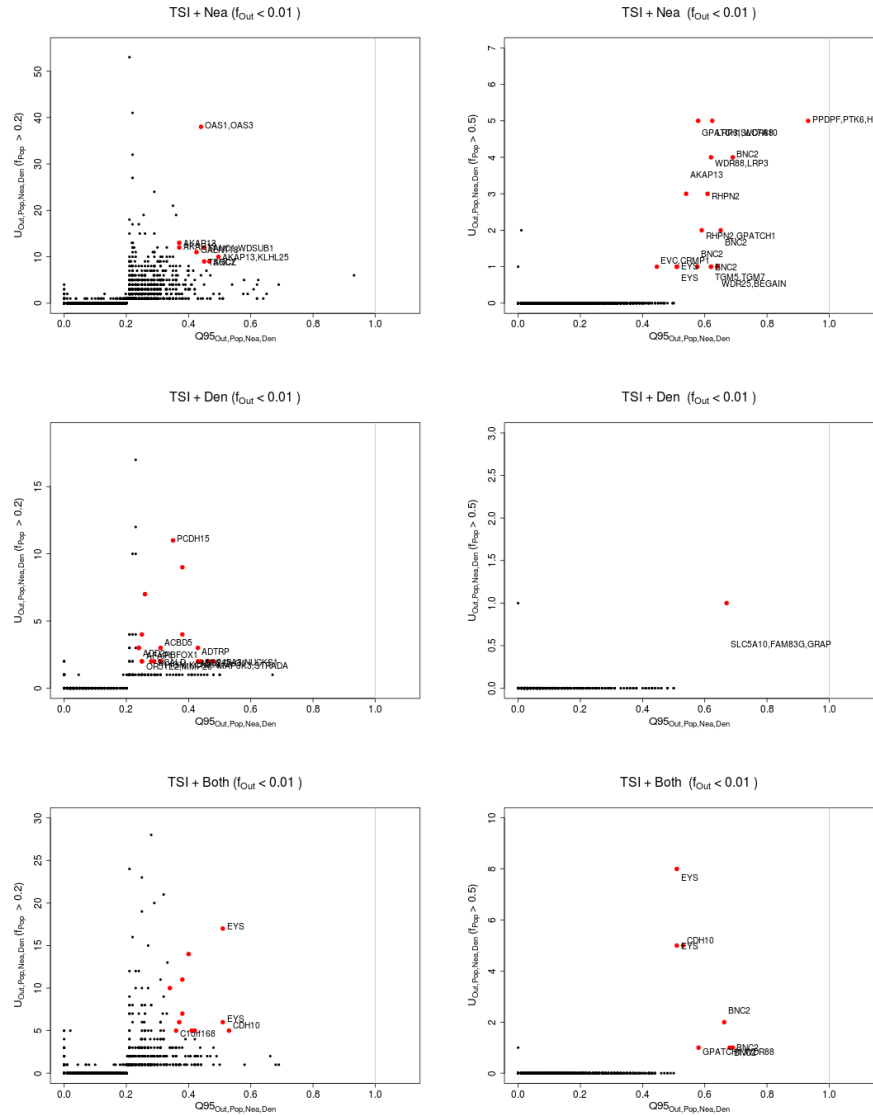


Figure S50: Uniquely shared archaic alleles in a Toscani (TSI) panel. Joint distribution of  $Q95_{AFR,TSI,Nea,Den}(1\%,y,z)$  and  $U_{AFR,TSI,Nea,Den}(1\%,x,y,z)$ , for 40kb non-overlapping regions along the genome, using two choices of  $x$  (20% in left column panels, 50% in right column panels). Red dots refer to regions that are in the 99.9% quantiles for both statistics. Neanderthal-specific shared alleles are displayed in the top panels, Denisovan-specific shared alleles are displayed in the middle-row panels, and alleles shared with both archaic human genome are displayed in the bottom panels.

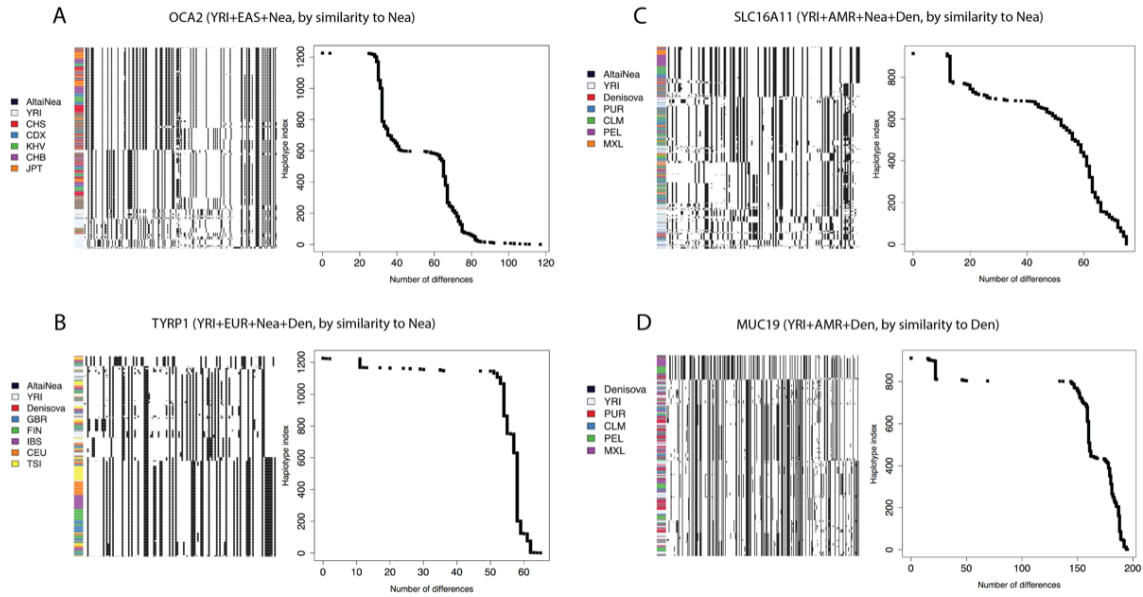


Figure S51: We explored the haplotype structure of *OCA2*, *TYRP1*, *SLC16A11* and *MUC19*. We applied a clustering algorithm to the haplotypes of particular human populations and then ordered the clusters by decreasing similarity to the archaic human genome with the larger number of uniquely shared sites. We also plotted the number of differences to the closest archaic haplotype for each human haplotype and sorted them simply by decreasing similarity. Note that, in the latter case, no clustering was performed, so the rows in the cumulative difference plots do not necessarily correspond to the rows in the adjacent haplotype structure plots. *OCA2*: chr15:28160001-28200000. *TYRP1*: chr9:12680001-12720000. *SLC16A11*: chr17:6880001-6960000. *MUC19*: chr12:40800001-40840000.

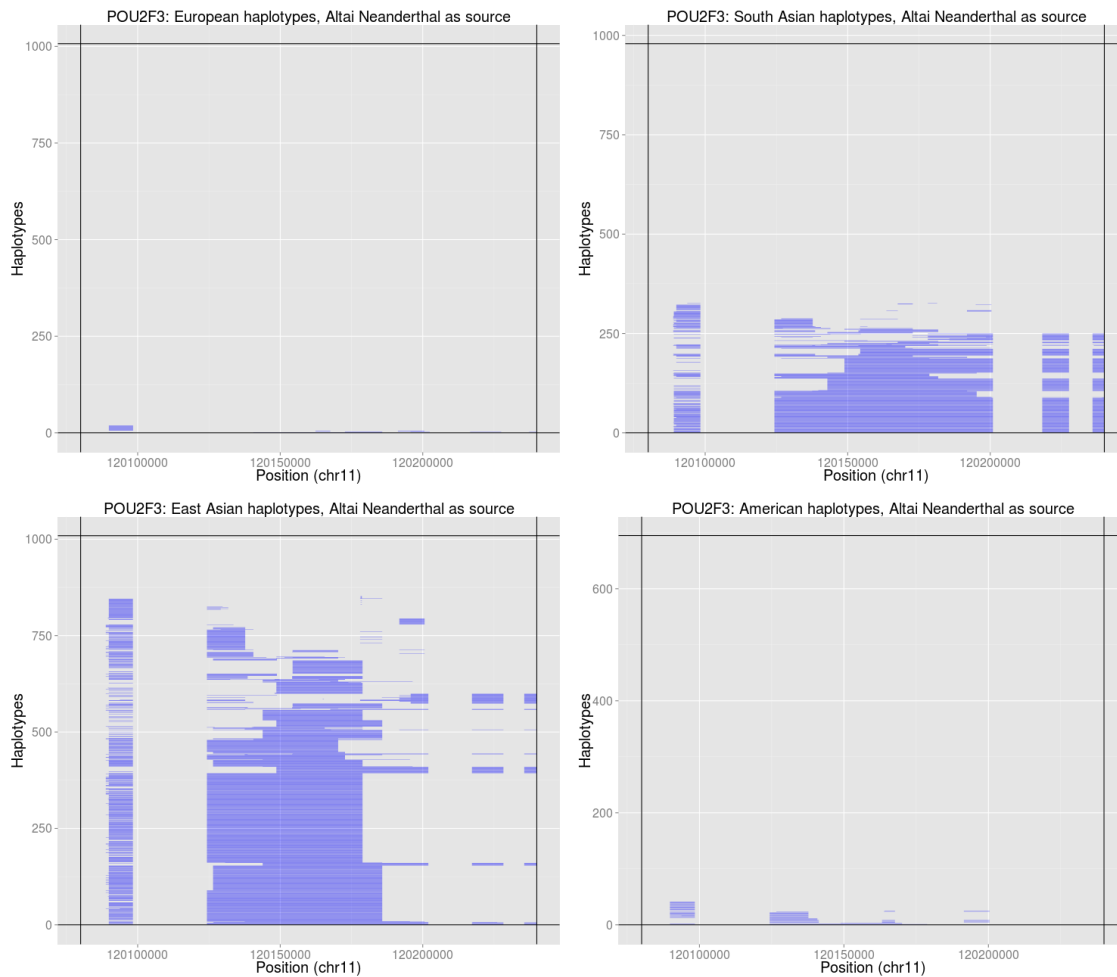


Figure S52: Introgred tracks inferred in the four Non-African 1000 Genomes continental panels by an HMM [21] in the *POU2F3* region, using the Altai Neanderthal genome as the archaic source.

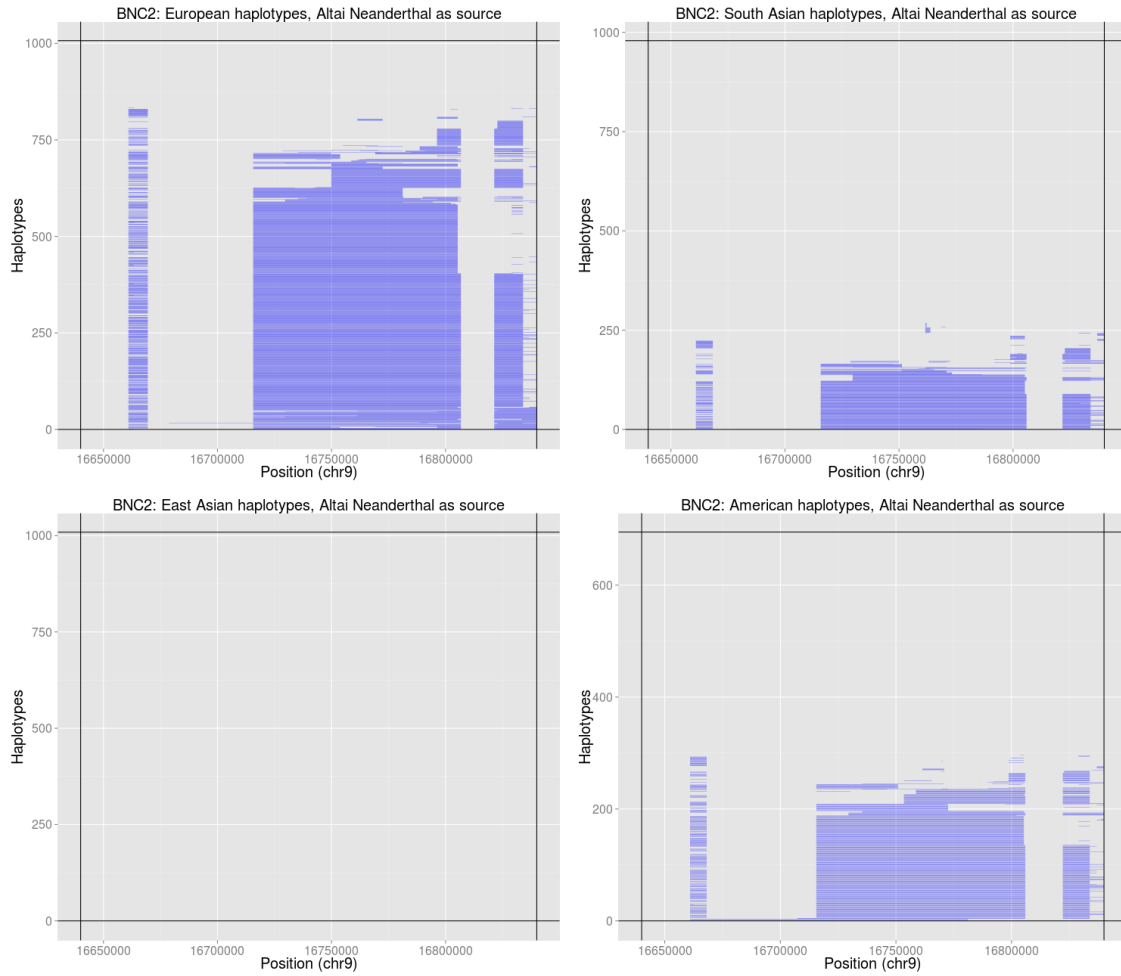


Figure S53: Introgressed tracks inferred in the four Non-African 1000 Genomes continental panels by an HMM [21] in the *BNC2* region, using the Altai Neanderthal genome as the archaic source.

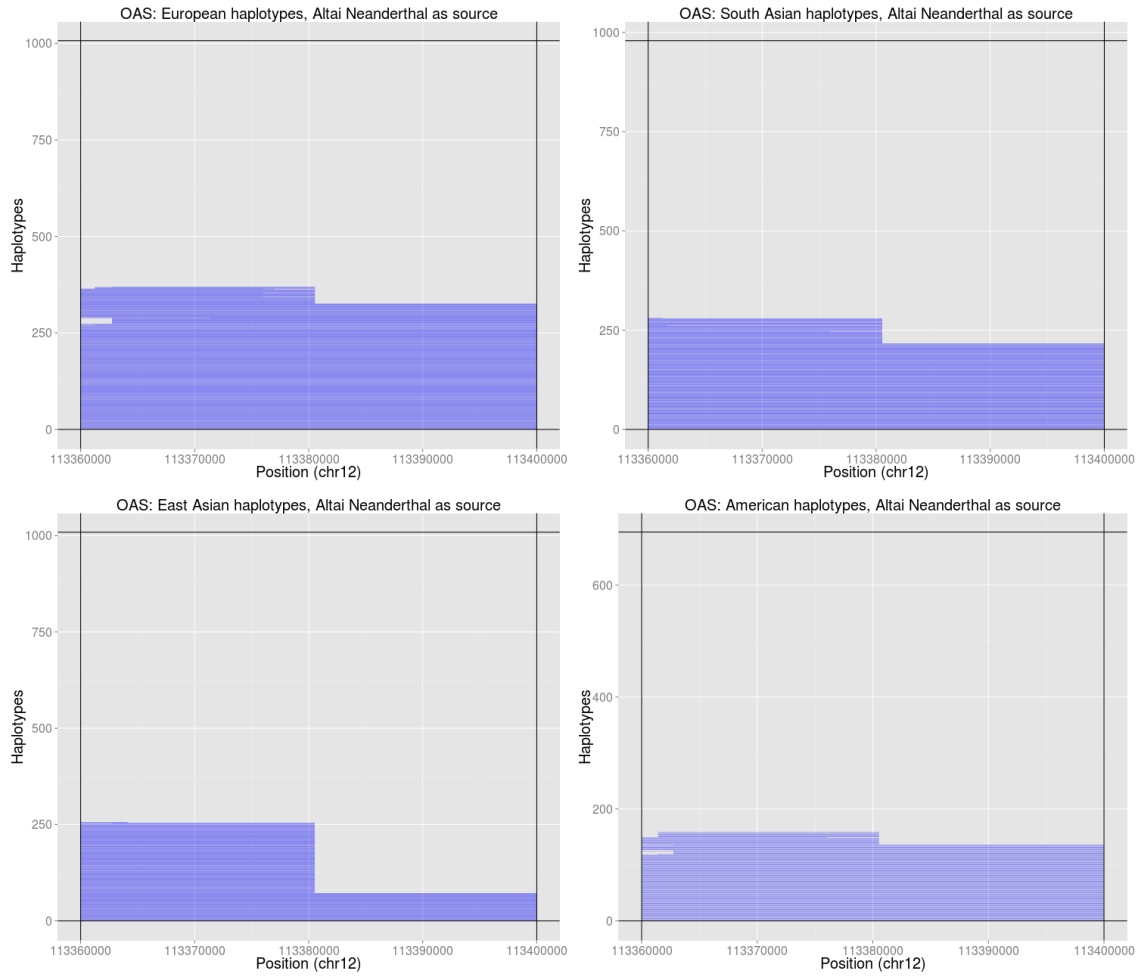


Figure S54: Introgressed tracks inferred in the four Non-African 1000 Genomes continental panels by an HMM [21] in the OAS region, using the Altai Neanderthal genome as the archaic source.



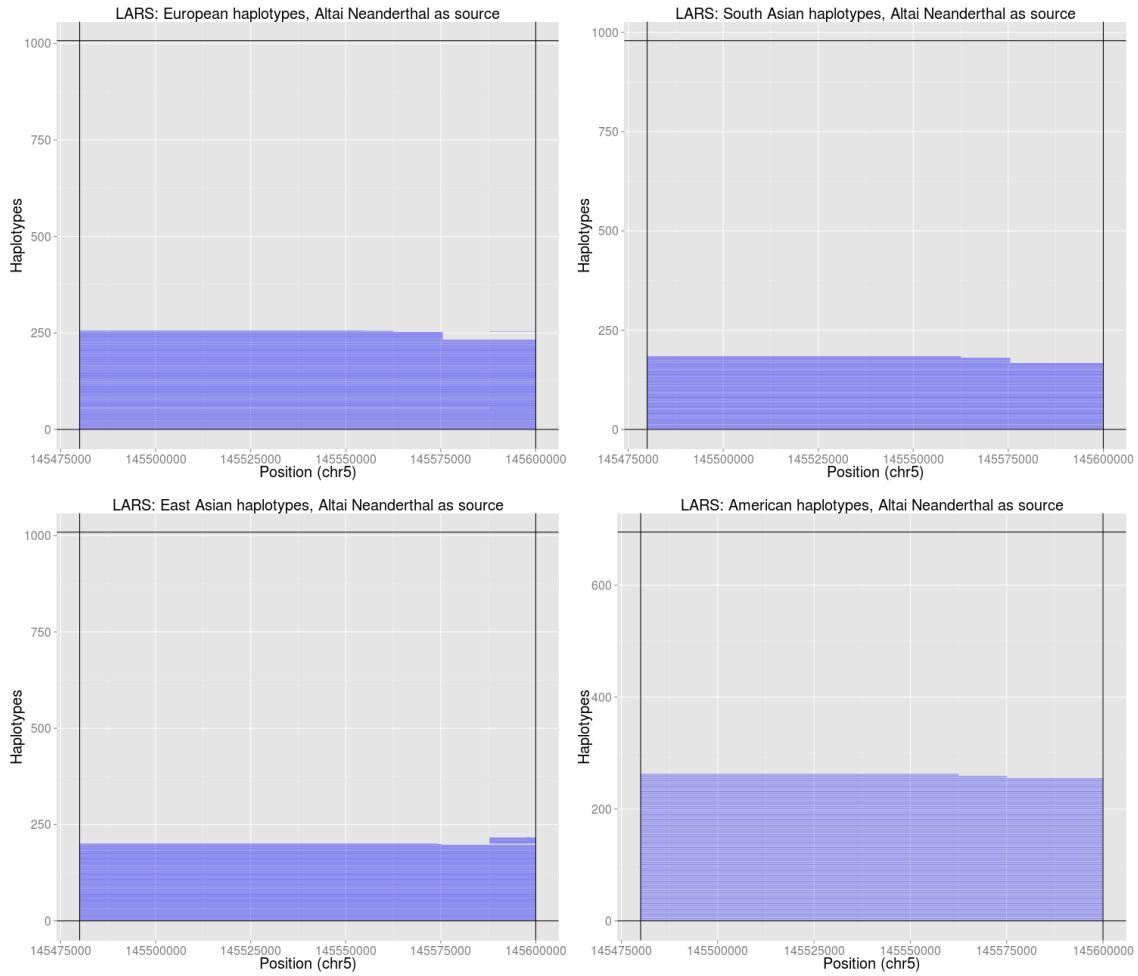


Figure S55: Introgressed tracks inferred in the four Non-African 1000 Genomes continental panels by an HMM [21] in the *LARS* region, using the Altai Neanderthal genome as the archaic source.

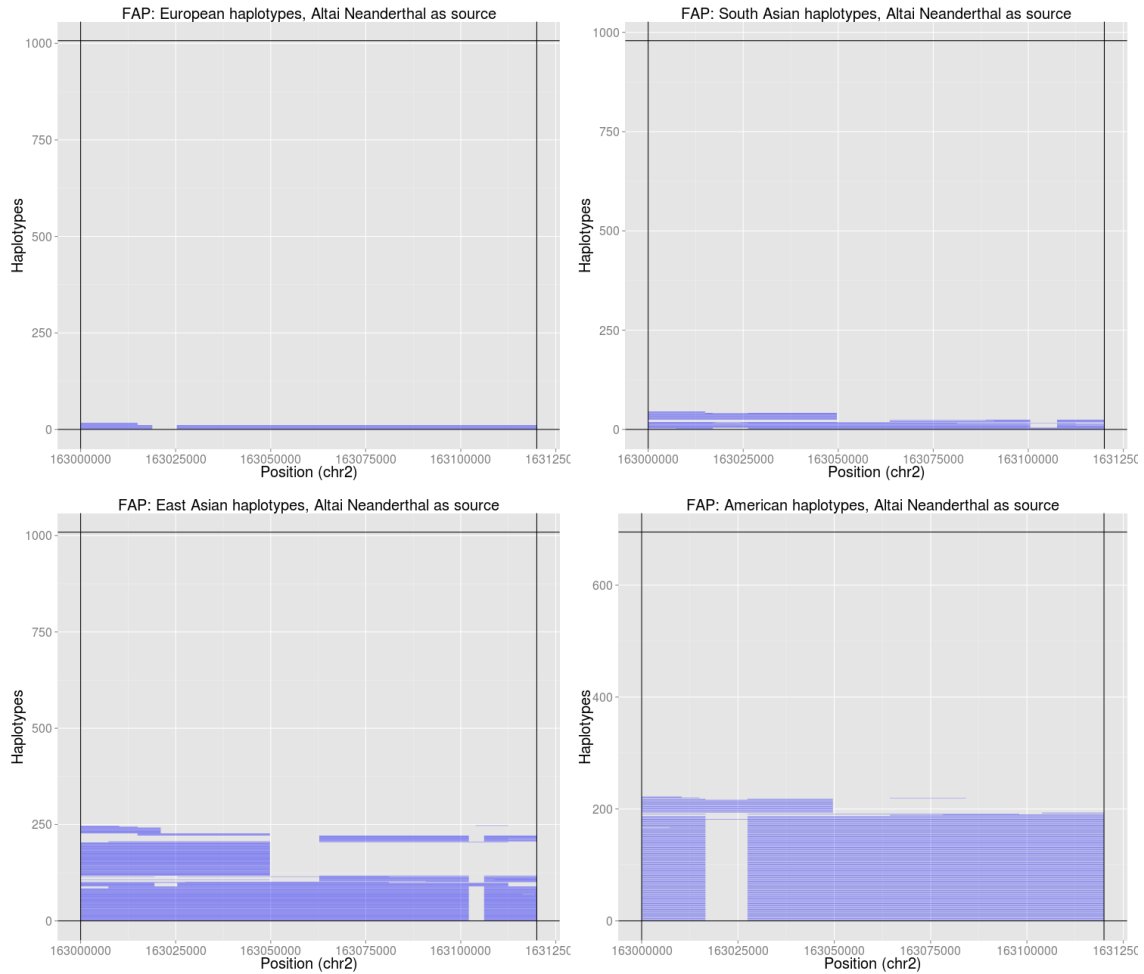


Figure S56: Introgressed tracks inferred in the four Non-African 1000 Genomes continental panels by an HMM [21] in the *FAP/IFIH1* region, using the Altai Neanderthal as the archaic source.

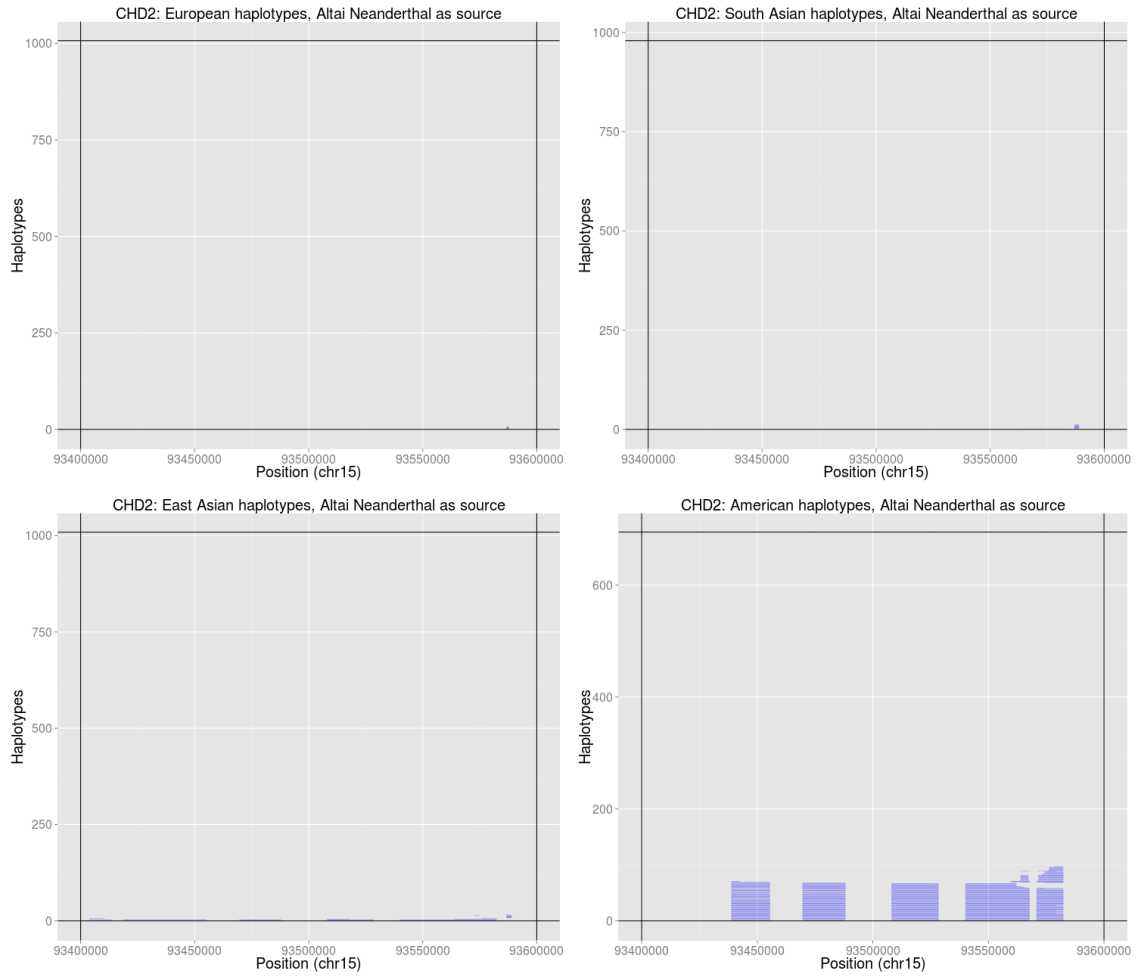


Figure S57: Introgressed tracks inferred in the four Non-African 1000 Genomes continental panels by an HMM [21] in the *CHD2* region, using the Altai Neanderthal genome as the archaic source.

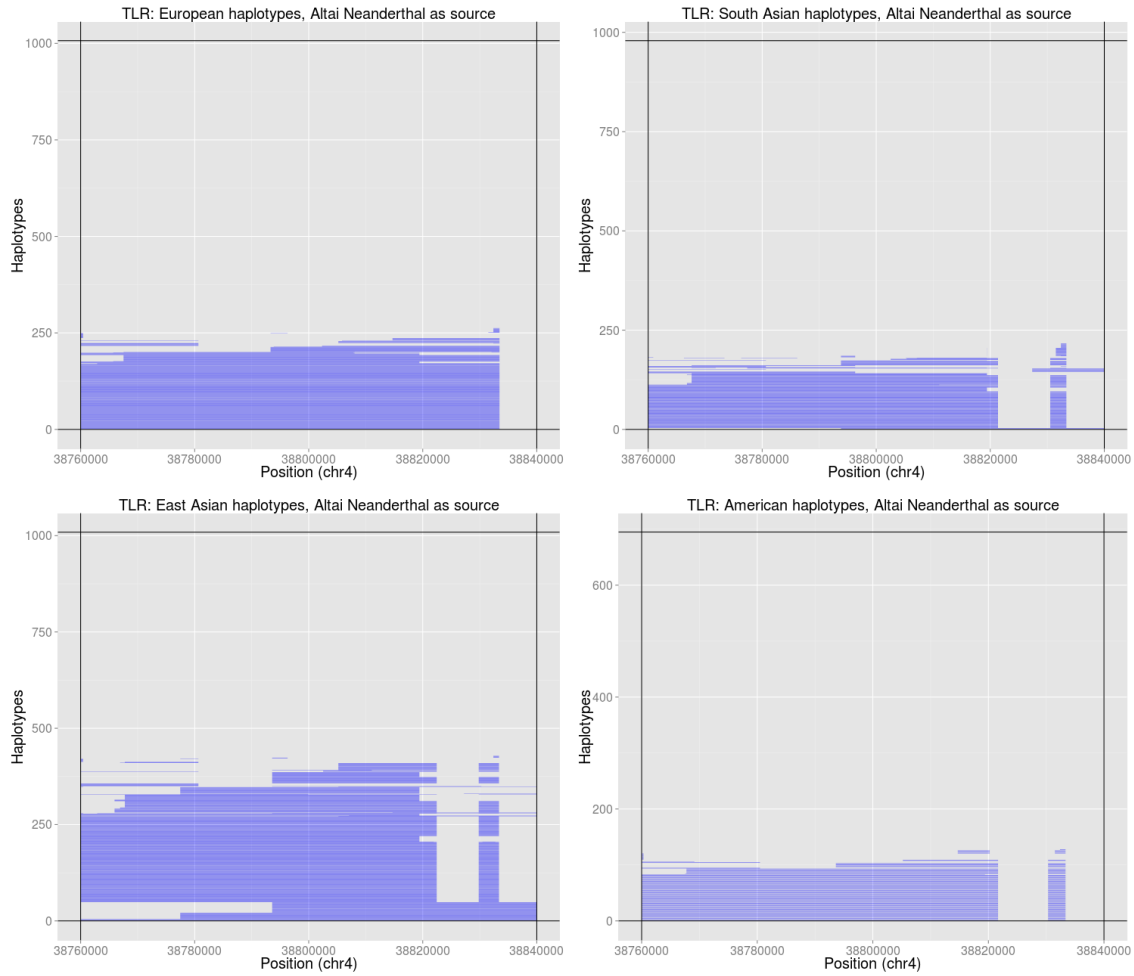


Figure S58: Introgressed tracks inferred in the four Non-African 1000 Genomes continental panels by an HMM [21] in the *TLR1-6* region, using the Altai Neanderthal genome as the archaic source.

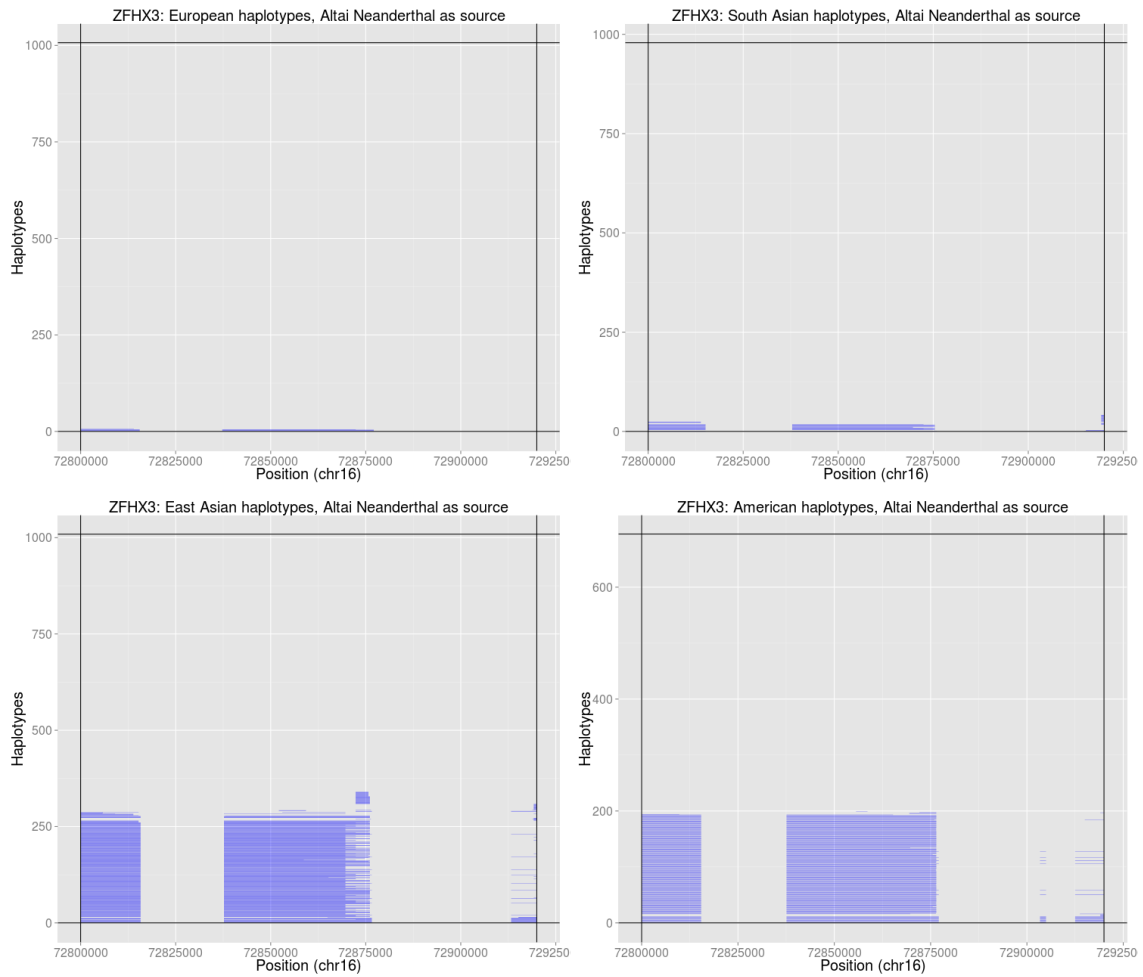


Figure S59: Introgressed tracks inferred in the four Non-African 1000 Genomes continental panels by an HMM [21] in the *ZFH3* region, using the Altai Neanderthal genome as the archaic source.

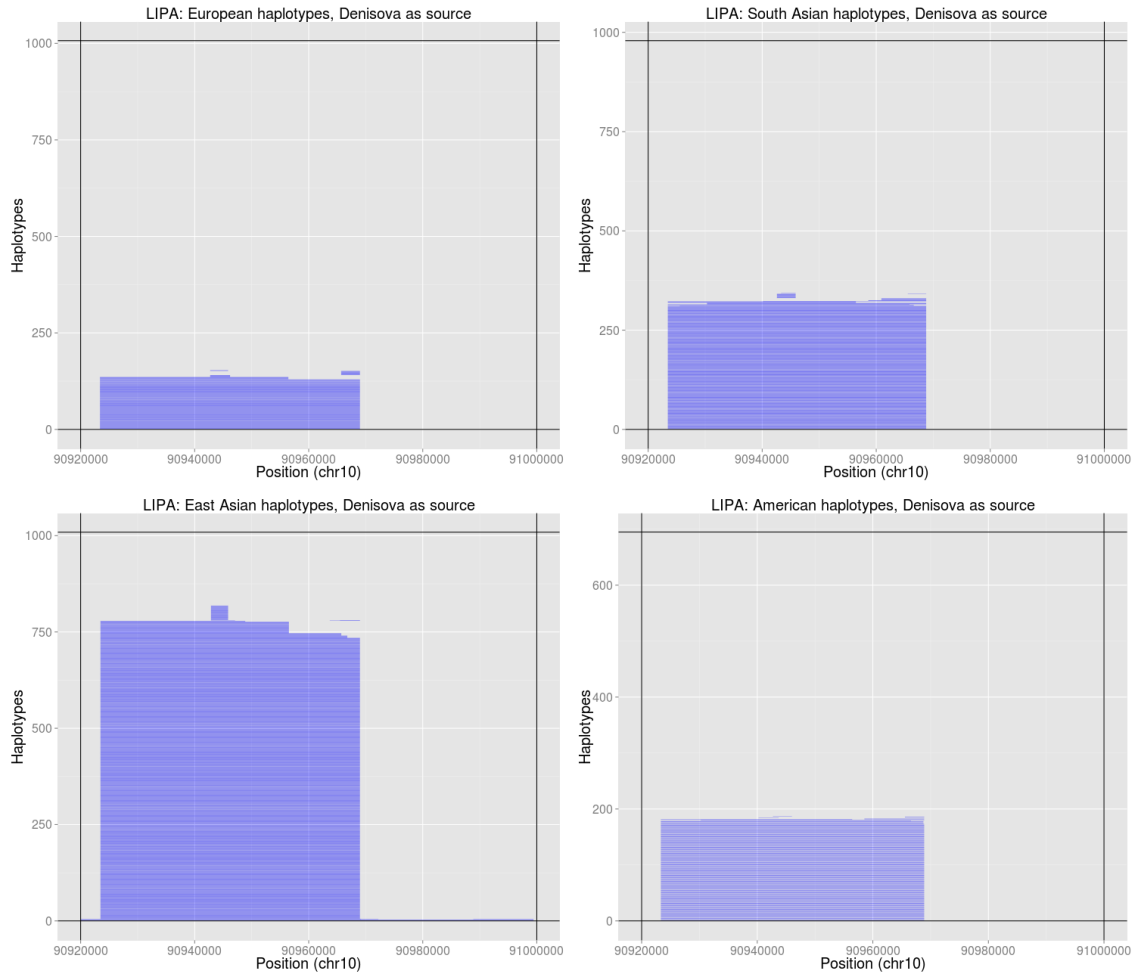


Figure S60: Introgressed tracks inferred in the four Non-African 1000 Genomes continental panels by an HMM [21] in the *LIPA* region, using the Denisova genome as the archaic source.

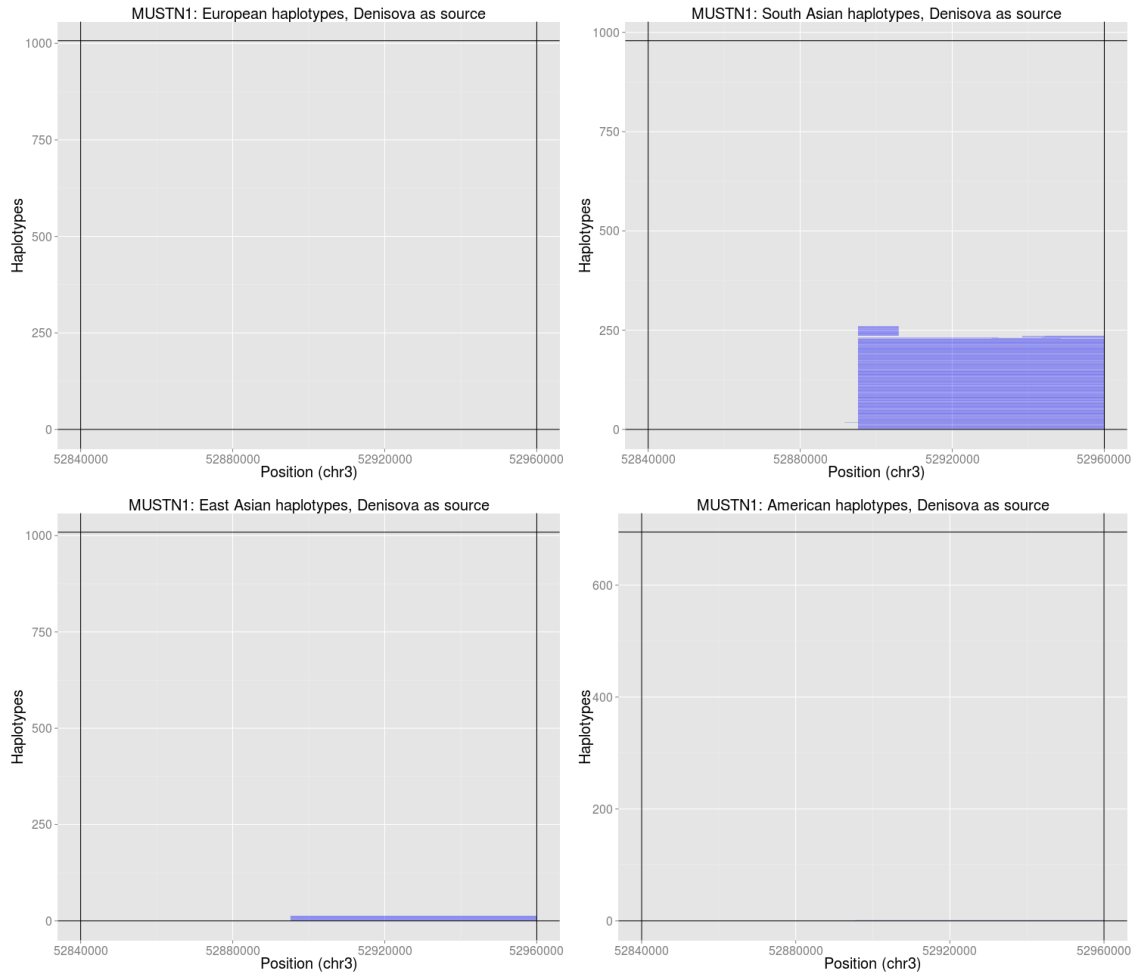


Figure S61: Introgressed tracks inferred in the four Non-African 1000 Genomes continental panels by an HMM [21] in the *MUSTN1* region, using the Denisova genome as the archaic source.